UNIVERSITY OF CALIFORNIA
RIVERSIDE

Structural Characterization of Proteins, Peptides and Oligosaccharides Based on Radical Chemistry and Mass Spectrometry

A Dissertation submitted in partial satisfaction
of the requirements for the degree of

Doctor of Philosophy

in

Chemistry

by

Xing Zhang

August 2014

Dissertation Committee:
Dr. Ryan Julian, Chairperson
Dr. Yinsheng Wang
Dr. Jingsong Zhang

The Dissertation of Xing Zhang is approved:

_____

_____

_____

Committee Chairperson

University of California, Riverside

ACKNOWLEDGMENTS

I would like to express my sincere gratitude to my graduate advisor Ryan Julian. Without his support and help this dissertation would not have become possible.

It is my pleasure to graduate from Julian group. I sincerely appreciate the research opportunities that ryan has given me. I sincerely appreciate the financial support for being a student research assistant. I sincerely appreciate the opportunities for attending and presenting in a lot conferences. I sincerely appreciate his suggestions and comments in every respect. I sincerely appreciate all the training I obtained in the past four years.

I would like to thank all the knowledge and help I obtained from Dr. Jason Cheng, Dr. Cindy Larive, Dr. Wenwan Zhong, Dr. Yinsheng Wang, Dr. Jingsong Zhang, Dr. Huiwang Ai, Dr. Angelina Chang, Dr. Beran Gregory, Dr. Roger Atkinson. My thanks also go to our collaborators Dr. Kathrin Breuker, Consuelo Beecher, Dr. Daniel Gallie, Dr. Joseph Loo, Dr. Rachel R. Loo, Pete Wongkongkathep, Huilin Li. Special thanks go to Dr. Shijun Cheng and Dr. Zhong Chen, who kindly teach me molecular biology skills.

I would like to thank all the help from my friends and peers at UCR: Yuanqi Tao, Benjamin Moore, Helen Sun, Jolene Diedrich, Tony Ly, Eric Knudsen, Nicole Pham, Omar Hamdy, Nathan Hendricks, Chris Nellessen, Yana Lyon; Yongsheng Xiao, Si Chen, Lijuan Fu, Qian Cai, Pengcheng Wang, Jicheng Duan; Zhijiang Lv, Mindy Huang, Yi Wang, Yenan Lin.

I would like to thank Mrs Barbara Outzen for help in preparation of documents.

I would like to thank my teachers from primary school to college: Mr. Chen Di, Mrs. Wang Qi, Mr. Duan Yimei, Mr. Yang Libo, Mr. Yao Jianming, Dr. Shao Yuanhua, Dr. Yan Li, Dr. Xinxiang Zhang. They help me to lay a foundation of graduate study.

My apologies for not being able to list everyone who ever gave me help.

Most text of this dissertation is a reprint of the material cited from the following published papers:

Chapter 2: Zhang, X.; Julian, R. R., Investigating the gas phase structure of KIX with radical directed dissociation and molecular dynamics: Retention of the native structure. *Int. J. Mass Spectrom.* **2011,** *308* (2-3), 225-231.

Chapter 3: Zhang, X.; Julian, R. R., Photoinitiated intramolecular diradical cross-linking of polyproline peptides in the gas phase, *Phys. Chem. Chem. Phys.* **2012,** *14*,16243-16249.

Chapter 4: Zhang, X.; Julian, R. R., Exploring radical migration pathways in peptides with positional isomers, deuterium labeling, and molecular dynamics simulations, *J. Am. Soc. Mass Spectrom.* **2013,** *24*, 524-533.

Chapter 5: Zhang, X.; Julian, R. R., Radical additions to aromatic residues in peptides facilitate unexpected side chain and backbone losses, *J. Am. Soc. Mass Spectrom.* **2014,** *25*, 626-635.

Chapter 6: Zhang, X.; Julian, R. R., Radical mediated dissection of oligosaccharides, *Int. J. Mass Spectrom.* **2014,** *372*, 22-28.

ABSTRACT OF THE DISSERTATION

Structural Characterization of Proteins, Peptides and Oligosaccharides Based on Radical Chemistry and Mass Spectrometry

by

Xing Zhang

Doctor of Philosophy, Graduate Program in Chemistry
University of California, Riverside, August 2014
Dr. Ryan Julian, Chairperson

Mass spectrometry (MS) is best known for measuring molecular weight and probing the chemical structure. Radical directed dissociation (RDD) is a tandem MS fragmentation method for hydrogen deficient radical precursors, which provides complementary structure information compared to other tandem MS methods.

Fragmentation pathways of peptide radical isomers in collision induced dissociation are radical site dependent. The purpose of my first project is to use RDD fragmentation patterns from peptide radical isomers as probes of peptides gas phase structure and conformation flexibility. Radicals are site-specifically generated by photodissociation of carbon-iodine bonds at ortho-, meta-, or para- position of a benzoyl ring labeled at peptide amine group. Radicals at these sites have almost identical bond dissociation

energies and thus the only difference comes from the steric effect. We utilized the steric effect and isotope deuterium labeling to study peptide gas phase structure and its influence on intramolecular radical migration.

Evaluating protein structure in the gas phase is useful for understanding the intrinsic forces which influence protein folding and for determining the feasibility of probing condensed phase structure with gas phase interrogation. KIX is a three-helix bundle protein that has been reported previously to preserve the condensed phase structure in the gas phase. In another project, structure dependent RDD is used to examine the gas phase structure of KIX by establishing residue specific distance constraints which can be used to assess candidate structures obtained from molecular dynamics simulations. The data obtained by RDD is consistent with KIX structures that largely retain condensed phase structure as determined previously by NMR.

A new method is developed to probe peptide structure in vacuo utilizing di-radical recombination reaction. Commonly, the pairing of electrons which occurs when two radicals interact is a *radical* exothermic process without an activation barrier. In the case of a separated peptide ion containing two radicals in the gas phase, such radical coupling reaction is an intramolecular cyclization process and generates a cyclic peptide. Therefore, examining the sites where the di-radical recombination occurs can provide local contact information. Herein, two radical precursors are site specifically introduced to polyproline at the N and C terminal residue, respectively. Internal fragments from cyclized polyproline peptides and ion-molecule reaction data indicate that polyprolines

no longer adopts a helical structure as in the solution which would prevent diradical interaction.

Intermolecular homolytic aromatic substitution (HAS) reaction between benzoate phenyl radical and aromatic side chains in large peptide is observed and investigated. Compared to those radical precursors we previously used, 2-iodo benzoic acid has a much higher propensity to add to the aromatic rings in peptides. HAS is in competitive with radical migration reaction and the product branching ratio depends on specific complex structure. The reaction mechanisms are verified by labeling at various key positions for tryptophan and tyrosine. Novel side chain losses (C_β-C_γ bond cleavage) from aromatic residues (-116W, -93Y, -77F) are rationalized by HAS. Phenylalanine is a chemically inert residue. Such unique side chain loss (i.e., -77F) allows identification of phenylalanine residue in peptides. Study of phenyl radical damage to oligopeptides in the gas phase by radical substitution reaction is achieved for the first time.

We have developed new methods to dissociate oligosaccharides based on RDD. Radical saccharides can be generated by either intermolecular radical migrations or covalent labeling with radical precursors. Compared to CID of even electron saccharides, RDD provides rich fragmentations including cross-ring cleavages. Positional isomers of oligosaccharides (e.g., lacto-N-fucopentaose isomers and lacto-N-difucohexaose isomers) are able to be distinguished by RDD owing to observed signature fragments.

TABLE OF CONTENTS

LIST OF FIGURES

LIST OF TABLES

LIST OF SCHEMES

Chapter 1

General Overview

1.1 Protein sequence and structure

Proteins are a class of large biological molecules that were discovered in the eighteenth century. The word “protein” comes from the greek word “proteios”, meaning “primary”. Indeed, proteins are the most abundant polymers in the body. Proteins are the molecules that carry out various functions encoded in genes. Proteins are the major structural component of cells and body organs including muscle, hair and skin. Some proteins such as enzymes, can bind to other molecules and catalyze chemical reactions involved in metabolism. Proteins also play an important role in cell signaling and other cellular functions.

Amino acids are the building blocks of proteins. They have a general formula of $H_2NCHRCOOH$, where R is one of twenty side chains. Based on structure and chemical characteristics, side chains can be categorized into different groups. All these twenty amino acid residues have one letter and three-letter codes. The diversity of organic

groups in amino acid side chains gives proteins a variety of functions such as conjugation, binding, folding, charging, etc.

The function of proteins is determined by structure. There are distinct levels of depth to describe protein structure. The primary structure of a protein refers to the sequence of amino acids. Since proteins are translated from mRNA by the ribosome and tRNA, protein sequence can be utilized to identify mRNA that has been transcribed from DNA. Post translational modifications such as disulfide bonds, phosphorylations and glycosylations can increase the complexity of primary structure. Secondary structure is mainly defined by the hydrogen bonds in local segments of proteins. Alpha-helix and beta-sheet are two main types of secondary structure. Tertiary structure refers to the three-dimensional structure of covalently bonded polypeptide chain. Under proper conditions, a protein will fold into a stable tertiary structure. In most cases, this is solely determined by its primary sequence.

Current experimental methods to identify protein tertiary structure with high resolution include X-ray crystallography, nuclear magnetic resonance (NMR) spectroscopy and electron microscopy. X-ray crystallography can only determine the structure of protein in a crystal. Therefore, protein crystallization is essential to obtain high resolution atomic-level resolution. For many proteins or protein complexes, this is hard to achieve because of many important factors. For example, a large quantity of protein in solution is required for nucleation and growth of well-ordered crystals. Also, some proteins like membrane

proteins tend to self-assemble and do not form crystals. NMR has a high requirement on the purity of protein in solution as signals from impurity may severely perturb the measurement. NMR has slightly lower resolution compared with X-ray crystallography. NMR measures the quantum mechanical properties of the nuclei of atoms in proteins, which are determined by their local molecular environment. The absorption signals of different nuclei are influenced by adjacent nuclei in space. NMR provides information on how close atoms are and how they could be linked chemically. These distance information in turn are used with complex software to determine the tertiary structure of protein.

1.2 Mass spectrometry in protein and peptide identification

Mass spectrometry (MS) records the mass over charge ratio (m/z) of ionized molecules in the gas phase. In the early development of ionization methods, electron ionization is the main approach for volatile small organic molecules. For analysis of large biomolecules, it is desired to transfer intact molecules into the gas phase without breaking them. Since late 1980s, with the development of soft ionization techniques for large biomolecules such as electrospray ionization (ESI) and matrix assisted laser desorption/ionization (MALDI), mass spectrometry has been widely used in analysis of biomolecules. [1-2]

1.2.1 Peptide identification by mass spectrometry

MS is particularly robust in peptide sequencing. Tandem mass spectrometry dissociates peptides into pieces of fragments in the gas phase and then measure the m/z for each fragment. Based on tandem MS data, peptide is identified by de novo sequencing, database search or a combination of the two.

Currently, collision induced dissociation (CID) is the most widely used method to dissociate peptides.[3-5] The precursor ions are accelerated by electrical potential to obtain high kinetic energy and then collide with neutral molecules such as helium, nitrogen or argon. The kinetic energy is converted into internal energy and initiates non-covalent or covalent bond cleavage. All charged fragments are then detected and recorded in tandem mass spectrum. Mobile proton initiated dissociations follow the lowest energy pathway when the kinetic energy is accumulated during multiple collisions.

Although CID of protonated peptides has great dissociation efficiency, the fragmentation pathways have not been fully understood. There are still some peptide fragments that could not be explained by current knowledge of fragmentation mechanisms. In addition to charge directed pathways such as mobile proton, there are many other fragmentation channels (charge remote pathways) that do not involve charge at all. Small molecule losses such as water and ammonia are typical product of charge remote fragmentation pathways. They often accompany charge directed pathways so that backbone fragments with additional small molecule loss may have even higher intensity

than original backbone fragment peaks. Sequence scrambling of some fragments (e.g., b ions) [6] are also commonly observed. As a result, some fragment peaks may be composed of different isomers and thus not accurately identified. A deeper understanding of the fragmentation pathways, especially the kinetics of different pathways, should greatly increase the accuracy of de novo sequencing by improving the accuracy of selected parameters in algorithms. [7-8]

1.2.2 Protein characterization by mass spectrometry

Fast protein characterization by mass spectrometry is important. There are two aspects in terms of protein characterization. Normally, protein characterization is based on sequence identification. The proteome represents a complete set of expressed proteins by a genome, cell, or tissue under defined conditions. A map of expressed proteins can reflect the status of cells or organism and are thus valuable for monitoring the function and disease diagnosis. Identified protein sequence can also be used to discover new gene and identify gene mutation because primary protein sequence is transcribed and translated from DNA. In typical shotgun proteomics (bottom up approach) studies, digested peptides from complex protein mixtures are separated using high performance liquid chromatography (HPLC) and identified by tandem MS and database search. A variety of techniques including isobaric labeling have also been developed for quantitative proteomics.

Protein characterization may also refer to investigation of tertiary structure. The structural aspects of individual protein or protein complex can also be studied by mass spectrometry-based approaches.[9-12] One MS approach is to monitor conformation-dependent charge state distribution.[13] In ESI mass spectra of protonated proteins, the distribution of protein peaks at different charge states can sometimes reflect protein structure in the gas phase. Generally, a compact globular protein tends to take a small number of protons whereas unfolded protein may have a high charge state. Analysis of a single charge state distribution spectrum is not informative because there are a lot other factors that can influence charge states. For examples, solvent, ion source parameter, salt, etc. However, when two mass spectra that are taken under the same experimental condition are compared, it is possible to get some structural change information. For example, alpha-helical peptide has been shown to be more stable when there is one charge located at the C-terminus of peptide fragment. Therefore, a protein structure that has more alpha-helical fragments may have different probability for protonation compared with a denatured structure. One of the biggest concerns in charge state distribution analysis is whether the gas phase protein structure can reflect its solution state. The importance of this question depends on what information is expected to be obtained. It should be mentioned that, charge state distribution may not be sensitive enough to tell the difference when two proteins in two samples are known to adopt different solution structures.

Another approach is to use structure dependent chemical reactions to evaluate protein structure including hydrogen/deuterium (H/D) exchange, covalent labeling, non-covalent binding, cross-linking and radical-mediated oxidation. The overall H/D exchange pattern is strongly influenced by protein folding and dynamics in solution. H/D exchange detects the strength of hydrogen bonding or labile hydrogen atoms within a protein in solution. If an exchangeable hydrogen atom is involved in a strong hydrogen bonding network, H/D exchange may be slow. Protein backbone amide deuterium exchange is influenced by many reactions. For example, reversible protein folding could break the hydrogen bonding network and accelerate H/D exchange. One of the characteristic properties of H/D exchange is high resolution, which is at amino acid residue level.

Protein cross-linking is also a widely used method to study individual protein structure (intramolecular cross-linking) or protein interaction network (intermolecular cross-linking). Compared with H/D exchange, cross-linking has lower resolution because the cross-linkers can only react with specific amino acid side chains, which is limited by protein sequence. Cross-linking experiments on individual protein with known sequence can potentially provide distance information between two amino acid residues. If tertiary structure of one protein has been determined by NMR or X-ray crystallography, these distance information can be used to evaluate protein structure stability. It is also possible to characterize conformational change by mapping these distance information to protein tertiary structure. If NMR or X-ray crystallography structure is unknown, this approach

would be less robust. Overall, cross-linking strategy is fast and able to probe protein structure without thorough protein purification.

Radical mediated oxidation reactions have a long history. It is similar to covalent labeling but has much higher resolution since most residues can react with radicals in solution. [14] One advantage of radical reagent is that radicals can be generated by chemical reactions or UV photodissociation. For example, hydroxyl radical can be formed via UV photolysis of hydrogen peroxide or by the reduction of hydrogen peroxide with Fe^{2+}. There are three main reactions in protein modification experiments with radicals: side chain modification, backbone cleavage and cross-linking. The modified protein can then be characterized with the aid of mass spectrometry.

1.3 Radical directed dissociation mass spectrometry

Extensive studies of radical reactions with proteins or peptides in solution have been reported for several decades. With the development of soft-ionization technique such as ESI and MALDI, it is possible to transfer large biopolymers into gas phase. Almost all solution techniques for protein structure characterization can be implemented in the gas phase, such as H/D exchange, cross-linking and covalent labeling. Tandem MS is then used to identify the modification sites. In early 1990s, CID has been used to dissociate proteins in Fourier transform ion cyclotron resonance mass spectrometer. However, low sequence coverage limits the application of top-down characterization by CID. This is

mainly caused by the fragmentation mechanisms of multiple collisions induced dissociation. CID of even-electron proteins is a slow activation method, which has a strong tendency to dissociate through the lowest energy pathway. In late 1990s, electron capture dissociation (ECD) has been developed for positively charged proteins and peptides. Electron is captured by isolated ions and then a radical protein cation is generated, which can spontaneously initiate radical fragmentation pathways. For highly charged protein ions, radical can be generated at most residues and thus high sequence coverage is expected. ECD facilitates the renaissance of radical chemistry in tandem MS. [15-16]

In 2000, Ivan Chu et al. generated radical peptides in the gas phase using peptide-metal complex and studied hydrogen deficient radicals initiated peptide dissociation pathways. [17] Since then, numerous methods have been developed to generate hydrogen deficient radicals in the gas phase including oxidative dissociation of peptide-metal complexes, homolytic bond cleavage in modified groups such as nitrate ester, peroxycarbamate, nitroso, tempo, etc. All of these methods use CID to facilitate bond cleavages in radical precursors and then generate hydrogen deficient radicals. Additionally, photodissociation (PD) mass spectrometry offers an advantage of selective activation of specific chromophores to generate radicals. UVPD at 266 nm has been used to selectively cleave carbon–iodine (C–I, see Scheme 1.1), carbon–sulfur bonds that are present in chromophore modified peptides and proteins or native sulfur–sulfur bonds. [18-25] After generation of radical peptides, further dissociation (either spontaneously or aided by

collisional activation) leads to radical directed dissociation (RDD) pathways including backbone fragmentation and side chain loss.

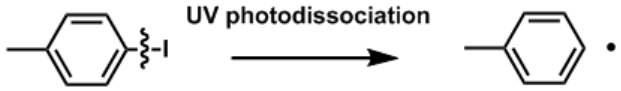

Scheme 1. Ultra violet photodissociation of carbon-iodine bond

There are many radical fragmentation pathways (see Scheme 2 to Scheme 6) in solution: hydrogen atom abstraction (radical migration), β scission dissociation, radical rearrangement, homolytic aromatic substitution (radical addition to aromatic residues), diradical cross-linking, etc. Almost all radical reactions that were discovered in solution can be observed in gas phase RDD of peptides and proteins.

Scheme 2. Radical migration reaction

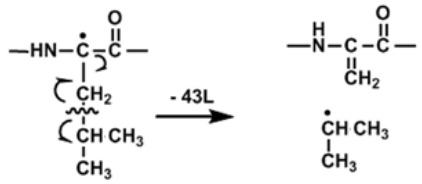

Scheme 3. β scission dissociation reaction at leucine side chain. -43L represents 43 Da loss from leucine

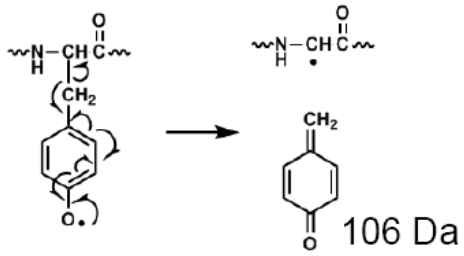

Scheme 4. Radical rearrangement reaction initiated tyrosine side chain loss

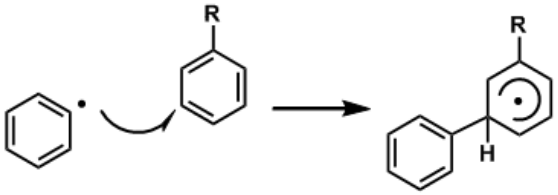

Scheme 5. Homolytic aromatic substitution reaction (radical addition to aromatic ring)

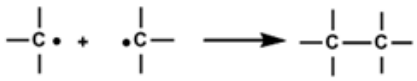

Scheme 6. Diradical cross-linking reaction

Radical migration reaction is essential in RDD of peptides and proteins because it makes radical mobile. C_α hydrogens in amino acid backbone, hydrogen atoms in aliphatic side chains, C_β hydrogens in aromatic residues, hydrogens in carboxyl group and phenol group are all good destination sites for radical migration. The enthalpy of radical migration reaction is determined by the relevant carbon-hydrogen (C-H) bond dissociation energies (BDEs) of both the radical donor and acceptor. Large BDEs indicate highly reactive radicals can easily migrate to other sites with lower BDEs in the absence of kinetic constraints. Normally, the relative abundance of backbone fragments and side chain losses observed for a series of peptides correlated well with the relevant

BDEs; radical directed dissociation was favored for those sites with low C-H BDEs. [19] However, radical migration within *any individual* peptide will be kinetically influenced by the relevant activation energies, which are a function of three-dimensional structure and sequence dependent steric constraints. For example, in very small, rigidly constrained peptides, high barriers to radical migration prevent radical isomerization and lead to different fragmentation patterns. The activation energy for intramolecular reactions strongly depends on transition state configuration, which is determined by distance and also alignment orientation. In addition radical migration reaction, β scission reaction is the dominant pathway for both backbone and side chain dissociation. Radical rearrangement reaction and homolytic aromatic substitution reactions are particularly favored at aromatic side chains.

One significant difference between low energy CID of even-electron species and RDD is extensive side chain fragmentation pathways in RDD. Most amino acid side chains are chemically inert but these residues become reactive upon reaction with carbon centered radicals. As a result, more fragmentation pathways are observed and thus can potentially provide more structural information. For example, leucine and isoleucine can be distinguished based on side chain loss. But for backbone dissociation, RDD is less robust than CID. This is caused by the mechanism of RDD initiated backbone fragmentation, where the radical must migrate to side chain C_β atom before β scission initiated backbone cleavage. Therefore, backbone fragmentation cannot be observed in some residues. For example, glycine residue has no side chain; proline residue is cyclic. In addition, radical

can hardly migrate to side chain of some residues such as alanine. In many cases, side chain fragmentations at favorable residues are abundant compared with backbone cleavage pathways. [19]

Detection of radicals in the gas phase can be performed with ion-molecule reaction. Neutral molecules such as dimethyl disulfide can react with radical ions and thus can be used to detect the existence of radicals. Dioxygen molecules inside mass spectrometers, although with low pressure, can also react with highly reactive radicals such as phenyl radicals (see Scheme 7). For example, after isolation of radical ions for several seconds, a decent yield of dioxygen addition product can be observed [22]. The yield of dioxygen addition product is determined by both radical reactivity and reaction time. Therefore, it is possible to characterize radical location based on the yield of ion-molecule reaction, which is determined by reactivity.

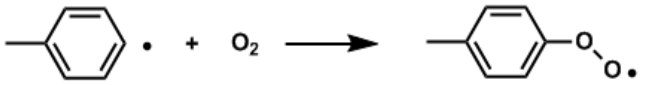

Scheme 7. Radical reaction with dioxygen molecule

Although H/D exchange reactions have been implemented inside mass spectrometers to monitor protein structure in the gas phase, residue contact information cannot be obtained. Ion mobility experiments measure the average cross-section of proteins ions without residue contact information either. Ion mobility data strongly rely on accurate molecular dynamics modeling to elucidate protein tertiary structure. ECD has been used to probe intramolecular non-covalent interactions. However, the exact location of residue

contact is hard to measure. Method based on fluorescence resonance energy transfer (FRET) has been used to probe peptide structure in the gas phase. [26]

Compared with these methods, RDD is another method that is able to examine protein structure in the gas phase. Based on radical migration and dissociation, distance constraints between radical donors and radical acceptors in a protein can be determined and used to evaluate candidate structures (see Scheme 8). However, this method requires not only a radical donor with strong reactivity but also a good radical acceptor in close proximity. This strategy is analogous to chemical cross-linking. However, radical migration reaction functions as a zero-length cross-linker since two groups are connected by a single chemical bond. Therefore, RDD has significant advantages that can monitor intramolecular interactions and is useful to probe protein tertiary structure in the gas phase.

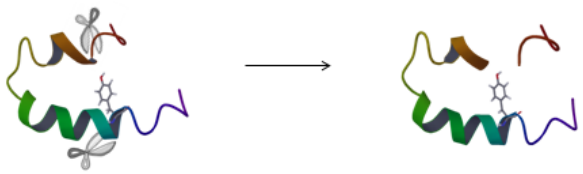

Scheme 8. Radical directed protein dissociation at residues that are close in space

In addition to intramolecular radical migration reaction, diradical cross-linking reaction can also be used to probe the distance between two radicals. Characterization of diradical cross-linking product can be performed by ion-molecule reaction or tandem MS such as CID. Accurate determination of radical initiation and termination sites are important in both

diradical cross-linking and radical migration reactions. Radical termination sites can be inferred from characterization of fragments.

Among all existing methods to generate radical peptides, photodissociation (PD) is very robust to generate radicals at specific positions without activating the whole molecules, which makes PD combined with RDD a particularly effective method in probing protein structure in the gas phase.

1.4 Scope of the dissertation

In chapter 2, RDD is used in combination with iodination chemistry to probe the tertiary structure of a small protein. KIX is a three-helix bundle protein that has been reported previously to preserve the condensed phase structure in the gas phase. Herein, structure dependent radical directed dissociation (RDD) is used to examine the gas phase structure of KIX by establishing residue specific distance constraints which can be used to assess candidate structures obtained from molecular dynamics simulations. The data obtained by RDD is consistent with KIX structures that largely retain condensed phase structure as determined previously by NMR. There are several factors that favor retention of the KIX native fold in the gas phase. The structure is largely comprised of alpha helices, which are known to be stable in the gas phase. Thus under appropriate conditions, solution phase structure can be largely retained and meaningfully examined in the gas phase.

In chapter 3, diradical cross-linking method is developed to probe the gas phase structure of polyproline peptide modified with radical precursor in the two ends. Polyproline is a fascinating polymer with interesting structural properties that have been studied in both solution and the gas phase. Herein, a method capable of measuring structural dynamics over long timescales is developed and applied to examination of polyproline in the gas phase. This method is based on measuring the probability of two radicals recombining to form a new covalent bond within a single molecule, which provides distance constraint information. To examine polyproline peptides of various lengths, radical precursors were selectively placed at the termini. Photoactivation with 266nm light can then be used to create a diradical species, and recombination of the two radicals can be used to evaluate end-to-end distances and structural flexibility. The results reveal that interaction of the polyproline termini is more favorable for shorter chain lengths and lower charge states. As charge states increase, Coulombic repulsion favors formation of more extended structures where the termini no longer come in close contact. With increasing chain length, the greater conformational space also appears to decrease the likelihood of the termini being able to recombine. The amount of radical recombination observed for short polyproline peptides in low charge states is not consistent with what would be expected for helical conformations.

In chapter 4, the influence of steric hindrance on radical migration is investigated. One of the keys for understanding radical directed dissociation in peptides is a detailed knowledge of the factors which mediate radical migration. Peptide radicals can be created

by a variety of means; however, in most circumstances the originally created radicals must migrate to alternate locations in order to facilitate fragmentation such as backbone cleavage or side chain loss. The kinetics of radical migration are examined herein by comparing results from *ortho*-, *meta*-, and *para*- benzoyl radical positional isomers for several peptides. Isomers of a constrained cyclic peptide generated by several orthogonal radical initiators are also probed as a function of charge state. Cumulatively, the results suggest that small changes in radical position can significantly impact radical migration, and overall structural flexibility of the peptide is also an important controlling factor. A particularly interesting pathway for the peptide RGYALG that is sensitive to *ortho* versus *meta* or *para* substitution was fully mapped out by a suite of deuterium labeled peptides. This data was then used to optimize parameters in molecular dynamics based simulations, which were subsequently used to obtain further insight into the structural underpinnings which most strongly influence the kinetics of radical migration.

In chapter 5, radical addition reactions initialized C_β–C_γ bond cleavage and C_α–C_β cleavage at aromatic residues are studied. Novel radical addition reactions that direct unexpected side chain dissociations at tryptophan and tyrosine residues are reported. Various mechanisms that can account for the observed dissociation channels are investigated by experiment and theory. The propensity for radical addition at a particular site is found to be primarily under kinetic control, which is largely dictated by molecular structure. In certain peptides intramolecular radical addition reactions are favored, which leads to the observation of numerous unexpected fragments. In one pathway, radical

addition leads to migration of an aromatic side chain to another residue. Alternatively, radical addition followed by hydrogen atom loss leads to cyclization of the peptide and increased observation of internal sequence fragments. Radical addition reactions should be considered when assigning fragmentation spectra of hydrogen deficient peptides.

In chapter 6, RDD is performed on oligosaccharides. Oligosaccharides represent a very important class of target molecules that require structural characterization in terms of both monosaccharide identity and overall connectivity. Two methods that generate radical oligosaccharides for subsequent activation are described. In one approach, a radical precursor is covalently attached to the oligosaccharide by reductive amination. Radicals can then be generated by homolytic bond cleavage of specific carbon-iodine bonds in protonated systems by either collisional activation or photodissociation. Subsequent activation of the radical species generates information rich spectra including numerous cross-ring fragments. Alternatively, noncovalent complexation with iodophthalic acid can be used to generate radical disaccharides by photoactivation. Subsequent radical transfer, loss of the radical precursor adduct, and collisional activation of the radical disaccharide results in characteristic glycosidic bond cleavage and cross-ring cleavage products that can easily distinguish isomeric species. Radical chemistry is demonstrated to have several advantages for the characterization of oligosaccharides relative to other approaches.

References

[1] Fenn, J.B., Mann, M., Meng, C.K., Wong, S.F., Whitehouse, C.M.: Electrospray Ionization for Mass-Spectrometry of Large Biomolecules. *Science* **246**, 64-71 (1989)

[2] Karas, M., Bachmann, D., Bahr, U., Hillenkamp, F.: Matrix-Assisted Ultraviolet-Laser Desorption of Nonvolatile Compounds. *Int. J. Mass Spectrom. Ion Processes* **78**, 53-68 (1987)

[3] Louris, J.N., Cooks, R.G., Syka, J.E.P., Kelley, P.E., Stafford, G.C., Todd, J.F.J.: Instrumentation, Applications, and Energy Deposition in Quadrupole Ion-Trap Tandem Mass-Spectrometry. *Anal. Chem.* **59**, 1677-1685 (1987)[4] Papayannopoulos, I.A.: The Interpretation of Collision-Induced Dissociation Tandem Mass-Spectra of Peptides. *Mass Spectrom. Rev.* **14**, 49-73 (1995)

[5] Paizs, B., Suhai, S.: Fragmentation pathways of protonated peptides. *Mass Spectrom. Rev.* **24**, 508-548 (2005)

[6] Roepstorff, P., Fohlman, J.: Proposal for a Common Nomenclature for Sequence Ions in Mass-Spectra of Peptides. *Biomed. Mass Spectrom.* **11**, 601-601 (1984)

[7] Zhang, Z.Q.: Prediction of low-energy collision-induced dissociation spectra of peptides. *Anal. Chem.* **76**, 3908-3922 (2004)

[8] Zhang, Z.Q.: Prediction of low-energy collision-induced dissociation spectra of peptides with three or more charges. *Anal. Chem.* **77**, 6364-6373 (2005)

[9] Loo, J.A.: Studying noncovalent protein complexes by electrospray ionization mass spectrometry. *Mass Spectrom. Rev.* **16**, 1-23 (1997)

[10] Kaltashov, I.A., Eyles, S.J.: Studies of biomolecular conformations and conformational dynamics by mass spectrometry. *Mass Spectrom. Rev.* **21**, 37-71 (2002)

[11] Maleknia, S.D., Downard, K.: Radical approaches to probe protein structure, folding, and interactions by mass spectrometry. *Mass Spectrom. Rev.* **20**, 388-401 (2001)

[12] Sinz, A.: Chemical cross-linking and mass spectrometry to map three-dimensional protein structures and protein-protein interactions. *Mass Spectrom. Rev.* **25**, 663-682 (2006)

[13] Chowdhury, S.K., Katta, V., Chait, B.T.: Probing Conformational-Changes in Proteins by Mass-Spectrometry. *J. Am. Chem. Soc.* **112**, 9012-9013 (1990)

[14] Konermann, L., Stocks, B.B., Pan, Y., Tong, X.: Mass Spectrometry Combined with Oxidative Labeling for Exploring Protein Structure and Folding. *Mass Spectrom. Rev.* **29**, 651-667 (2010)

[15] Zubarev, R.A.: Reactions of polypeptide ions with electrons in the gas phase. *Mass Spectrom. Rev.* **22**, 57-77 (2003)

[16] Cooper, H.J., Hakansson, K., Marshall, A.G.: The role of electron capture dissociation in biomolecular analysis. *Mass Spectrom. Rev.* **24**, 201-222 (2005)

[17] Chu, I.K., Rodriquez, C.F., Lau, T.C., Hopkinson, A.C., Siu, K.W.M.: Molecular radical cations of oligopeptides. *J. Phys. Chem. B* **104**, 3393-3397 (2000)

[18] Turecek, F., Julian, R.R.: Peptide Radicals and Cation Radicals in the Gas Phase. *Chem. Rev.* **113**, 6691-6733 (2013)

[19] Sun, Q.Y., Nelson, H., Ly, T., Stoltz, B.M., Julian, R.R.: Side Chain Chemistry Mediates Backbone Fragmentation in Hydrogen Deficient Peptide Radicals. *J. Proteome Res.* **8**, 958-966 (2009)

[20] Ly, T., Julian, R.R.: Residue-specific radical-directed dissociation of whole proteins in the gas phase. *J. Am. Chem. Soc.* **130**, 351-358 (2008)

[21] Ly, T., Julian, R.R.: Tracking Radical Migration in Large Hydrogen Deficient Peptides with Covalent Labels: Facile Movement does not Equal Indiscriminate Fragmentation. *J. Am. Soc. Mass Spectrom.* **20**, 1148-1158 (2009)

[22] Moore, B.N., Blanksby, S.J., Julian, R.R.: Ion-molecule reactions reveal facile radical migration in peptides. *Chem. Commun.* 5015-5017 (2009)

[23] Diedrich, J.K., Julian, R.R.: Site-Selective Fragmentation of Peptides and Proteins at Quinone-Modified Cysteine Residues Investigated by ESI-MS. *Anal. Chem.* **82**, 4006-4014 (2010)

[24] Ly, T., Julian, R.R.: Elucidating the Tertiary Structure of Protein Ions in Vacuo with Site Specific Photoinitiated Radical Reactions. *J. Am. Chem. Soc.* **132**, 8602-8609 (2010)

[25] Turecek, F., Julian, R.R.: Peptide Radicals and Cation Radicals in the Gas Phase. *Chem. Rev.* **113**, 6691-6733 (2013)

[26] Talbot, F.O., Rullo, A., Yao, H., Jockusch, R.A.: Fluorescence Resonance Energy Transfer in Gaseous, Mass-Selected Polyproline Peptides. *J. Am. Chem. Soc.* **132**, 16156-16164 (2010)

Chapter 2

Investigating the Gas Phase Structure of KIX with Radical Directed Dissociation and Molecular Dynamics: Retention of the Native Structure

2.1 Introduction

Protein structure is a subject of intense interest in a variety of different contexts.[1] From a chemical perspective, determination of protein structure is one of the primary prerequisites for understanding (and ultimately controlling) functionality. Ideally protein structure should be examined within the framework of conditions that are present in cells where proteins carry out their various duties.[2] In reality, all experimental methods for examining protein structure fall short in this regard, although arguably some are closer than others. The gas phase is not typically an environment which is considered to be similar to a cell, yet methods for examining protein structure in the gas phase continue to increase in popularity, including those utilizing mass spectrometry, ion mobility, and spectroscopy. [3-4] Reasons for this are clear, gas phase experiments can be carried out rapidly with minimal sample consumption;[5] therefore, proteins which are present in very small abundance can be targeted. Perhaps even more importantly, several gas phase

techniques can easily accommodate increasing protein size, allowing for the interrogation of large systems.[6] However, despite the increasing popularity, it is more difficult to ascertain whether the information obtained in the gas phase is relevant to the condensed phase, and if so, under what conditions.

Ion mobility is the most frequently used method for examining the structures of large molecules in the gas phase.[7-12] Although there are now several varieties of experimental setups, all utilize electric fields and a buffer gas to separate ions according to their average collision cross section or "size". This experimentally determined parameter can be used to evaluate candidate structures, typically derived from molecular dynamics simulations. The strengths of the ion mobility approach include direct measurement of a structural parameter and the ability to easily accommodate increasing molecular size. It is equally easy to measure the collision cross section of a small peptide or a large protein. The primary disadvantage of ion mobility is that only a single parameter (collision cross section) can be obtained, regardless of the experimental setup. Constraining all of protein structural space with a single parameter can be quite challenging.

Electron capture dissociation (ECD) has also been used to investigate protein structure.[13-15] In these experiments, it is assumed that dissociation into c/z ions occurs throughout the protein backbone. Failure to observe fragmentation is interpreted to signify that noncovalent interactions are holding the two fragments together. The noncovalent interactions could originate from secondary or tertiary structural features. With ECD, it is possible to map out which portions of a protein have the least contact

with the remaining structure as a function of the charge state. The relative stability of structural features can in theory be mapped this way because all proteins adopt more elongated structures in the gas phase as the charge state increases. Unfortunately, for compact structures which are frequently most likely to be similar to those found in solution, little information is obtained by ECD since the primary observation is simply lack of fragmentation. Similarly, this method cannot distinguish between close contacts which are strongly interacting with one another and contacts which are merely in close proximity, but not strongly interacting.

Radical directed dissociation (RDD) is a new method which can examine protein structure.[16] In these experiments, radical precursors are placed site specifically at particular residues within a protein. Photodissociation is then used to generate a radical by homolytic cleavage of a photolabile carbon-iodine bond. The initially formed radicals are reactive, but not well placed to induce dissociation.[17] Thus migration of the radical species to locations where dissociation is favorable occurs rapidly.[18] Mild collisional activation can then be used to facilitate fragmentation, and the locations of the radical directed dissociation sites can be easily determined by evaluation of the fragments which are produced. In this fashion, a series of distance constraints between radical initiation and termination points can be determined and used to evaluate candidate structures. Ideally, the distance constraints can be used to actually drive molecular dynamics simulations towards relevant conformational space.[16] Multiple structure parameters are obtained in a typical experiment, and compact structures can be investigated along with extended conformations. The primary drawback for this methodology is that the protein

must be modified, and that structure will only be probed in the vicinity of the site of modification. Iodination of the most reactive tyrosine residue is simple [19] and the preferred starting point for RDD structure probing. Of course, modification at additional sites is possible for most proteins, but only at the cost of significant efforts to install other modifications site specifically.[20]

KIX is a three-helix domain within the larger CREB binding protein which is involved in the regulation of transcriptional processes.[21] The KIX domain itself is a recognition motif, which can bind simultaneously to two other proteins to form a ternary complex. The structure of KIX has been investigated by both NMR in solution [22] and in the gas phase by ECD. [23] Evaluation of the ECD data suggested that the solution phase structure of KIX is largely retained in the gas phase and stable for at least 4 seconds due to favorable electrostatic interactions. This conclusion was primarily based on evaluation of data related to secondary structure from high charge states (+10 or larger), which likely represent more extended conformations of the protein. For reasons explained above, examination of the structure of the lower charge states was not possible. Herein, RDD is used to examine the gas phase structure of KIX in the +6 and +7 charge states. Comparison with the solution phase structure reveals that the RDD data is consistent with the solution phase structure being largely retained in the gas phase. Exploration of potential alternate structures based on the RDD data by molecular dynamics failed to yield any substantially lower energy structures. KIX is a three-helix bundle protein, with the helices connected by fairly flexible linkers. Desolvation of KIX is accompanied by only slight shifting of the helical regions to accommodate charge

solvation. KIX contains a high density of basic and acidic residues, which is important for several reasons. It enables the formation of favorable electrostatic interactions, as noted previously

2.2 Experiment Section

Materials. KIX domain from CREB binding protein was expressed in Escherichia coli cells using a plasmid that includes residues 586-672, with residue 586 corresponding to residue 5 here. KIX was provided as a generous gift by Dr. Kathrin Breuker and Dr. Martin Tollinger. α-Cyano-4-hydroxycinnamic acid (CHCA) and trypsin (porcine pancreas) were purchased from Sigma-Aldrich (St. Louis, MO). Lysyl endopeptidase (Lys C) and endoproteinase Asp N were purchased from Wako Chemicals USA (Richmond, VA). Methanol, glacial acetic acid, sodium iodide, chloramine-T, sodium metabisulfite were purchased from Fisher Scientific (Fairlawn, NJ).

Iodination of Protein. Ortho position of tyrosine side chains in KIX protein were iodinated by sodium iodide and chloramine-T at room temperature, after a short reaction time of about 10 minutes, excess sodium metabisulfite was added to quench the reaction. Diluted solution (10 μM protein) and stoichiometric quantities of reagents (1:2:1:2 molar ratio of KIX/sodium iodide/chloramine-T/sodium metabisulfite) were used to limit the iodination extent and produce mainly mono-iodinated KIX. Iodinated KIX was then purified by a desalting trap (Michrom Bioresources, Inc., Auburn, CA) to remove excess iodination reagents.

Enzymatic Digestion. Iodinated KIX was digested by trypsin, endopeptidase Asp N or Lys C separately in 20 μL 50 mM sodium bicarbonate buffer at 37ºC overnight. Enzyme to substrate ratio 1:10 (w/w) was used. The protein cleavage was stopped by adding 0.1 μL trifluoroacetic acid to a final concentration of 0.5% (v/v). Digested mixtures were desalted with C_{18} ZipTip (Millipore, Billerica, MA) and then directly eluted onto a MALDI sample plate. CHCA was used as matrix for on plate mixing. MALDI-TOF analysis was carried out with Voyager-DE STR mass spectrometer (Applied Biosystems, Framingham, MA), equipped with a 337 nm nitrogen laser. The spectra were averaged and recorded in the positive reflector mode at an accelerated voltage of 20 kV in the range from 500 to 3500 Da.

Photodissociation. Iodinated KIX (2 μM) in 80:20 H_2O:CH_3OH with 0.1% acetic acid was electrosprayed into an LTQ linear quadrupole ion trap mass spectrometer (Thermo Fisher Scientific, San Jose, CA). The back plate of the instrument was modified with a quartz window to transmit 266 nm UV photons into the linear ion trap, from the 4^{th} harmonic generation of a Nd:YAG laser (Continuum, Santa Clara, CA). Laser pulses were synchronized to the isolation step via a digital delay generator. Charge state of fragments after collision activated dissociation (CAD) were assigned using the zoom or ultrazoom scan modes, which can typically resolve isotope peaks of up to +8 charge state. Protein fragments were assigned manually with the aid of Fragmentor 1.2.2 (http://www.faculty.ucr.edu/~ryanj/fragmentor.html) and UCSF ProteinProspector program v.5.7.3 (http://prospector.ucsf.edu/prospector/mshome.htm). Assignments do not

distinguish between even electron fragments vs. radical fragments with only one Da difference.

2.3 Results and Discussion

2.3.1 Localization of iodinated tyrosine

To obtain information about protein structure through radical migration and dissociation, the initial radical site should ideally be known. In the present work, radicals are generated by photodissociation of carbon-iodine bonds present in iodinated tyrosine residues. In order to favor single site modification, iodination was carried out under mild conditions which produce primarily mono-iodinated KIX and avoid histidine modification. KIX contains five tyrosine residues with Tyr50 and Tyr59 in the α2 helical region, and Tyr68, Tyr69 and Tyr77 in α3. Based on aqueous NMR structures, Tyr68 is buried inside the three-helix bundle and Tyr59 is partially buried, while the other three tyrosines are well exposed at the surface. The surface accessibilities to iodine as calculated from the NMR structure for each tyrosine residue are shown in Table 2.1. Previous work has shown that solvent accessibility alone cannot determine probability of iodination, presumably due to the influence of other factors within the local chemical environment surrounding the tyrosine side chain such as intramolecular hydrogen bonds or salt bridges.

Table 2.1. Surface accessibility ($Å^2$) of tyrosine side chain defined at 1.4 Å van der Waals sphere.

	Tyr50	Tyr59	Tyr68	Tyr69	Tyr77
Two ortho carbon atoms	10.8	3.7	0.0	12.7	14.6
Phenol ring	85.3	29.8	0.0	78.5	134

Identifying the site of iodination for mono-iodinated KIX is not achievable by simple CAD of the entire protein due to incomplete sequence coverage and numerous uninformative fragmentation pathways. Instead, enzymatic digestion of the mixture of unmodified, mono- and multiple-iodinated KIX was carried out. MALDI-MS was used to analyze the proteolytic digest fragments. The results are summarized in Figure 2.1. The bar height represents the iodination extent for each tyrosine, which is determined by the ratio of the relative intensity of the mono-iodinated to non-iodinated peptide. If the corresponding peptide fragment was not observed, then the bar is absent in Figure 2.1. Those bars with a value of zero indicate a measured quantity. Three enzymes, trypsin, Lys C and Asp N were each used in an effort to increase the sequence coverage and to obtain overlapping results. Although the final results are semi-quantitative, Tyr50 is obviously the primary iodination site. Tyr59, which is partially buried inside the three-helix bundle, is not iodinated at all. Tyr68 and Tyr69 cannot be distinguished as both are present in all digested peptides, therefore they are grouped together as one potential iodination site. Tyr77 was only observed in the Asp N digestion, but the relevant peptide in that case also includes Tyr68 and Tyr69, confounding independent analysis. Considering that Tyr68 and Tyr69 are partially iodinated as shown by the results obtained with Lys C, it is likely that Tyr77 may only be iodinated to a small extent. It is important to point out that the digestion results include some information about secondary sites of iodination as the doubly iodinated species could not be separated out prior to analysis. In summary, Tyr50 in KIX is the likely primary iodination site, Tyr68-69 and Tyr77 may also be iodinated to a smaller extent. These results are in agreement with those obtained

by photodissociation, which has been demonstrated previously to provide iodination site identification in very high charge states.

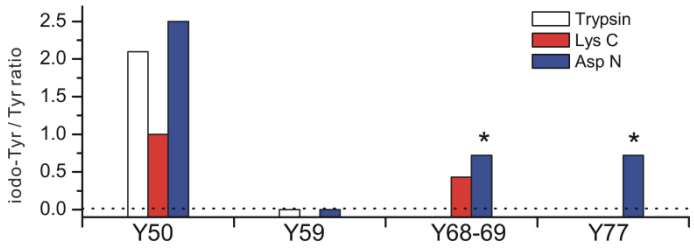

Figure 2.1. Iodination extent at each tyrosine in KIX quantified by MALDI analysis of enzyme digested iodinated KIX. * indicates a peptide containing Tyr68, Tyr69 and Tyr77.

2.3.2 Radical directed dissociation

The iodinated KIX mixture was electrosprayed from a solution of 80:20 H_2O:CH_3OH with 0.1% acetic acid. The mono-iodinated KIX was then isolated in the ion trap and subjected to photodissociation with a single pulse of 266 nm photons, which led to homolytic cleavage of the carbon-iodine bond as shown in Figure 2.2a for the +10 charge state. After loss of I•, a radical is generated at tyrosine side chain. The CAD spectrum of this re-isolated +10 protein radical is shown in Figure 2.2b. Radical initiated a, c, w, and z fragment ions are produced as well as some abundant proton initiated b/y ions. These b/y ions are also produced by CAD of the even-electron +10 KIX as shown in Figure 2.2c, in addition to several other b/y ions. RDD of peptides frequently occurs at a lower dissociation threshold than proton initiated dissociation, but some of the proton initiated pathways are competitive in CAD of radical KIX protein. The most abundant fragmentation channel in CAD of radical +10 KIX is non-radical initiated cleavage of Asp17/Leu18 to produce b_{17}/y_{74} ions, presumably due to the aspartic acid effect. Other competitive fragmentations such as those yielding the b_{31}/y_{60} and b_{35}/y_{56} ion pairs occur at proline. Most of the remaining proton initiated dissociation pathways observed in Figure 2.2c are substantially suppressed in Figure 2.2b. Similar results and conclusions can be drawn for most other charge states of KIX.

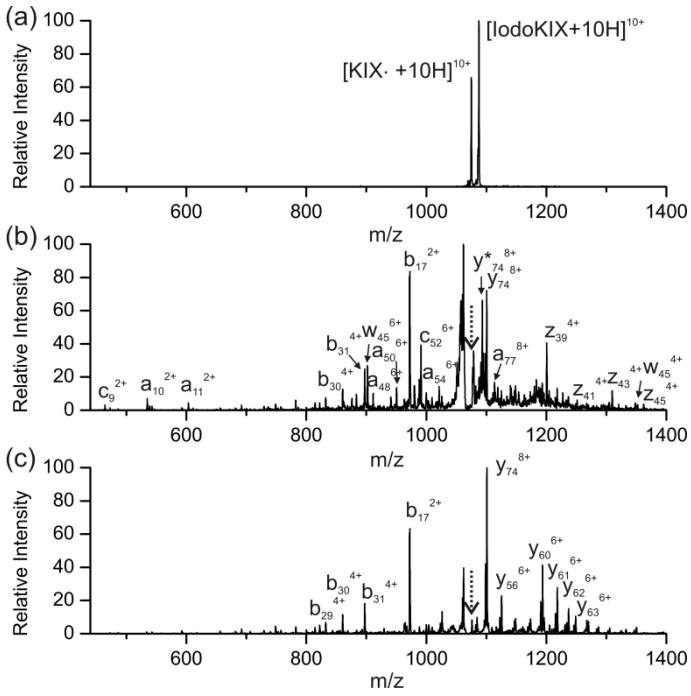

Figure 2.2. (a) Photodissociation of the +10 charge state of iodo-KIX generates odd electron KIX radical. (b) CAD of the KIX radical from (a) generates radical directed fragment ions (backbone a, c/z, w series and side chain loss peaks) and also some proton directed b/y fragments. (c) CAD of the even electron +10 KIX generates mainly b/y fragments. * represents side chain loss from the corresponding fragment.

The radical can migrate from the initial tyrosine side chain to other specific residues, leading to subsequent dissociation (e.g. β-scission) at those residues. RDD of proteins can results in both backbone dissociation (e.g., a50, c52, w45, z39 in Figure 2.2b) and various side chain losses. The broad peak with a trailing edge at lower m/z in Figure 2.2b results from overlapping (and sometimes multiple) side chain losses from the radical precursor. These side chain loss peaks are unresolvable with an ion trap and cannot be included in our analysis. In Figure 2.3, the relative intensities of radical directed backbone fragments that appear only in CAD of KIX radical species (i.e. they are not present in CAD of the corresponding even electron cation), are plotted as a function of sequence from charge states +6 through +12 and +16. In +8 and higher charge states, RDD fragments are primarily localized by sequence in close proximity to Tyr50, Tyr68-69 and Tyr77, which all correspond to potential radical initiating residues. At even higher charge states, fragmentation around Tyr50 becomes dominant, in agreement with the previous MALDI-MS data that suggested Tyr50 is the primary iodination site. However, the gradual disappearance of some RDD peaks in higher charge states is due to several factors: (i) less favored through-space radical migration in more extended structure, (ii) decreased dissociation threshold for mobile proton initiated competitive fragmentation channels, (iii) limited resolution for high charge state fragment ions in the LTQ linear ion trap. In CAD of KIX +16 radical protein, only RDD fragments around Tyr50 have sufficient signal intensities and resolution to allow assignment of charge state. This data does not rule out the possibility of small amounts of iodination at Tyr68-69 and Tyr77. Therefore,

analysis of the compact structures will need to consider all three potential radical initiation points.

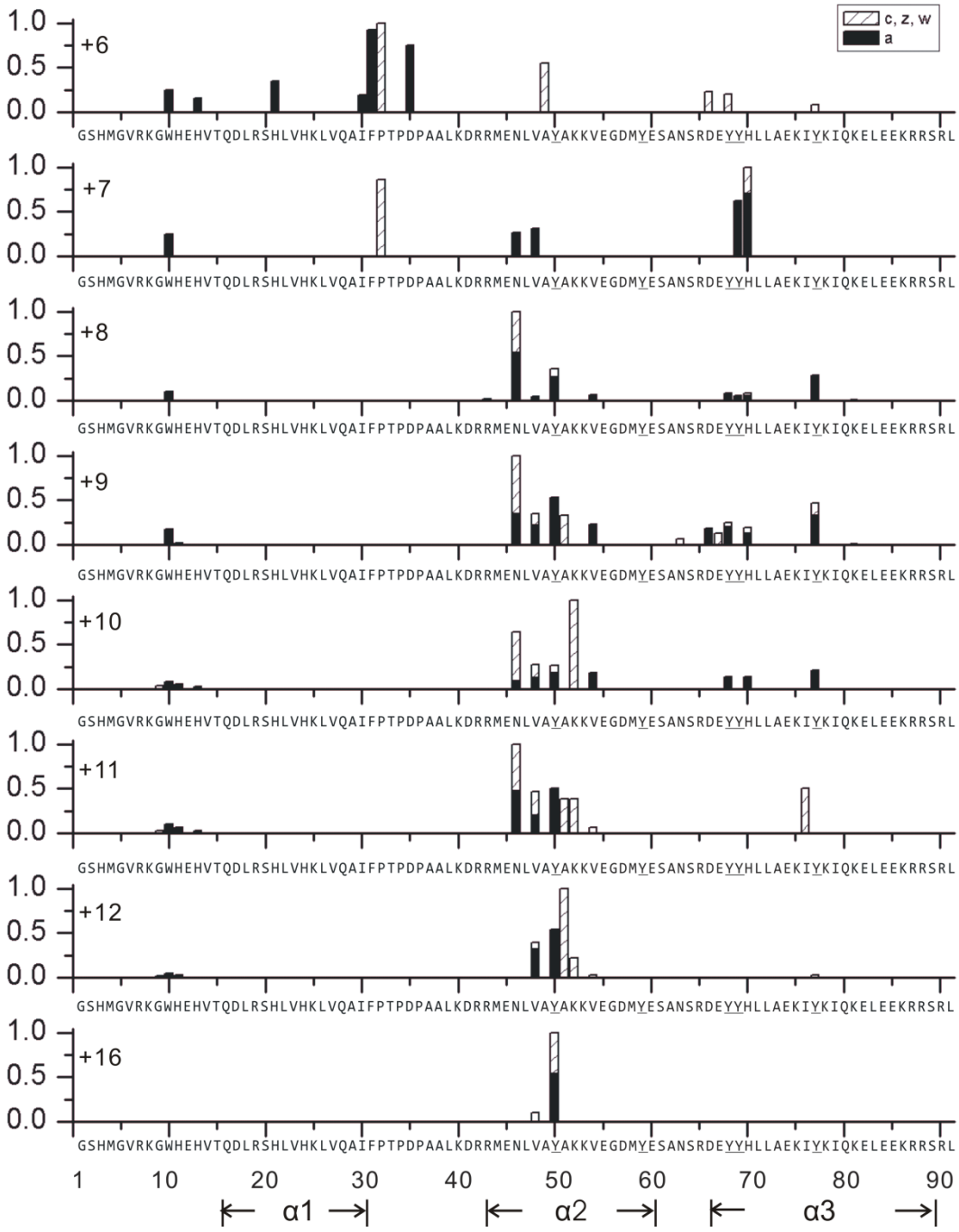

Figure 2.3. Relative abundance of fragments resulting from radical directed backbone dissociation of KIX along the amino acid sequence in different charge states. The sum of fragments at each residue is normalized to the highest sum.

Radical migration occurs only when kinetic and thermodynamic considerations are favorable. The kinetics are largely determined by structure, requiring that the radical donor has direct contact with the radical acceptor and that the relative orientation is favorable. The relevant C-H bond dissociation energies (BDEs) can generally be used to predict whether a reaction will be energetically favorable. The BDE of the C-H bond corresponding to the initial tyrosine radical generated by photodissociation is higher than most other non-aromatic hydrogens present in proteins, making hydrogen abstraction from most other residues exothermic. In other words, the initial tyrosine radical is highly reactive and will abstract hydrogen from most other C-H groups if the structure of the protein allows. Subsequent migrations are also possible, though less likely because the radical favors migration to more stable locations which become less abundant as the radical migrates downhill. The ultimate radical destination can be identified by assignment of the RDD fragments that are observed following activation of the protein radical, and connections with protein structure can be determined as explained previously. RDD backbone fragments are typically initiated from a β-carbon radical in the side chain, which undergoes β-scission to cleave the adjacent C_α-C or N-C_α bond to generate a/x ions or c/z ions. Radical x ions will generally dissociate further into z or w ions.

2.3.3 Secondary structure

For the +8 through +11 charge states, one of the most abundant radical directed backbone cleavages is at residue Asn46 as shown in Figure 2.3. Asn46 is four residues away from the primary initial radical site at Tyr50. Facile radical migration to an amino

acid four residues away can be easily rationalized if the protein is α-helical in this region. The condensed phase structure reveals that Tyr50 and Asn46 are located in the α2 helix region. There are 3.6 residues per turn in an α helix, which places the side chain of Asn46 in close proximity to Tyr50 and allows abstraction of the β-hydrogen to proceed without distortion of the helical structure. This suggests that the secondary structure in this region is preserved when KIX is transferred from the solution phase to the gas phase in these charge states, as suggested previously. In the +16 charge state, this fragmentation pathway is no longer favorable, indicating loss of α-helical structure in the higher charge states. The RDD results examining secondary structure are consistent with the data previously obtained for KIX by ECD.

2.3.4 Tertiary structure

As demonstrated previously, radical migration can also be used to examine protein tertiary structure. Tertiary structural information is inferred from radical migrations which are distant in sequence from the initial residue where the radical is generated. These residues must be spatially proximate to the initial radical site in order for migration to occur, and therefore contain information about the three dimensional organization of the protein. These distance constraints can then be used to drive molecular dynamics simulations towards relevant conformational space and help evaluate potential structures. In the case of KIX, analysis of the RDD data is complicated slightly by the presence of multiple sites of iodination. In this situation, each dissociation endpoint must be considered in relation to several potential radical initiation sites. For evaluation of a

known structure, agreement with the RDD data is determined by evaluating whether each radical endpoint is within proximity of any of the potential radical initiation points. Multiple radical initiation points will actually provide more diverse spatial proximity information which could in theory be better for probing a particular protein conformation. KIX has been reported previously to preserve the known solution structure in the gas phase for +7 and lower charge states. Determining whether the RDD data is consistent with retention of the solution phase structure in the gas phase is therefore a fairly straightforward endeavor.

Backbone dissociation at favorable radical acceptor residues (i.e. Trp10, His21, and Phe31 which have side chains with low β C-H BDEs) which are sequence remote from tyrosine residues is most prevalent for the +6 charge state of KIX, as observed in Figure 3. The RDD data for the +7 charge state appears to bridge the results for the +6 and +8 charge states, suggesting that a structural transition may take place at this charge state. Evaluation of the spatial proximity for the solution phase structure between iodinated tyrosine residues and sites of dissociation such as Trp10, His21, and Phe31 (8.2Å, 7.6Å, and 6.2Å, respectively) are larger than would be expected for radical migration to be able to occur. However, local minima structures on the potential energy surface that are within 80 kJ/mol energy of the solution phase structure are easily obtained when these distances are reduced below 5Å. The Trp10 and His21 sites represent different, mutually exclusive conformations where Tyr69 can bind to one or the other, but not both simultaneously as can be seen in Figure 2.4. The overall folds for both conformers are very similar to the solution phase structure with root mean square deviations (RMSD) of 3.4Å and 2.7Å for

the structures in Figure 2.4a and Figure 2.4b, respectively. Based on the backbone atoms in α helical regions only, all structures are within an RMSD of 2.1Å, suggesting that random coil regions are more flexible than α helices. Alternative folds were explored by constraining tyrosine residues to sites of dissociation in various combinations and subjecting these structures to simulated annealing from 2500K to 50K; however, no lower energy structures were obtained in this fashion. Furthermore, the solution phase three-helix bundle structure of KIX is stable when subjected to stochastic molecular dynamics simulations at 300K for one nanosecond. Although this timescale may be too short to reflect potential structure changes that might eventually occur at longer timescales, the observed stability is in agreement with the RDD data acquired on the millisecond timescale. The influence of charge site selection was also investigated. The relative energies and conformations adopted by KIX are not extremely sensitive to choice of charge locations. This suggests that multiple protonation conformers may exist in reality, which may influence local structural preferences (e.g. binding of Tyr69 to Trp10 or His21).

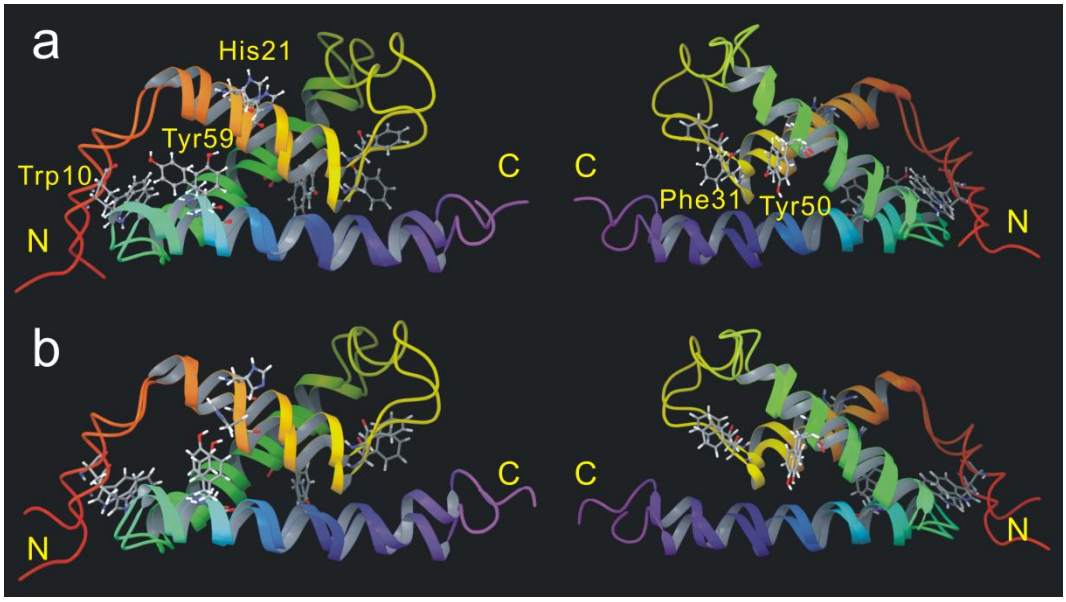

Figure 2.4. Two local minima structures calculated by constraining and releasing distance pairs for +7 KIX in the gas phase overlapped with the native NMR structure. (a) Tyr59-Trp10 and Tyr50-Phe31 are proximate. RMSD is 3.4Å. The picture on the right is the reverse viewpoint. (b) Tyr59-His21 and Tyr50-Phe31 are proximate. RMSD is 2.7Å. N and C indicate the N- and C-termini, respectively.

Why is the gas phase structure of KIX similar to that found in solution? Favorable electrostatic contributions, including salt bridges, have been suggested previously and likely are important. However, it is important to recognize that not all salt bridges present in solution can be retained in the gas phase. The body of work which has been done on the stabilization of charge separation in the gas phase (as is required for salt bridge formation) suggests that only arginine containing salt bridges will be stable in the gas phase. The significantly reduced basicity of lysine in comparison makes salt bridge stabilization much more difficult to achieve. With that in mind, there are several salt bridges which should survive in the gas phase. In particular, the Arg19-Glu55 salt bridge is potentially important. This salt bridge is partially buried, suggesting structural importance in solution, and serves to anchor α1 to α2. In addition, the Arg42-Asp41 salt bridge may be important to stabilize α2. Alpha helices are known to be stable in the gas phase, particularly when a positive charge resides at the C-terminus. The Arg42-Asp41 salt bridge is at the N-terminus of the α2 helix, and the salt bridge dipole is oriented to interact favorably with the macrodipole of the helix. Protonation of Arg42 in the absence of the salt bridge would destabilize the α2 helix. The C-terminus of α2 is stabilized with a proton by Lys8. In addition, a (net) protonated salt bridge may form between Arg90, the C-terminus, and Arg88. This salt bridge would anchor α3 by strongly connecting the terminal residues, and placing a positive charge in the proper location to interact with the helix macrodipole. This salt bridge may explain why α3 is the most stable helical region according to ECD. Similarly, the lack of charge stabilization of the helix macrodipole may explain why α1 is the least stable helix. Charges which do not interact with the

helices can be placed at several different locations due to the multiplicity of basic sites which are available in KIX. The large number of side chains with polar groups additionally helps to ensure that these charges can be solvated without significant rearrangement of the backbone.

2.4 Conclusions

Results obtained by radical directed dissociation are consistent with the KIX domain retaining a three-helix bundle structure in the gas phase which is very similar to the native structure determined by NMR in solution. The native structure is retained due to a combination of factors. KIX secondary structure is primarily alpha helical, a motif which has been demonstrated to be stable in the gas phase. The solvation of charge for the +6 and +7 charge states of KIX can be accommodated without significant structural rearrangement. Furthermore, there are numerous potential sites where the charges can be placed, increasing the likelihood that charges will be able to reside in locations that do not require structural rearrangement. There are also several key salt bridges and favorable ion-helix dipole interactions which likely help hold the structure together in the gas phase once solvent has been removed.

References

[1] C.-I. Brändén, J. Tooze, Introduction to protein structure, 2nd ed., Garland Pub., New York, NY, 2009.

[2] J.N. Sachs, D.M. Engelman, Introduction to the membrane protein reviews: The interplay of structure, dynamics, and environment in membrane protein function, Annu. Rev. Biochem., 75 (2006) 707-712.

[3] D.E. Clemmer, M.F. Jarrold, Ion mobility measurements and their applications to clusters and biomolecules, J. Mass Spectrom., 32 (1997) 577-592.

[4] J.R. Eyler, Infrared Multiple Photon Dissociation Spectroscopy of Ions in Penning Traps, Mass Spectrom. Rev., 28 (2009) 448-467.

[5] M.E. Belov, M.V. Gorshkov, H.R. Udseth, G.A. Anderson, R.D. Smith, Zeptomole-sensitivity electrospray ionization - Fourier transform ion cyclotron resonance mass spectrometry of proteins, Anal. Chem., 72 (2000) 2271-2279.

[6] M. Han, M. Jin, K. Breuker, F.W. McLafferty, Extending top-down mass spectrometry to proteins with masses greater than 200 kilodaltons, Science, 314 (2006) 109-112.

[7] K.J. Gillig, B. Ruotolo, E.G. Stone, D.H. Russell, K. Fuhrer, M. Gonin, A.J. Schultz, Coupling high-pressure MALDI with ion mobility/orthogonal time-of flight mass spectrometry, Anal. Chem., 72 (2000) 3965-3971.

[8] C. Uetrecht, I.M. Barbu, G.K. Shoemaker, E. van Duijn, A.J.R. Heck, Interrogating viral capsid assembly with ion mobility-mass spectrometry, Nature Chem., 3 (2011) 126-132.

[9] C. Bleiholder, N.F. Dupuis, T. Wyttenbach, M.T. Bowers, Ion mobility-mass spectrometry reveals a conformational conversion from random assembly to beta-sheet in amyloid fibril formation, Nature Chem., 3 (2011) 172-177.

[10] J.J. Thomas, B. Bothner, J. Traina, W.H. Benner, G. Siuzdak, Electrospray ion mobility spectrometry of intact viruses, Spectrosc-Int J, 18 (2004) 31-36.

[11] D.E. Clemmer, R.R. Hudgins, M.F. Jarrold, Naked Protein Conformations - Cytochrome-C in the Gas-Phase, J. Am. Chem. Soc., 117 (1995) 10141-10142.

[12] B.T. Ruotolo, K. Giles, I. Campuzano, A.M. Sandercock, R.H. Bateman, C.V. Robinson, Evidence for macromolecular protein rings in the absence of bulk water, Science, 310 (2005) 1658-1661.

[13] D.M. Horn, K. Breuker, A.J. Frank, F.W. McLafferty, Kinetic intermediates in the folding of gaseous protein ions characterized by electron capture dissociation mass spectrometry, J. Am. Chem. Soc., 123 (2001) 9792-9799.

[14] R.B.J. Geels, S.M. van der Vies, A.J.R. Heck, R.M.A. Heeren, Electron capture dissociation as structural probe for noncovalent gas-phase protein assemblies, Anal. Chem., 78 (2006) 7191-7196.

[15] K. Breuker, H.B. Oh, D.M. Horn, B.A. Cerda, F.W. McLafferty, Detailed unfolding and folding of gaseous ubiquitin ions characterized by electron capture dissociation, J. Am. Chem. Soc., 124 (2002) 6407-6420.

[16] T. Ly, R.R. Julian, Elucidating the Tertiary Structure of Protein Ions in Vacuo with Site Specific Photoinitiated Radical Reactions, J. Am. Chem. Soc., 132 (2010) 8602-8609.

[17] T. Ly, R.R. Julian, Tracking Radical Migration in Large Hydrogen Deficient Peptides with Covalent Labels: Facile Movement does not Equal Indiscriminate Fragmentation, J. Am. Soc. Mass. Spectrom., 20 (2009) 1148-1158.

[18] B.N. Moore, S.J. Blanksby, R.R. Julian, Ion-molecule reactions reveal facile radical migration in peptides, Chem. Commun., (2009) 5015-5017.

[19] Q.Y. Sun, S. Yin, J.A. Loo, R.R. Julian, Radical Directed Dissociation for Facile Identification of Iodotyrosine Residues Using Electrospray Ionization Mass Spectrometry, Anal. Chem., 82 (2010) 3826-3833.

[20] P. Carter, Site-Directed Mutagenesis, Biochem. J., 237 (1986) 1-7.

[21] N. Vo, R.H. Goodman, CREB-binding protein and p300 in transcriptional regulation, J. Biol. Chem., 276 (2001) 13505-13508.

[22] R.N. De Guzman, N.K. Goto, H.J. Dyson, P.E. Wright, Structural basis for cooperative transcription factor binding to the CBP coactivator, J. Mol. Biol., 355 (2006) 1005-1013.

[23] K. Breuker, S. Bruschweiler, M. Tollinger, Electrostatic Stabilization of a Native Protein Structure in the Gas Phase, Angew. Chem. Int. Ed., 50 (2011) 873-877.

Chapter 3

Photoinitiated Intramolecular Diradical Cross-Linking of Polyproline Peptides in the Gas Phase

3.1 Introduction

Polyproline peptides are well known as molecular rulers in the condensed phase and are often used for distance calibration in structural molecular biology.[1-2] Of the twenty natural amino acids, proline is unique because the side chain is cyclized to the backbone. This ring structure restricts the conformational flexibility of proline, which is often found in turns in proteins. There are two distinctly different helical conformations which polyproline can adopt: polyproline type I (PPI) helix where all peptide bonds are in the *cis* configuration, and the polyproline type II (PPII) helix with all proline residues in the *trans* form.[3] PPI is stabilized by intramolecular van der Waals forces and is favored in nonpolar solvents (such as n-propanol), whereas PPII is more extended and is favored in aqueous solution. Although PPII has long been assumed to adopt a rigid structure in water, significant deviations from the regular all-*trans* helix have been reported in a variety of experiments including osmometry,[4] NMR,[5] single-molecule fluorescence resonance energy transfer (FRET),[6-7] and fluorescence quenching by photoinduced-electron transfer.[8] Theoretical studies on polyproline have suggested that other low

energy non-helical conformers with various amounts of interspersed *cis* or *trans* residues are also stable.[9]

Polyproline peptide conformation in the gas phase has been studied by ion mobility,[10] fluorescence quenching,[11] and FRET.[12] Molecular mechanics calculations were also used to help evaluate the data in each experiment. In all cases, evidence for multiple conformations that deviated from ideal helical structures was found. Radical directed dissociation (RDD) is another method developed in Julian group that can be applied to examine protein structure in the gas phase.[13-14] Based on radical migration and dissociation, distance constraints between radical donors and radical acceptors in a protein can be determined and used to evaluate candidate structures. However, this method requires not only a radical donor with strong reactivity (such as tyrosine) but also a good radical acceptor in close proximity. Polyproline peptides have neither good radical initiation sites nor good radical migration sites, dictating that an alternative approach should be utilized.

Chemical cross-linking combined with mass spectrometry is a common method for protein structure analysis.[15-18] Cross-linked residues are assumed to be within a certain distance of each other that is determined by the length of the cross-linker. These distance constraints can be leveraged to build up information about the three-dimensional structure of the protein. In this work, we have developed a zero length cross-linking strategy based on diradical recombination to monitor the end-to-end distances in polyproline peptides of various lengths and charge states in the gas phase. Diradical recombination can be monitored by comparing the collision induced dissociation (CID)

spectra of the diradical to that of the non-radical. When cross-linking occurs, a cyclic molecule is formed and the CID spectrum no longer yields the typical b and y ions characteristic of linear polyproline. Ion-molecule reactions with dioxygen can also be used to monitor the extent and rate of radical recombination.

The results from these experiments suggest that low charge state ions in short polyprolines have much closer end-to-end distances than that would be expected for PPII. More extended conformations with larger end-to-end distances are observed for highly charged longer polyproline ions. The population of ions which undergo rapid recombination decreases with increasing charge state or peptide length. Singly charged anions formed from 1-propanol solution are also found not to maintain PPI helical structure, which is in agreement with molecular dynamics calculations that indicate the existence of many lower energy conformations.

3.2 Experiment Section

Materials Polyproline peptides (Ac-KP_mK, m=5, 9, 16, 23, KP_nK, n=7, 12, 13, 18, 21, 26) were synthesized by Genscript (Piscataway, NJ). N-hydroxysuccinimide (NHS) activated iodo-benzoyl ester was synthesized previously. All organic solvents were purchased from Fisher Scientific (Fairlawn, NJ).

Peptide derivatization All polyproline peptides were labeled at N-terminal and C-terminal lysine ε-amines with NHS activated iodo-benzoyl ester (2X molar ratio) in 1:1 borate buffer (pH 8.5) : dioxane solution for 30 mins at 40 ℃. A reversed phase cartridge (Michrom Bioresources, Inc., Auburn, CA) was used for desalting.

Photodissociation mass spectrometry. Iodo-benzoyl derivatized polyproline peptide (10 μM) in 50:50 H_2O:CH_3OH with 0.1% acetic acid was electrosprayed into an LTQ linear quadrupole ion trap mass spectrometer (Thermo Fisher Scientific, San Jose, CA). The back plate of the instrument was modified with a quartz window to transmit 266 nm UV photons into the linear ion trap, from the 4^{th} harmonic generation of a Nd:YAG laser (Continuum, Santa Clara, CA). Laser pulses were synchronized to the isolation step via a digital delay generator. Isolation window for collision induced dissociation and photodissociation and was 3 to 10 m/z with activation value q=0.25 and activation time as 30 ms. For ion-molecule reaction following photodissociation, all ions including radical precursor ions and photodissociation product were trapped for a specific time (30 ms ~ 9 s) to allow reaction with background dioxygen in the ion trap. In the negative mode, polyproline peptides were dissolved in n-propanol. Fragments were analyzed manually with the aid of Fragmentor 1.2.2.

C-H Bond dissociation energy calculation GaussView 5.0 was used to build proline amino acid with backbone dihedral angles at polyproline type I (φ= -83°,ψ=158°,ω=0°) or type II (φ= -78°,ψ=149°,ω=180°) configuration. Proline was extended with acetyl group at N-terminus and amine at C-terminus. Isodesmic reactions were used to calculate C-H bond dissociation energies (BDE) with $(CH_3)_2CH$-H or glycine as reference molecules for secondary (β-, γ- or δ-carbon) or tertiary (α-carbon) radical centers at proline. Restricted structural optimization with fixed dihedral angles and energy calculations were performed at the B3LYP/6-31G(d) level of theory using Gaussian 09 Version 8.0.

Molecular Modeling. MacroModel, version 9.9, Schrödinger, LLC, New York, NY, molecular mechanics software package was used to build deprotonated $KP_{13}K$ at carboxyl group and perform all molecular modeling simulations. The OPLS force field at constant dielectric, $\varepsilon = 1.0$, was used for all calculations. Extended cutoffs were used for dipole-dipole interactions. Energy minimization was performed using the Polak-Ribiere Conjugate Gradient method with a derivative convergence criterion of 0.05 kJ/Å·mol. Conformational searches with the mixed torsional/low-mode sampling method were used with a maximum of 10000 steps. The maximum number of unique structures to save per rotatable bond is 100.

3.3 Results and discussion

A series of polyproline peptides of varying chain lengths were prepared with an additional lysine residue placed on each end to allow for convenient modification. 4-iodobenzoyl (IB) radical precursor groups were covalently attached to both lysine side chains to yield Ac-$K^{IB}P_mK^{IB}$ and $K^{IB}P_nK^{IB}$ peptides (where m=5, 9, 16, 23, and n=7, 12, 13, 18, 21, 26, for simplicity, these will simply be referred to as P_x peptides where x indicates the number of proline residues). The CID spectrum for singly protonated non-radical P_9 is shown in Fig3.1a. The spectrum is not rich and yields only a few C- terminal fragments (i.e, y_{10}, y_8, y_6). Interestingly, proline residues are predominantly lost in pairs of two. The most abundant dissociation product is y_{10}. In contrast, y_8, y_6, and y_4 are

observed with decreasing intensity, suggesting that these ions may be secondary fragments produced by consecutive losses of proline dimers from y_{10}.

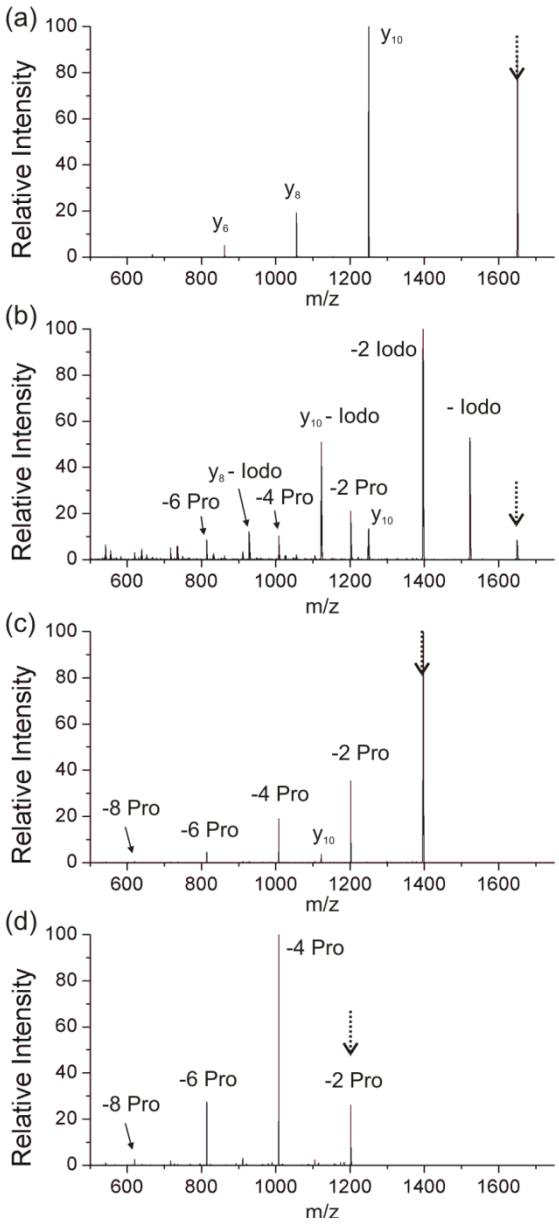

Figure 3.1. (a): CID and (b): photodissociation spectrum of di-iodobenzoyl labeled $[P_9+H]^+$, (c): CID spectrum of diradical peptide, $[P_9 \cdot\!\!+H]^+$, generated via photoinitiated cleavage of carbon-iodine bonds in (b), (d): CID spectrum of -2 Pro fragment in (c). P_x : x indicates the number of proline residues

Fig3.1b shows the photodissociation spectrum for di-iodobenzoyl labeled $[P_9+H]^+$. The highest intensity peak corresponds to the loss of two iodine atoms, creating (at least initially) a diradical peptide. Mono-radical peptide and other backbone fragments are also observed. CID of the re-isolated diradical peptide is shown in Fig3.1c, and demonstrates mainly loss of internal fragments (i.e., -2 Pro, -4 Pro, -6 Pro). The loss of internal fragments, rather than dominant backbone fragmentation, suggests that a significant fraction of the diradicals have recombined to yield cross-linked, cyclic peptides. The y_{10} ion, which was dominant in Figure 3.1a, is very small in Figure 3.1c, which is also consistent with significant cross-linking. Recombination of two radicals is extremely exothermic and will occur spontaneously if the two radicals are brought within proximity of each other. Radical-radical proximity is a function of polyproline ion conformation and dynamics. In addition to radical recombination, individual radicals are known to be able to migrate to lower energy sites via hydrogen atom abstraction. Migrated radicals could also then potentially recombine. In order to examine the likelihood of migration followed by recombination further, the primary product in Figure 3.1c was subjected to further collisional activation and the results are shown in Figure 3.1d. The only fragments of consequence in Figure 3.1d are additional sequential internal losses of proline dimers. There are no significant b or y ions in either Figure 3.1c or Figure 3.1d. This suggests that radical recombination of the originally generated diradicals is the dominant process, and that migration followed by recombination is less likely. The recombination pathway is shown generically in Scheme 3.1. The results in Figure 3.1 suggest that the terminal ends of $[P_9 \bullet\!+H]^+$ are in sufficiently close proximity with adequate dynamic flexibility to

enable facile diradical recombination. Even taking into account the rotational flexibility of lysine side chains, an extended polyproline type II helical structure would not allow interaction between the terminal ends for $[P_9 \cdot\!\!+H]^+$.

Scheme 3.1. Photoinitiated diradical cross-linking mechanism

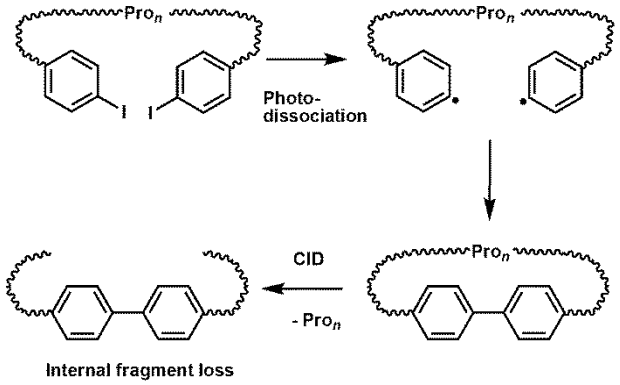

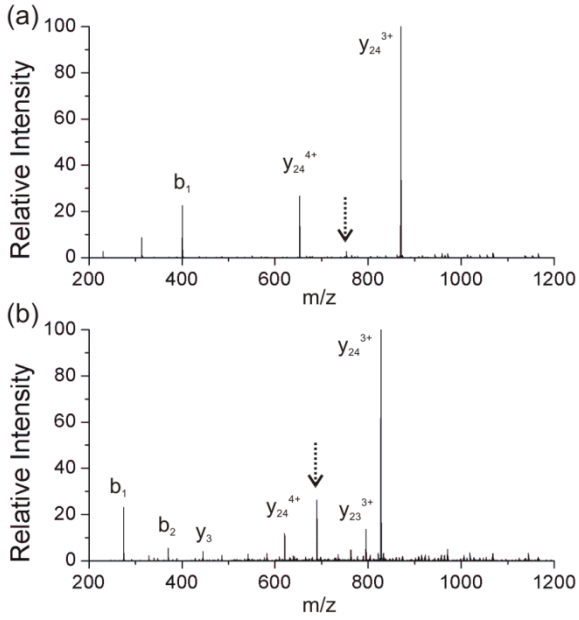

Figure 3.2. (a): CID spectrum of the di-iodobenzoyl labeled peptide $[P_{23}+4H]^{4+}$. (b): CID spectrum of the same peptide with two radicals, $[P_{23}{\cdot}+4H]^{4+}$, generated by photodissociation.

Results from experiments on $[P_{23}+4H]^{4+}$ are shown in Figure 3.2. The CID spectrum for the non-radical (Figure 3.2a) is dominated by fragmentation of the backbone between N-terminal lysine and adjacent proline residue to yield the y_{24} ion. The complementary b_1 ion is also observed. Figure 3.2b shows the CID spectrum of the di-radical, which behaves very similarly to the non-radical with a few additional backbone fragments. Internal fragment losses are not observed as noted previously for $[P_9 \cdot+H]^+$, which suggests that recombination for $[P_{23} \cdot+4H]^{4+}$ is not favorable. There are at least two factors that disfavor cross-linking in longer and more highly charged peptides. First, Coulomb repulsion will tend to elongate the peptide into an extended structure which places the two lysine residues far away. Second, the likelihood of interaction between the two ends of a linear peptide becomes lower with increasing chain length due to increased entropic factors. It is likely that both of these issues contribute to the lack of di-radical recombination observed for $[P_{23} \cdot+4H]^{4+}$. The consistency of the two CID spectra in Figure 3.2 is also further evidence for crosslinking in Figure 3.1, where the corresponding CID spectra were quite different. Isotopic analysis of the fragments in Figure 3.2 confirms that radical migration to the proline backbone is not a favorable pathway for the longer peptide.

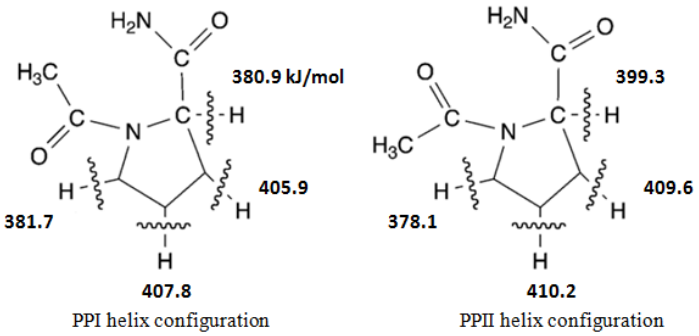

Scheme 3.2. C-H bond dissociation energies on proline residue in the configuration of polyproline type I helix (φ = -83 °, ψ = 158 °, ω = 0 °) or type II helix (φ = -78 °, ψ = 149 °, ω = 180 °).

There are several potential factors which may suppress radical migration in polyproline peptides. In general, radical migration is favored when a newly created radical is more stable than the original, and sufficient structural flexibility exists to allow the two sites to come into close proximity with the proper geometrical alignment. Radical stabilities are easily predicted by C-H bond dissociation energies (BDEs). The original phenyl radical at the modified lysine side chain is very reactive with a BDE of 473 kJ/mol. For comparison, various BDEs associated with proline in the PPI and PPII helical structures are shown in Scheme 3.2. The primary difference between the two occurs at the alpha position due to cis/trans isomerization of the peptide bond. Although hydrogen abstraction from proline by the original phenyl radical would be exothermic, the BDEs for proline relative to the most common sites for migration are still fairly high. Therefore, there is not an extremely large thermodynamic driving force behind potential migration. Perhaps more importantly, the cyclic nature of proline significantly restricts structural flexibility, which impedes both the number of potential radical donor and acceptor sites that might come into close proximity and the proper alignment of the donor and acceptor sites. Therefore, it is very likely that radical migration is kinetically constrained by the rigidity of the polyproline structure. In contrast, radical recombination has a tremendous thermodynamic driving force (>450kJ/mol) with significantly looser geometrical alignment constraints.

$$X = \frac{\sum I_{\text{internal fragment}}}{\sum I_{\text{all fragments}}} \times 100\% \qquad (1)$$

In order to quantitatively evaluate the effect of size and charge on polyproline structure in the gas phase, we calculated the extent of diradical cross-linking using formula (1), where *I* represents the intensity of the relevant fragment ion. In (1), it is assumed that all internal fragments are generated due to crosslinking, which is reasonable because no internal fragments were observed for the linear polyprolines examined herein and internal fragments are in general rarely observed in peptide fragmentation. An X score of 100% implies that all observed fragments are consistent with cross-linking and that the probability for contact between the terminal residues is high. Lower X scores will indicate lower probabilities for cross-linking. Figure 3.3 summarizes the X scores from four peptides in various charge states.

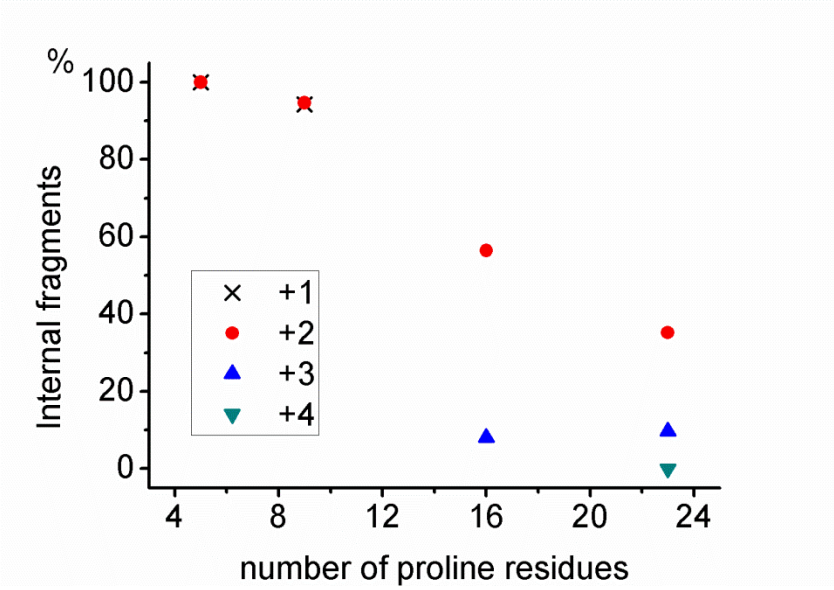

Figure 3.3. Fractions of diradical cross-linking initiated CID fragments intensities (X is defined in formula 1) as a function of peptide chain length and charge state.

For P_5 and P_9, charge state (+1 and +2) has little influence on the X score in Figure 3.3. The observation of abundant internal fragments in both charge states suggests that significant diradical cross-linking occurs for these short peptides. The situation changes for P_{16}, where the X score varies significantly between the +2 and +3 charge states, with the score dropping for the higher charge state. This observation is consistent with Coulombic repulsion leading to a more extended structure where the terminal ends are less likely to interact. Similar trends are observed as a function of charge state for P_{23}. For the +2 charge state of all four peptides, there is also a consistent trend where the X score decreases as peptide length increases. The probability for ring closing due to cross-linking is expected to decrease as peptide length increases due to entropic factors. A similar trend is not observed for the +3 charge state; however, we note that there are only two data points for the +3 charge state and that the X score is very low in both cases.

Ion-molecule reactions with dioxygen

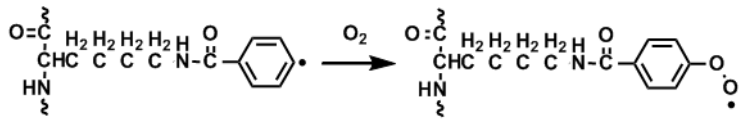

Scheme 3.3. Ion-molecule reaction for polyproline peptide ions.

Dioxygen is present as a background gas in ion traps and is able to form adducts with some radicals following storage on the second timescale. We have previously demonstrated that ion-molecule reactions with dioxygen (Scheme 3.3) can be used to detect phenyl radicals and monitor radical migration in peptides. Cross-linked peptides are no longer radicals and will not react with dioxygen, but if the originally generated diradicals persist, they will readily form dioxygen adducts. Cross-linked polyproline ions can therefore be easily distinguished from non-recombined diradical ions by reaction with background dioxygen. Fig. 3.4a shows the mass spectrum obtained after simultaneously trapping both $[P_{21}\cdot+2H]^{2+}$ and $[P_{21}\cdot\cdot+2H]^{2+}$ for 4 seconds. Monoradical dioxygen adduct ions were observed with 6.7% intensity relative to the unreacted monoradical ion. It should be pointed out that the monoradicals will be generated at both potential sites (either terminal end of the polyproline) in these experiments, and to first approximation should be equally distributed between the two sites. If there is no intramolecular interaction between the two separated radicals, the theoretical ion-molecule reaction yield for the diradical should be approximately twice that for a monoradical (~13.4%). The actual relative intensity of dioxygen adduct ions was only 2.0%, indicating significantly reduced radical availability relative to the monoradical. The most likely explanation for this result is significant recombination of the diradicals to yield cross-linked peptides. Furthermore, diradical recombination in these ion molecule reactions occurs without collisional activation, suggesting that the peptides are sufficiently dynamic to enable recombination without heating.

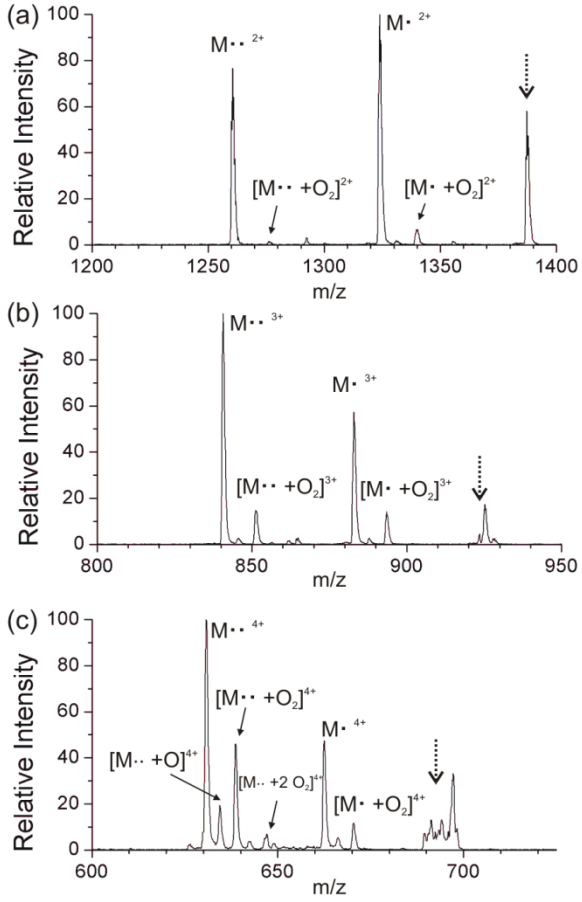

Figure 3.4. The mass spectrum resulting from the reaction of O_2 with photodissociation generated radical P_{21} peptides in different charge states: (a) +2, (b) +3, and (c) +4. M ⋯- P_{21} ⋅; M ⋅- P_{21} :

In an attempt to semi-quantitatively characterize the extent of radical annihilation in diradical peptides, we used formula (2) as follows:

$$\text{Radical annihilation percentage} = \left(1 - \frac{\text{Ion molecule reaction yield for diradical}}{2 \times \text{monoradical yield}}\right) \times 100\% \quad (2)$$

Using formula (2), the percentage of original radicals that have undergone annihilation reactions for $[P_{21}{\cdot}+2H]^{2+}$ is 85%, suggesting significant interaction between the terminal residues and a large population of the conformations with a compact structure. As charge state increases for P_{21}, the radical annihilation percentage decreases substantially (70% for $[P_{21}{\cdot}+3H]^{3+}$ in Fig. 3.4b and 8.4% for $[P_{21}{\cdot}+4H]^{4+}$ in Fig. 3.4c). These values are consistent with Coulombic repulsion causing peptide unfolding, which decreases the chance of interaction between terminal residues. Further evidence for diradical non-recombination is observed in the spectrum for $[P_{21}{\cdot}+4H]^{4+}$, where it is clear that two O_2 molecules have attached to the peptide (see Fig. 3.4c).

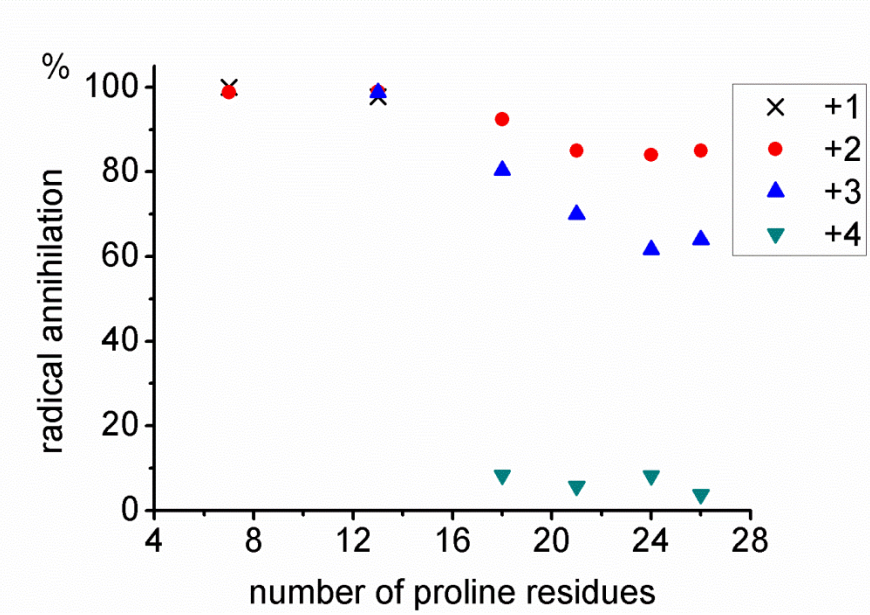

Figure 3.5. Percentage of radical annihilation in diradical polyproline peptides $[P_x$ ·+ nH$]^{n+}$ (x = 7, 13, 18, 21, 24, 26, n = 1, 2 , 3, 4) as a function of charge state and chain length. The percentage is approximately calculated from ion-molecule reaction yield by formula (2).

We also applied ion-molecule reactions to other polyproline peptides (P_7, P_{13}, P_{18}, P_{24}, P_{26}) with the same strategy and the radical annihilation values are plotted in Fig. 3.5 as a function of the charge state or the number of proline residues. For small peptides (i.e. P_7, P_{13}), the radical annihilation percentage is nearly 100% regardless of charge state. This suggests that these peptides are able to adopt conformations with proximal ends even for the highest charge states which are observed. For larger peptides (P_{18}, P_{24}, P_{26}), there is a clear effect due to charge state. As the charge state increases, less radical recombination is observed. In fact, for the +4 charge states, the data indicate that very little radical recombination is able to occur. The most likely explanation for these observations is again elongation of the peptides due to Coulombic repulsion. Trends due to increasing size are more difficult to sort out from the data in Figure 3.5, which was all acquired at a set point in time. However, the kinetics of dioxygen addition can also be explored and may reveal additional information.

Singly charged polyproline anions

All previous studies on the structure of polyproline peptides in the gas phase examined positively charged ions. The structures of negatively charged polyproline peptides catch our interest for several reasons. First, peptide ions in low charge states are ideal for structural characterization because there is less Coulombic repulsion to interfere with the intrinsic structure. Furthermore, polyproline peptides have only one acidic site at the C-terminus, which should carry the charge after electrospray ionization. Accurate

assignment of the charge position facilitates molecular mechanics structure calculations. Finally, polyproline type I helices have a macrodipole moment oriented with the positive end towards the C-terminus, which should maximize the chances for stabilization of the helix structure in the gas phase by analogy with previous work on alpha helices.

Table 3.1. Ion Molecule Reactions with Polyproline Anions

	P_5	P_7	P_9	P_{12}	P_{13}
$M^{\cdot +} + O_2$ (%) [a]	3.6	7.4	9.7	26	28
$M^{\cdot\cdot +} + O_2$ (%) [b]	0.16	0.14	0.34	0.16	0.34

a - abundance relative to monoradical,
b - abundance relative to diradical.

Polyproline peptides in n-propanol (which should favor formation of PPI) were electrosprayed in negative ion mode and ion-molecule reactions were used to characterize the extent of radical annihilation as previously discussed. The dioxygen addition yields for negatively charged monoradical and diradical polyproline (P_x, x = 5, 7, 9, 12, 13) are shown in Table 3.1. The yield is approximately defined as the peak intensity ratio of ion-molecule adduct peak relative to the radical precursor. The low yield for $[M^{\bullet\bullet} + O_2]^{-1}$ diradical ions suggests that almost all radicals have recombined. The variation of monoradical adduct yield in Table 3.1 is likely due to the influence of peptide structure.

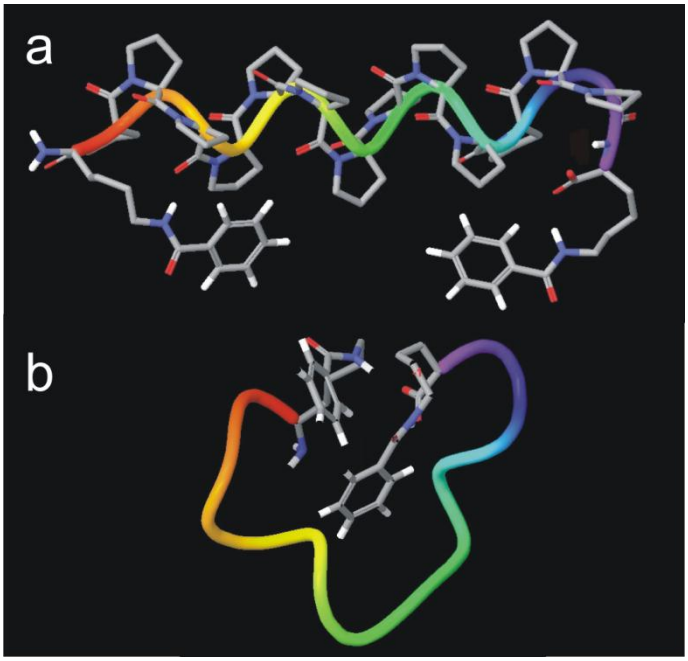

Figure 3.6. Molecular mechanics simulation of polyproline anion $[P_{13} - H]^-$. (a): sampled structure (-46.1 kJ/mol potential energy) with polyproline type I helix and the shortest distance between two lysine side chains during molecular dynamics, (b): lowest potential energy structure (-77.2 kJ/mol) resulting from conformational search.

Molecular dynamics calculations were used to examine potential conformations of polyproline anions. Fig. 3.6a shows a sampled P13 structure with a PPI helical conformation where the distance between two lysine side chains was at a minimum. It is clear that even at this shortest distance, the benzoyl group on one end cannot approach the other. Therefore, extensive diradical cross-linking in P_{13} suggests that it does not adopt a PPI helix structure in the gas phase. A conformational search was then used to look for the most stable structure for P_{13} in the gas phase. The lowest energy structure that was found is shown in Fig. 3.6b. The calculated potential energy, -77.2 kJ/mol, is lower than the PPI helical structure in Fig. 3.6a (-46.1 kJ/mol). In the lowest energy state, a compact globular structure is adopted with two proline residues in the *trans* orientation. This severely bent structure puts the two benzoyl groups in close proximity to each other. Although the static orientations of the two benzoyl groups in Fig. 3.6b would likely not allow for spontaneous diradical recombination, amino acid side chain dynamics could easily enable the required geometry. In summary, our experimental data and calculations both suggest that negatively charged PPI helical structure is not the major conformation observed in the gas phase.

3.4 Conclusions

The present results illustrate that photoinitiated diradical cross-linking can be utilized to probe the conformations of biomolecules in the gas phase. Radical recombination leads to cross-linked peptides that are easily identified by CID. In the case of polyproline,

cross-linking leads to dominant observation of internal fragment ions. Radical recombination can also be examined without activation via ion-molecule reactions with dioxygen. The extent of recombination can be determined by comparing diradical reactivity with the corresponding monoradical reactivity of the same ion. In the end, cross-linking establishes distance constraints that can be used to evaluate potential structures. The results indicate that polyproline does not favor PPI or PPII helical structures in the gas phase in either positive or negative charge states. It is clear that increasing charge leads to more extended structures, which would be expected due to Coulombic repulsion. Kinetic data also suggests that cross-linking is less favorable for longer peptides, which would be consistent with entropic effects that would be expected to disfavor ring closing. The potential utility of polyproline as a molecular ruler in the gas phase is questionable.

References

[1] Stryer, L., Haugland, R.P.: Energy Transfer - a Spectroscopic Ruler. *Proc. Natl. Acad. Sci. U. S. A.* **58**, 719-& (1967)

[2] Schuler, B., Lipman, E.A., Eaton, W.A.: Probing the free-energy surface for protein folding with single-molecule fluorescence spectroscopy. *Nature* **419**, 743-747 (2002) [3] Watkins, L.P., Chang, H.Y., Yang, H.: Quantitative single-molecule conformational distributions: A case study with poly-(L-proline). *J. Phys. Chem. A* **110**, 5191-5203 (2006)

[3] Commission on Biochemical Nomenclature - Abbreviations and Symbols for Description of Conformation of Polypeptide Chains - Tentative Rules (1969). *Biochemistry* **9**, 3471-& (1970)

[4] Mattice, W.L., Mandelke.L: Conformational Properties of Poly-L-Proline Form-Ii in Dilute Solution. *J. Am. Chem. Soc.* **93**, 1769-& (1971)

[5] Stryer, L., Haugland, R.P.: Energy Transfer - a Spectroscopic Ruler. *Proc. Natl. Acad. Sci. U. S. A.* **58**, 719-& (1967)

[6] Schuler, B., Lipman, E.A., Steinbach, P.J., Kumke, M., Eaton, W.A.: Polyproline and the "spectroscopic ruler" revisited with single-molecule fluorescence. *Proc. Natl. Acad. Sci. U. S. A.* **102**, 2754-2759 (2005)

[7] Sinz, A.: Chemical cross-linking and mass spectrometry to map three-dimensional protein structures and protein-protein interactions. *Mass Spectrom. Rev.* **25**, 663-682 (2006)

[8] Doose, S., Neuweiler, H., Barsch, H., Sauer, M.: Probing polyproline structure and dynamics by photoinduced electron transfer provides evidence for deviations from a regular polyproline type II helix. *Proc. Natl. Acad. Sci. U. S. A.* **104**, 17400-17405 (2007)

[9] Moradi, M., Lee, J.G., Babin, V., Roland, C., Sagui, C.: Free Energy and Structure of Polyproline Peptides: An Ab Initio and Classical Molecular Dynamics Investigation. *Int. J. Quantum Chem.* **110**, 2865-2879 (2010)

[10] Counterman, A.E., Clemmer, D.E.: Anhydrous polyproline helices and globules. *J. Phys. Chem. B* **108**, 4885-4898 (2004)

[11] Shi, X.G., Duft, D., Parks, J.H.: Fluorescence quenching induced by conformational fluctuations in unsolvated polypeptides. *J. Phys. Chem. B* **112**, 12801-12815 (2008)

[12] Moradi, M., Lee, J.G., Babin, V., Roland, C., Sagui, C.: Free Energy and Structure of Polyproline Peptides: An Ab Initio and Classical Molecular Dynamics Investigation. *Int. J. Quantum Chem.* **110**, 2865-2879 (2010)

[13] Ly, T., Julian, R.R.: Elucidating the Tertiary Structure of Protein Ions in Vacuo with Site Specific Photoinitiated Radical Reactions. *J. Am. Chem. Soc.* **132**, 8602-8609 (2010)

[14] Zhang, X., Julian, R.R.: Investigating the gas phase structure of KIX with radical directed dissociation and molecular dynamics: Retention of the native structure. *Int. J. Mass Spectrom.* **308**, 225-231 (2011)

[15] Sinz, A.: Chemical cross-linking and mass spectrometry to map three-dimensional protein structures and protein-protein interactions. *Mass Spectrom. Rev.* **25**, 663-682 (2006)

[16] Sohn, C.H., Agnew, H.D., Lee, J.E., Sweredoski, M.J., Graham, R.L.J., Smith, G.T., Hess, S., Czerwieniec, G., Loo, J.A., Heath, J.R., Deshaies, R.J., Beauchamp, J.L.: Designer Reagents for Mass Spectrometry-Based Proteomics: Clickable Cross-Linkers for Elucidation of Protein Structures and Interactions. *Anal. Chem.* **84**, 2662-2669 (2012)

[17] Ly, T., Liu, Z.J., Pujanauski, B.G., Sarpong, R., Julian, R.R.: Surveying ubiquitin structure by noncovalent attachment of distance constrained bis(crown) ethers. *Anal. Chem.* **80**, 5059-5064 (2008)

[18] Mentinova, M., McLuckey, S.A.: Intra- and Inter-Molecular Cross-Linking of Peptide Ions in the Gas Phase: Reagents and Conditions. *J. Am. Soc. Mass Spectrom.* **22**, 912-921 (2011)

Chapter 4

Exploring radical migration pathways in peptides with positional isomers, deuterium labeling, and molecular dynamics simulations

4.1 Introduction

Free radicals play various important roles in biology in both useful and destructive contexts. [1] For example, nitric oxide is a small endogenous diatomic radical which regulates blood flow. Radical chemistry is also key in the synthesis of nucleotides by ribonucleotide reductase for eventual synthesis of DNA. Reactive oxygen species such as hydroxyl and peroxide radicals are utilized beneficially by the immune system to attack invading organisms. On the other hand, reactive oxygen species are also bi-products of respiration or can be generated by other exogenous sources, and can harmfully attack lipids, proteins, and DNA.[2]

Radical chemistry also plays an important role in mass spectrometry, where information about sequence and structure can be derived from the radical driven fragmentation of peptides or proteins via methods such as electron capture dissociation (ECD) or electron transfer dissociation (ETD). Both of these methods (at least initially) generate hydrogen abundant radicals, so called because the number of hydrogen atoms exceeds the number required for an even electron molecule. Most free radicals (including all discussed in the previous paragraph) are hydrogen deficient species, where essentially

a hydrogen atom is missing relative to an even electron molecule. Collision induced dissociation (CID) based methods have been recently developed to generate hydrogen deficient radical peptides in the gas phase through various modification strategies, including oxidative dissociation of peptide-metal complexes, [3] homolytic cleavage of labile bonds such as nitrate ester, [4] peroxycarbamate, [5] azo, [6] nitroso, [7] tempo, [8] etc. One typical concern in generating radical peptides by CID is that charge directed backbone dissociation processes compete with desired radical generation, which may lead to suppression of radical yield in some situations. In comparison, photodissociation (PD) is capable of generating radical biomolecules via dissociative excited state chemistry that results in homolytic bond cleavage at specific chromophores. In particular, 266 nm UV photons can selectively cleave carbon-iodine (C-I), carbon–sulfur-, or sulfur-sulfur bonds in modified peptides and proteins. [9-11] This method works independently of molecular size, and a single radical in a whole protein can easily be generated with high yield. The motivation for creating such radical species is that the fragmentation chemistry of hydrogen deficient radicals differs from that of even electron species, which enables unique experiments to be carried out. Radical directed dissociation of biomolecules in the gas phase can directly identify post translational modification sites, distinguish peptide epimers, and even probe protein tertiary structure in vacuo. [12-15]

Radical directed dissociation (RDD) in hydrogen deficient radical peptides typically involves migration of the radical from the initial position where it was created to the site where dissociation is ultimately observed. These radical migration reactions, which all involve hydrogen atom transfers, are influenced by both thermodynamics and kinetics.

The enthalpy of any given radical migration reaction can be easily estimated by determination of the relevant carbon-hydrogen (C-H) bond dissociation energies (BDEs) of both the radical donor and acceptor. Large BDEs indicate highly reactive radicals which will be enthalpically favored to migrate to sites with lower BDEs in the absence of kinetic constraints. Previously, we have shown that, *on average,* the relative abundance of backbone fragments and side chain losses observed for a series of peptides correlated well with the relevant BDEs; radical directed dissociation was favored for those sites with low C-H BDEs. [16] However, radical migration within *any individual* peptide will be kinetically influenced by the relevant activation energies, which are a function of three-dimensional structure and sequence dependent steric constraints. For example, in very small, rigidly constrained peptides, high barriers to radical migration prevent radical isomerization and lead to different fragmentation patterns. [17-18] On the other hand, similar fragmentation patterns have been observed in small flexible peptides, indicating that radical migration can also be facile. [19-20]

In the present work, we focus on kinetic constraints rather than thermodynamics. More specifically, we have examined a series of isomers where dissociation was investigated as a function of radical initiation site. For example, *ortho*-, *meta*-, and *para*- benzoyl radical modified peptide isomers reveal that even minor changes in radical initiation site can significantly influence subsequent dissociation pathways. A cyclic peptide yields virtually identical fragmentation patterns for three distinct radical isomers in the +1 charge state, yet the +2 charge state of the same peptide produces highly distinct dissociation spectra for all three isomers. In order to obtain more detailed structural

insight into these results, we carried out molecular dynamics simulations. Deuterium labeling was used to experimentally map out one complete migration pathway, which was used to calibrate the molecular dynamics simulations. Subsequent investigation revealed that structural flexibility accounts for the different results in the +1 versus +2 charges states of the cyclic peptide. Alignment of the radical donors and acceptors is the primary controlling factor that distinguishes the results from *ortho* versus *meta* and *para* radical isomers.

4.2 Experimental methods

Materials. Peptides (RGYALG, RYLPT, cyclo-(RGDyK)) were purchased from American Peptide Company (Sunneyvale, CA). 2-(hydroxymethyl-iodobenzoate)-18-crown-6 ether and N-hydroxysuccinimide (NHS) activated iodo-benzoyl ester were synthesized previously. [21] Sodium iodide, chloramine-T, sodium metabisulfite and other organic solvents were purchased from Thermo-Fisher Scientific. α-d_2-Glycine, α-d_1-Alanine, iso-propyl-d_7-Leucine and α-d_1-Leucine were purchased from CDN Isotopes (Pointe-Claire, Quebec, Canada), while β-d_2-Tyrosine was purchased from Cambridge Isotope Laboratories (Andover, MA). Fmoc-protected amino acids were purchased from Anaspec (San Jose, CA) or LC Sciences (Houston, TX). Wang resin and 2,6-dichlorobenzoyl chloride (DCB) (Acros Organics), fluorenylmethyloxycarbonyl-O-succinimide (Fmoc-oSu) and tetramethylammonium hexafluorophosphate(HCTU) (ChemPep Inc., Miami, FL), isopropylsilane(TIPS)(Sigma Aldrich) were also purchased.

Peptide derivatization. Peptides were labeled at the *N*-terminus with NHS activated iodo-benzoyl ester (2X molar ratio) in 1:3 borate buffer (0.2M, pH 8.5) : dioxane solution for 30 mins at 40 ℃. The side product at arginine and tyrosine side chains were removed by incubation in 1M hydroxylamine (adjust pH to 8-9 by NaOH) for 4 hours. Tyrosine in cyclo-(RGDyK) was iodinated with sodium iodide and chloramine-T at room temperature, after 1 minute reaction time, excess sodium metabisulfite was added to quench the reaction. Stoichiometric quantities of reagents (1:2:1:2 molar ratio of peptide/sodium iodide/chloramine-T/sodium metabisulfite) were used to limit the iodination extent and produce mainly mono-iodinated tyrosine. A reversed phase cartridge (Michrom Bioresources, Inc., Auburn, CA) was used for peptide desalting and purification.

Synthesis of deuterium labeled RGYALG. Fmoc protected amino acids (e.g., α-d_2-Glycine, β-d_2-Tyrosine, etc) were synthesized by reaction with 1X Fmoc-oSu and 1X $NaHCO_3$in 1:1 dioxane: H_2O solution overnight. After dissolving reaction mixture in 5% HCl, the product was taken up using ethyl acetate and washed with 0.1M HCl and water. Following drying with anhydrous Na_2SO_4, organic solvent was evaporated away and the protected amino acid was crystallized. Peptides were synthesized by solid phase methodology using Wang-resin and Fmoc chemistry. HCTU and piperidine was used for carboxyl group activation and amine group deprotection, respectively, whereas DCB was used for adding the first residue to Wang resin. Peptides were cleaved from the resin with 95:2.5:2.5 TFA:H_2O:TIPS.

Photodissociation mass spectrometry. Peptides (10 μM) were dissolved in 50:50 H_2O:CH_3OH with 0.1% acetic acid and electrosprayed into an LTQ linear quadrupole ion trap mass spectrometer (Thermo Fisher Scientific, San Jose, CA). 50 μM 2-(hydroxymethyl-iodobenzoate)-18-crown-6 ether was mixed with 10 μM peptide to form peptide-crown complexes. 266 nm photons were generated from the 4th harmonic generation of a Nd:YAG laser (Continuum, Santa Clara, CA). The back plate of the instrument was modified with a quartz window to transmit UV photons into the linear ion trap. Laser pulses were synchronized to the isolation step via a digital delay generator. The isolation window for precursor ions in collision induced dissociation and photodissociation was set between 3 to 10 m/z with an activation value q=0.25 and default activation time 30 ms. For experiments utilizing deuterium labeled peptide to track the radical migration, the precursor ion isolation window was set at 1 m/z. Activation parameters were held constant for experiments where similarity scores are calculated.

Fragmentation pattern similarity score

$$S = 1 - \frac{\sum_i \left| I_m^1(i) - I_m^2(i) \right|}{\sum_i I_m^1(i) + I_m^2(i)}$$

Of all ions (*i*), I_m^1 and I_m^2 are intensities of an ion at m/z = " m " in two spectra excluding precursor ions. [22]A similarity score (S) value of 1 represents two spectra that are exactly the same. An in-house JAVA program was used to automatically calculate S from the peak lists of two mass spectra.

C-H bond dissociation energy calculations. GaussView 5.0 was used to build *N*-methyl-benzoylamide, which was used to model benzoic acid labeled peptides. Isodesmic reactions [23] were used to calculate C-H bond dissociation energies (BDEs) at *ortho*-, *meta*-, and *para*- positions of *N*-methyl-benzoylamide with C_6H_5-H (472 kJ/mol) [24] as reference molecule. Energy calculations were performed at the B3LYP/6-31G(d) level of theory using Gaussian 09 Version 8.0.

Molecular modeling. MacroModel, version 9.9, (Schrödinger, LLC, New York, NY) molecular mechanics software package was used to build benzoic acid modified RGYALG and cyclo-(RGDyK) and perform all molecular modeling simulations. Arginine side chains were protonated first, followed by lysine side chains for higher charge states. The OPLS force field [25] was used for all calculations with the dielectric constant, $\varepsilon = 1.0$. Extended cutoffs were used for dipole-dipole interactions. Energy minimization was performed using the Polak-Ribiere Conjugate Gradient method with a derivative convergence criterion of 0.05 kJ/Å·mol. Conformational searches with the Monte Carlo multiple minimum algorithm and enhanced torsional sampling were used with a maximum number of 10,000 steps. 100,000 conformations were saved with an interval of 0.1 ps during 10 ns molecular dynamics. We chose 500 K - 750 K as molecular dynamics temperature to explore the peptide potential energy surface. These values are comparable to previous MD calculations for peptides in the gas phase and work well in our systems.[26]

4.3 Results and discussion

4.3.1 Fragmentation of *ortho-*, *meta-*, and *para-* iodobenzoyl modified peptide radical isomers

Radical isomers with the initial radical site at the *ortho-*, *meta-*, or *para-* position of the benzoyl group in *N*-iodobenzoyl-RGYALG were generated by 266 nm UV photodissociation to selectively cleave the photolabile C-I bonds and leave σ radicals on the benzene rings. The radical ions were subsequently re-isolated and subjected to CID as shown in Figures 4.1a-c. The results are typical for dissociation of a hydrogen deficient radical peptide, i.e. side chain losses (e.g., -43L, -56L, -106Y) and selective backbone fragmentation (a_3 only) are observed. Consecutive side chain losses are also observed in low abundance (e.g., -56L-CO_2, -43L-CO_2) suggesting multistep radical migrations occur to a lesser degree. Although the observed fragmentation channels for the *ortho-*, *meta-*, or *para-* benzoyl radical modified RGYALG isomers are very similar, there is some variation in the degree to which each dissociation channel is populated. In particular, the relative intensity for the a_3 ion from the *ortho-* radical isomer is significantly more abundant than is observed for the *meta-* and *para-* radical isomers. A similarity score (S, defined in experimental methods) is used to quantitatively characterize the similarity between two fragmentation patterns. An S score of one implies that two spectra are identical with the same distributions of relative intensities; scores lower than one indicate less similarity. The reported similarity scores conservatively have uncertainties of ±0.05. Similarity scores are indicated with brackets between each pair of spectra in Figure 4.1. The *meta*-isomer (Figure 4.1b) is fairly similar (S=0.85) to the *para-* isomer (Figure

4.1c), whereas the *ortho*- isomer is more distinct relative to both other spectra (S=0.74, 0.59 for *para* and *meta*, respectively). The lower scores for the *ortho*-isomer are primarily due to significantly increased peak intensity for the a_3 and leucine side chain loss fragments.

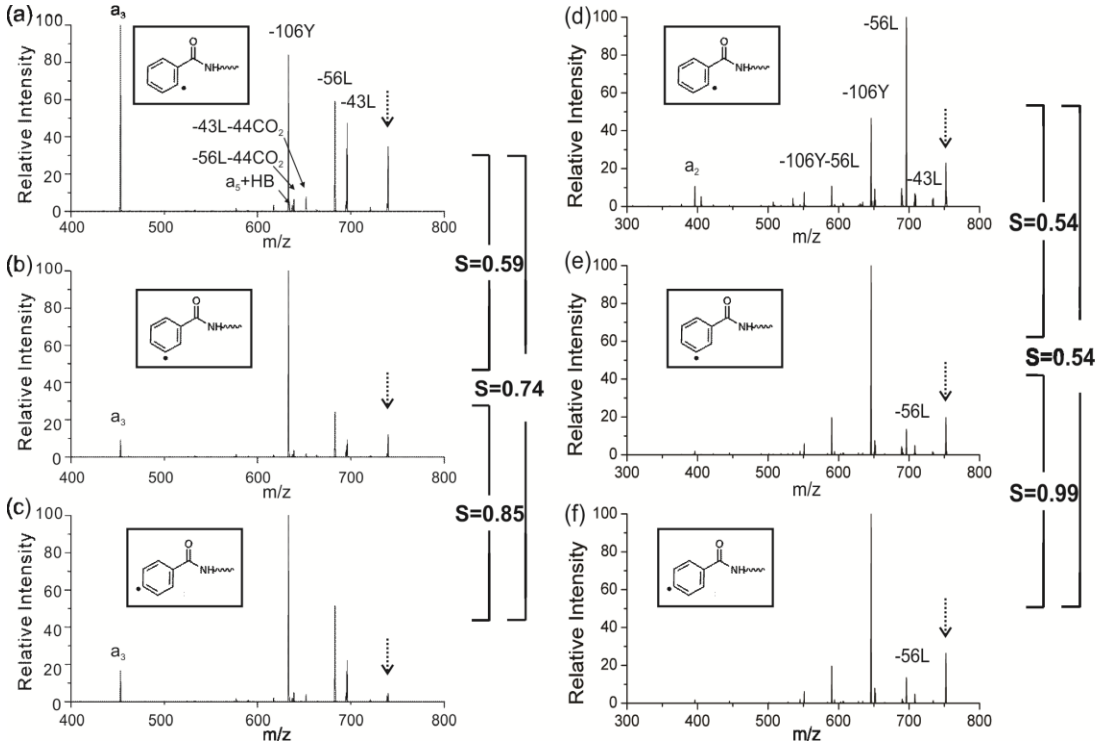

Figure 4.1.(a-c) CID spectrum of radical peptide *N*-benzoyl-RGYALG in the +1 charge state with initial radical at (a) *ortho*-, (b) *meta*-, or (c) *para*- position of benzoyl labeling group at *N*-terminus. (d-f) CID spectrum of radical peptide *N*-benzoyl-RYLPT in the +1 charge state with initial radical at (d) *ortho*-, (e) *meta*-, or (f) *para*- position of benzoyl labeling group at *N*-terminus. Side chain losses are abbreviated, i.e. -43L represents 43 Da side chain loss from leucine. Similarity scores (S) are indicated for each pair. The relevant radical precursor for each spectrum is indicated in the inset box, and precursor ions are indicated by a downward arrow.

As an approximation to benzoic acid modified RGYALG, the BDEs for the *ortho*-, *meta*- and *para*- C-H bonds in *N*-methyl-benzoylamide were calculated to be 461, 473, and 474 kJ/mol, respectively. These benzene radical isomers have very similar BDEs and

are predicted to be very reactive (e.g., the C-H BDE values of all tertiary carbons in 20 amino acids range from 319 to 399 kJ/mol). Thermodynamics are therefore not anticipated to dictate the behavior of these radical isomers to any significant extent. The nature of our experiments, which utilize low energy collisional activation, should also favor kinetic products. The variations in fragmentation observed in Figure 4.1 are therefore most likely due to the influence of positional isomerism on relevant transition state geometries that dictate radical migration. The details of migration in this system were mapped out with deuterium labeling and molecular mechanics calculations that are reported further below.

Figures 4.1d-f show the CID spectra of radical isomers for another peptide, *N*-benzoyl-RYLPT. Side chain losses (e.g., -56L, -106Y) along with few radical initiated backbone fragmentations (e.g., a_2) are observed. The spectrum for the *meta*- isomer shown in Figure 4.1e is very similar to that for the *para*- isomer in Figure 4.1f (S=0.99). Thus for RYLPT, the *para* and *meta* positional isomers are essentially identical in terms of influence on radical migration kinetics. In contrast, the *ortho*- isomer yields an obviously more distinct spectrum as shown in Figure 4.1d (S=0.54, 0.54). This is reminiscent of the results from the *N*-benzoyl-RGYALG isomers, where the *ortho*- isomer also exhibited the greatest difference. Taken together, these results suggest that the *ortho*- isomers are most distinct in terms of ability to influence the kinetics of radical migration. This observation is not unexpected given that both the *meta* and *para* isomers yield radicals which are on the end of the benzoyl addition, whereas the *ortho* isomer yields a radical that is directed back towards the point of attachment. Although it is clearly possible in some cases to

accommodate the *para* to *meta* shift by modest rotation or shifting of the benzoyl group, it is not possible to achieve similar alignment with the *ortho* isomer.

4.3.2 Fragmentation of cyclic peptide radical isomers

A series of radical isomers for a small cyclic peptide cyclo-(RGDyK) (the small cap y indicates D-tyrosine) were subjected to collisional activation and the results are shown in Figure 4.2. These radical isomers were produced by several methods, and the radical initiator is identified within each spectrum. Figure 4.2a shows CID of the +1 cyclo-(RGDyK)$^{\bullet}$ radical isomer, which was produced by intermolecular radical migration.**Error! Bookmark not defined.** In this method, a noncovalent complex between a peptide and a radical precursor (i.e., *ortho*-iodobenzoyl derivatized 18-crown-6) is isolated in the ion trap. The iodine atom in the radical precursor is then selectively removed by photodissociation. The resulting phenyl radical is very reactive and abstracts a hydrogen atom from the peptide. Subsequent activation steps isolate and then fragment the peptide radical. In Figure 4.2b, a *para*-iodobenzoyl derivatized 18-crown-6 radical precursor was used. In addition to the crown ether method, chemical iodination at tyrosine side chain was used as described previously. Figure 4.2c shows the dissociation spectrum of cyclo-(RGDy•K) radical generated by tyrosine iodination. Most peaks in Figures 4.2a-c correspond to radical directed side chain losses from lysine (-•NH_2, -43K, -58K, -71K), tyrosine (-106Y) and aspartic acid (-44D) residues. No backbone dissociation is detected, which is not surprising because at least two backbone bonds would need to be cleaved for fragmentation to be observable. A rich fragmentation

pattern originating from the lysine side chain indicates that the radical can freely migrate to almost every carbon on its aliphatic chain.[27] Although the arginine side chain provides a similar target for radical attack, no side chain losses from arginine are observed. The arginine side chain is also the most probable location for protonation, which may enhance kinetic barriers via restricted conformational flexibility and could also complicate detection if the side chain loss retained the proton.

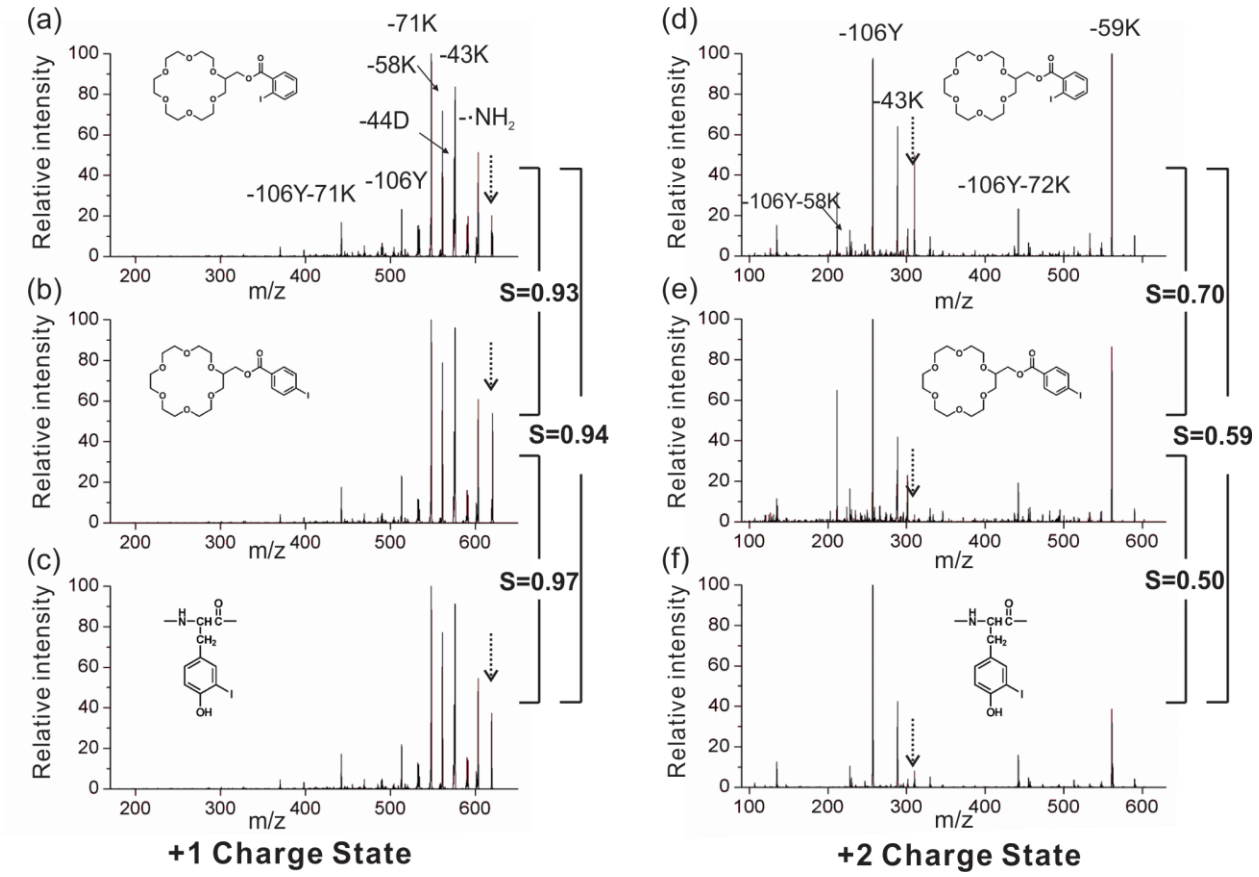

Figure 4.2. CID spectrum of cyclo-(RGDyK)• in the +1 (a, b, c) and +2 (d, e, f) charge state with the radical introduced by *ortho*-iodobenzoyl modified 18-crown-6 based non-covalent radical delivery (a, d), *para*-iodobenzoyl modified 18-crown-6 (b, e) and tyrosine side chain iodination (c, f). Labeling of the spectra follows the same pattern established in Figure 4.1.

In Figures 4.2a and 4.2b, the initial sites where the radical transfers to the peptide are unknown. Given the steric differences caused by the *ortho* versus *para* substitution, it is unlikely that the initial sites are the same for Figures 4.2a and 4.2b. Similarly, it is unlikely that radical transfer via abstraction of an aromatic tyrosine hydrogen atom will occur due to enthalpic considerations. Therefore, the precursor ions in Figures 4.2a, 4.2b and 4.2c should all be different isomers of cyclo-(RGDyK)•. The striking similarity between all three spectra obtained by activation of the different isomers is therefore quite unexpected. Analogous experiments conducted on RGYALG yielded significantly less similar spectra (see Figure 4.7).

The dissociation spectra for cyclo-(RGDyK)• isomers in Figures 4.2a-c have extremely high similarity scores (0.94, 0.97, and 0.93), indicating very little difference in fragmentation between the various isomers. This suggests that barriers to radical migration via numerous pathways for this peptide are likely low and comparable in magnitude. From an enthalpic standpoint, the radical sites which yield the fragments observed in Figures 4.2a-c are similar (BDEs ranging from 390 to 416 kJ/mol). A flat thermodynamic surface also favors a flat kinetic surface because endothermic reactions cannot contribute to kinetic barriers. Since the radicals initially start at different locations but ultimately yield very similar fragmentation patterns, the results further suggest that multiple migrations are occurring, which allows equilibration of the various isomers. The cyclic nature of the peptide restricts the overall available conformational space; however, this may actually facilitate interactions between the flexible lysine side chain and the remainder of the peptide, allowing migration to occur freely.

The situation changes dramatically when another charge is added to the peptide. Analogous experiments were conducted on the +2 charge state and are shown in Figures 4.2d, 4.2e and 4.2f. The relative intensities of several side chain losses are notably different compared with those observed in the +1 charge state. Interestingly, the similarity scores also change substantially (0.59, 0.50, 0.70), indicating that kinetic barriers are preventing the free migration observed in the +1 charge state. The addition of the second charge should occur on the side chain of lysine, which is by far the most basic available site. Intramolecular solvation of the additional charged site and Coulombic repulsion between the charges will likely lead to significant stiffening of the peptide structure and restriction of side chain flexibility, which will both serve to increase kinetic barriers to migration. This hypothesis is supported by molecular modeling which will be discussed further below.

4.3.3 Pinpointing radical migration with deuterium isotope labeling

In Figures 4.1a-c, the a_3 fragment intensity serves as a diagnostic feature to distinguish between the *ortho* and *meta* or *para* positional isomers. An abundant a_3 ion is only formed for the *ortho*-isomer, suggesting favorable kinetics exist for this migration pathway. In order to explore the structural features (which) that lead to these favorable kinetics in greater detail, it is necessary to determine the exact migration route. It has been well established previously that immediately prior to formation of the a_3 ion, the radical must migrate to the tyrosine β carbon as shown in Scheme 4.1c. However, the radical could arrive at the tyrosine β carbon via direct migration or through a multistep

route. To determine the exact radical migration pathway, we prepared a series of deuterium isotope labeled peptides. Collisional activation of deuterium labeled tyrosine (Tyr β d2) yields an abundant a_3(d1) ion as shown in Figure 4.3a. Direct migration of the initial radical would lead to deuterium on the N-terminus and generation of an a_3(d2) ion. The results are not consistent with direct migration but rather indicate that deuterium has migrated to a site within the ALG residues. It should be mentioned that some amount of direct migration cannot be completely excluded because a small quantity of a_3(d2) is observed in Figure 4.3a, but direct migration is clearly not the primary pathway. The results suggest that initial radical at the *N*-terminus migrates to an intermediate site within ALG first, followed by subsequent migration to the tyrosine β carbon.

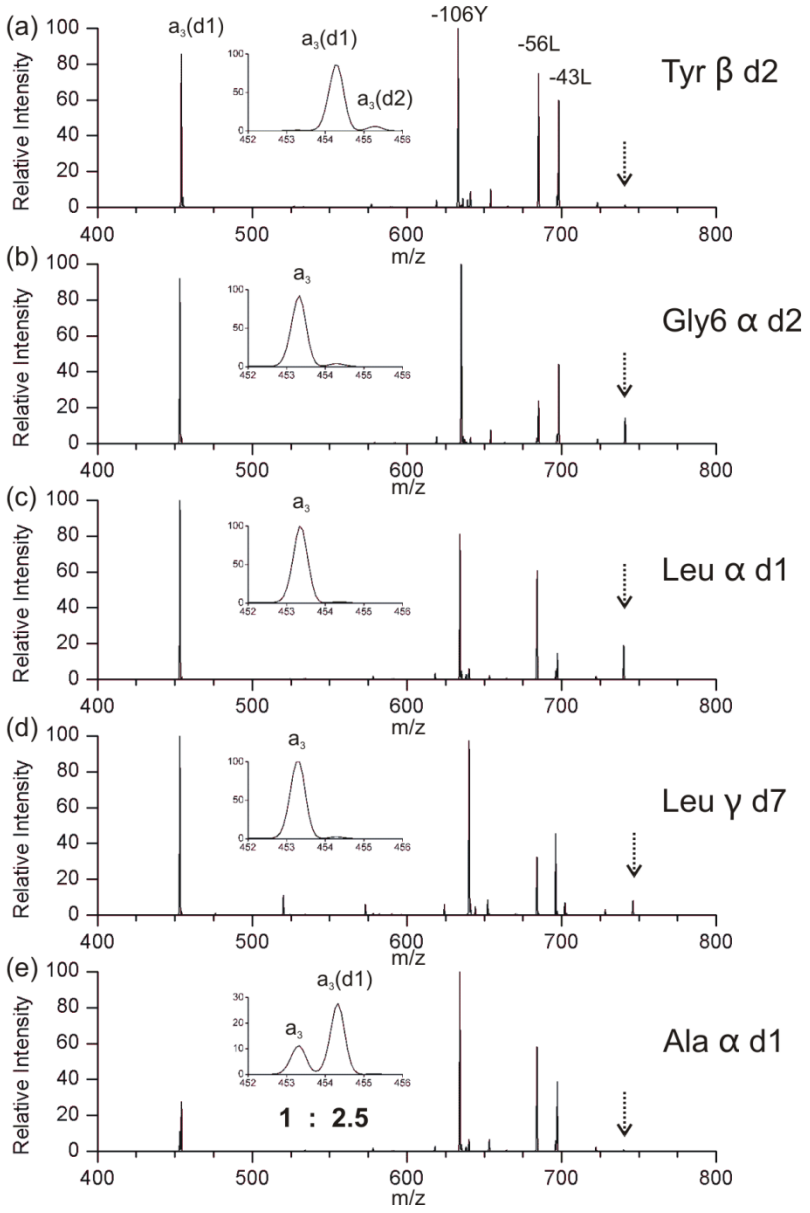

Figure 4.3. CID spectrum of *N*-benzoyl-RGYALG (+1) with radical at the *ortho*-position of benzoyl group and deuterium labeling at (a) Tyr β d2, (b) Gly6 α d2, (c) Leu α d1, (d) Leu γ d7 (isopropyl), and (e) Ala α d1. Down arrows indicate precursor ions.

In an attempt to determine which intermediate site within the ALG residues the *ortho*-benzoyl radical migrates to, additional deuterium labeled peptides (i.e, Gly6 α d2, Leu α d1, Leu d7 isopropyl, Ala α d1) were synthesized and the results are shown in Figures 4.3b-e, respectively. None of the labeling sites at Gly6 or Leu are attacked by the benzoyl radical, otherwise an a_3(d1) ion would be observed as the major peak in the isotope distribution. However, the observation of a_3(d1) in Figure 4.3e suggests that the Ala α deuterium was abstracted directly as shown in Scheme 4.1a. Successive radical migration from the Ala α carbon to the Tyr β carbon is expected to be a facile process through a transition state with a six-membered ring. Our previous work has shown that Tyr β radical can migrate from the carbon α position at an adjacent glycine residue.[28] Similarly, the Ala α radical should also be able to migrate to adjacent Tyr β carbon (Scheme 4.1b).

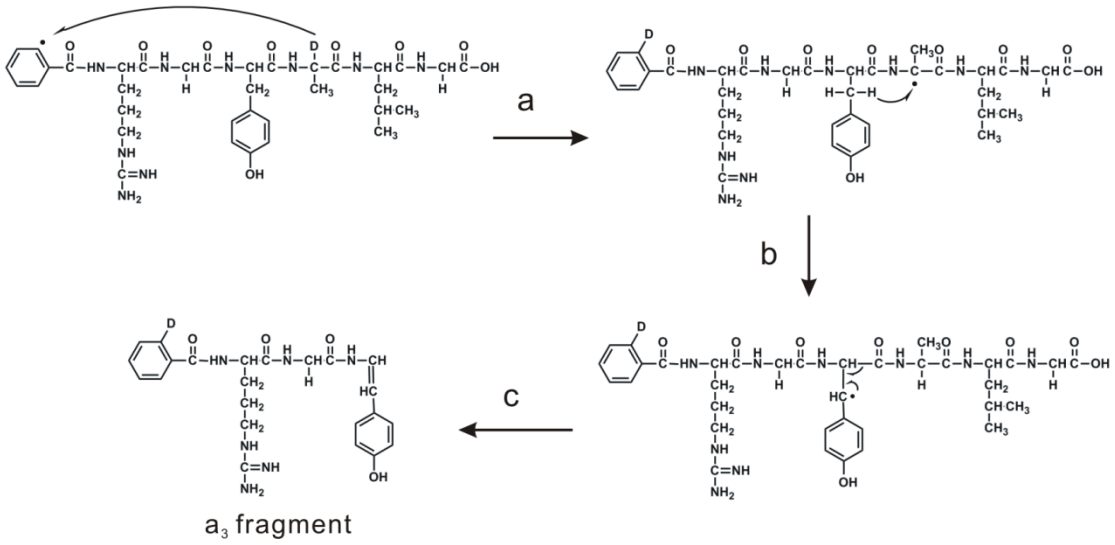

Scheme 4.1. Radical migration pathway and β scission mechanism for generation of a_3 fragment from *N*-benzoyl-RGYALG with the initial radical at *ortho*- position of benzoyl group.

In order to determine if there are additional intermediate sites between the initial *ortho*-benzoyl radical and the Ala α carbon (Scheme 4.1a), the a_3(d1) isotope peak in Figure 4.3e was reisolated and dissociated to identify the position of the deuterium. A benzoyl fragment containing a deuterium (Figure 4.8) suggests that the Ala α deuterium was abstracted directly by the benzoyl radical. Data from deuterium labeling at the Gly2 α position also suggests that Gly2 α hydrogens are not involved in the major fragmentation pathway for a_3 ion (Figure 4.9). It is worth noting that observation of the a_3(d0) isotope peak in Figure 4.3e is inconsistent with the proposed two step migration mechanism (Scheme 4.1) suggesting the existence of other minor migration routes not involving the Ala α carbon. The intensity ratio between a_3(d0) and a_3(d1) is 1: 2.5 in Figure 4.3e, suggesting the major pathway is the one outlined in Scheme 4.1. Kinetic isotope effects further support radical migration involving the Ala α hydrogen. The intensity of the a_3 ion in Figure 4.3e decreases significantly compared to that of the unlabeled peptide (see Figure 4.1a), which is consistent with a kinetic isotope effect disfavoring abstraction of deuterium.

Figure 4.4 shows the dissociation spectra of *meta*- and *para*- benzoyl radical RGYA(α d1)LG isomers. In contrast to *ortho*- isomer in Figure 4.3e, observation of a_3(d0) ion as the major isotope peak in Figure 4.4 indicates that the radical migration via the Ala α carbon is not a major pathway to generate the a_3 fragment for these two isomers. The relative intensity ratio between a_3(d0) and a_3(d1) is 1 : 0.63 for the *meta*- radical isomer (Figure 4.4a) and 1 : 0.47 for the *para*- isomer (Figure 4.4b). Compared with the 1: 2.5 ratio for the *ortho*- isomer in Figure 4.3e, the extent of radical migration to Ala α occurs

with the following preference: *ortho* > *meta* > *para*. This is consistent with the spectra in Figures 4.1a-c showing that *ortho*- radical isomer has the largest relative intensity of a_3. This order is found to be related to peptide 3D structure based on molecular dynamics calculations as discussed below.

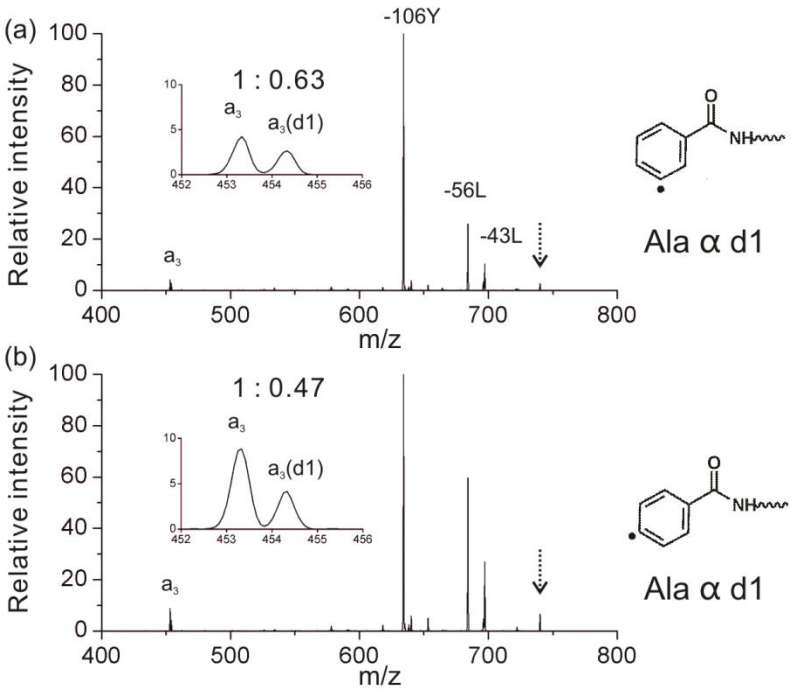

Figure 4.4. CID spectrum of *N*-benzoyl-RGYA(α d1)LG (+1) radical isomers with deuterium labeling at Ala α d1 and radical at the *meta*- position (a) and *para*- position (b) of the benzoyl group. Downward arrows indicate precursor ions.

4.3.4 Molecular modeling

Conformational searches and molecular dynamics (MD) simulations were carried out to determine in greater detail the influence of peptide structure and dynamics on radical migration. Force field parameters for odd-electron radicals are not readily available, so saturated peptides were constructed instead. Distances between hydrogen atoms representing potential radical donor and acceptor sites were monitored in lieu of calculating distances involving actual radical sites.

N-benzoyl-RGYALG

The lowest potential energy structure for *N*-benzoyl-RGYALG obtained from a molecular mechanics conformational search is shown in Figure 4.5a. Interestingly, the *N*-terminal benzoyl group is very close to the alanine residue, which should kinetically facilitate radical migration from the benzoyl group to the Ala α carbon. In an attempt to understand why the *ortho*- benzoyl radical isomer favors radical migration to the Ala α carbon more than the other two isomers, the distances from the Ala α hydrogen to benzoyl *ortho*-, *meta*-, and *para*-hydrogens, were monitored during a 10 ns MD simulation at 500K. Because hydrogen transfer can only occur when the donor is in very close proximity to the acceptor, the probability of residue contact at a distance below 4 Å was calculated for 100,000 sampled structures (Figure 4.10). The *ortho*- benzoyl hydrogen has the highest probability for close contact with the Ala α hydrogen (26%), whereas the probabilities for the *meta*- and *para*- hydrogens are 8.6% and 3.6%, respectively. This trend is consistent with the experimental data on the extent of radical migration to the Ala α carbon which follows the same order: *ortho* > *meta* > *para*.

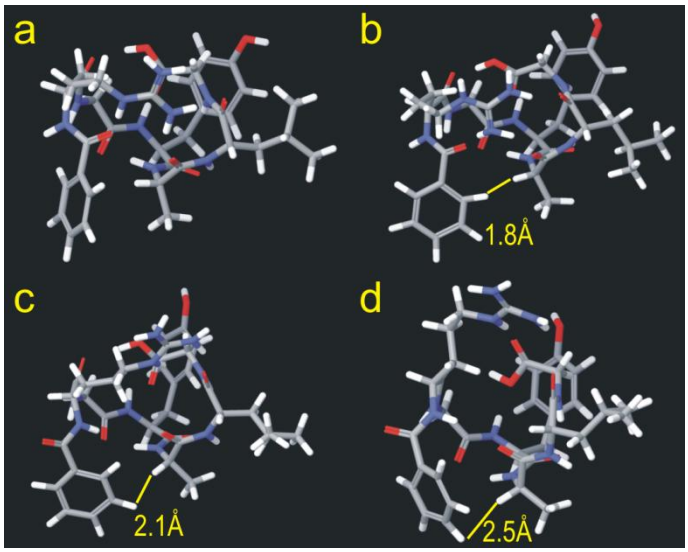

Figure 4.5. (a): The lowest potential energy structure of *N*-benzoyl-RGYALG resulting from a Monte Carlo Multiple Minimum conformational search. (b-d): Structures with the smallest distance from the Ala α hydrogen to the *ortho*-benzoyl hydrogen, *meta*-benzoyl hydrogen, or *para*-benzoyl hydrogen obtained during 10 ns of MD simulations at 500K are shown in (b), (c), (d), respectively.

Figures 4.5b-d show the conformations obtained during molecular dynamics with the smallest distance from the Ala α hydrogen to the *ortho*- (Figure 4.5b), *meta*- (Figure 4.5c), or *para*- (Figure 4.5d) benzoyl hydrogen. All distances are smaller than 3 Å and should be satisfactory for radical migration; however, distance is not the only structural parameter that can influence radical migration kinetics. Hydrogen transfer preferentially proceeds via a linear or near-linear pathway in the transition state.[29] The alignment of bonds involved in potential hydrogen transfer from benzoyl *ortho*- hydrogen to the Ala α carbon (Figure 4.5b) is near-linear and thus optimal for hydrogen transfer. In comparison, the *meta*- and *para*- isomers have unfavorable non-linear orientations and much higher activation barriers are expected as a consequence. The average results are also consistent with these snapshots, with a significantly higher fraction of the ortho-hydrogen isomer exhibiting near linear alignment (see Figure 4.11).

Cyclo-(RGDyK) in the +1 and +2 charge state

The fragmentation similarities for cyclo-(RGDyK) radical isomers in Figure 4.2 vary with charge state. As suggested above, this may be caused by restricted conformational space in the +2 charge state which may inhibit radical migration. We carried out MD simulations for both charge states and monitored several distances between side chains. Figure 4.6 shows the statistical analysis of distances from 100,000 conformations sampled during 10 ns of MD at 750K. Distances from the tyrosine *ortho*-hydrogen (the initial radical site in tyrosine-iodinated peptide) to the lysine δ-hydrogen are quite different between the +2 (Figure 4.6a) and +1 (Figure 4.6b) charge states. In the +1 charge state, the peptide exhibits a very broad distribution of distances, suggesting fairly

unbiased occupation of the conformational space. For the +2 charge state, two distinct populations are clearly observed. It should be mentioned that a slightly greater number of structures with close contact is observed in the +2 charge state, although the corresponding lysine side chain losses are not more abundant for the +2 charge state (Figures 4.2c and 4.2f). This may indicate that direct migration is not the primary mechanism that generates these fragments. The primary purpose of the data in Figures 4.6a and 6b is to illustrate potential differences in conformational space, not to elucidate migration pathways (as is the case in Figures 4.10 and 4.11).

In Figures 6c and 6d, the distances between the arginine δ hydrogen and the lysine δ hydrogen are shown. Both side chains are potential intermediate radical migration sites. In the +2 charge state, the protonation sites are most likely at lysine and arginine which leads to greater separation in space (> 6 Å) as shown in Figure 6c. In comparison, there is some contact (distance below 4 Å) between lysine and arginine side chains in the +1 charge state (Figure 4.6d), which again suggests larger conformational space which should be beneficial for radical migration. These MD simulations are consistent with the hypothesis that conformational flexibility and multiple migrations are the primary sources of the experimentally observed differences in dissociation between the +1 and +2 charge states as shown in Figure 4.2.

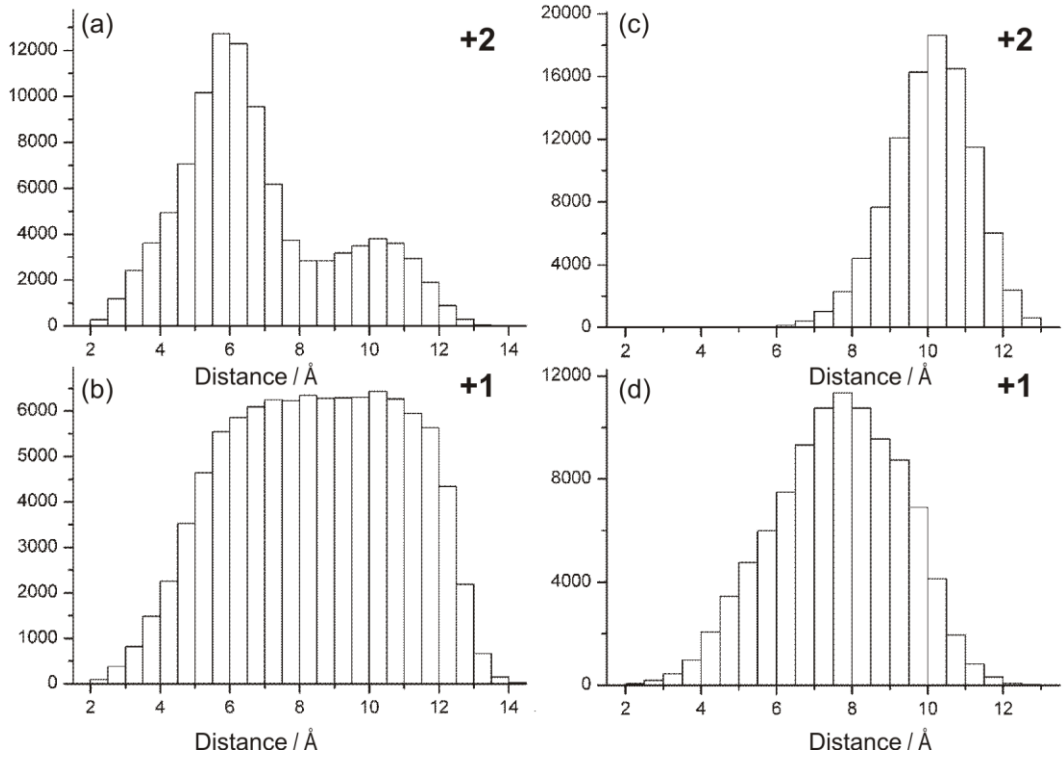

Figure 4.6. Histograms of monitored distances for cyclo-(RGDyK) in the +1 and +2 charge state during 10 ns molecular dynamics at 750K from 100,000 sampled conformations. Distances between the *ortho*-hydrogen in tyrosine side chain and the δ-hydrogen in lysine are plotted in (a) for the +2 charge state and (b) for +1. Distances between the δ-hydrogen in arginine side chain and the δ-hydrogen in lysine side chain are plotted in (c) for the +2 charge state and (d) for +1.

4.3.4 Conclusions

The present results illustrate that radical migrations in peptides are not unrestricted but can be significantly influenced by peptide 3D structure. Information on radical migration pathways can be derived from various approaches including evaluation of fragmentation pattern similarities among positional isomers, deuterium isotope labeling and molecular mechanics calculations. For example, site specific deuterium labeling in RGYALG reveals that the initial *ortho*-benzoyl radical at *N*-terminus prefers migration to the tyrosine β carbon indirectly via the alanine α carbon as an intermediate site. However, this radical migration pathway is kinetically disfavored for *meta*- and *para*- radical isomers as a result of steric hindrance. The charge state dependent fragmentation pattern similarities among cyclo-(RGDyK)• isomers indicate that radical migration pathways are sensitive to the peptide structural flexibility. A relatively wide conformational space in the +1 charge state allows sufficient residue contact to facilitate radical migration, whereas narrower conformational space in the +2 charge state results in higher energy barriers to radical migrations. Folded proteins are expected to have restricted conformational space due to high levels of intramolecular interactions, which should (in general) lead to larger kinetic barriers for migration. Results from this work suggest that radical migrations in proteins should be highly structure dependent, which should be beneficial for structure investigation.

4.3.5 Supplementary information

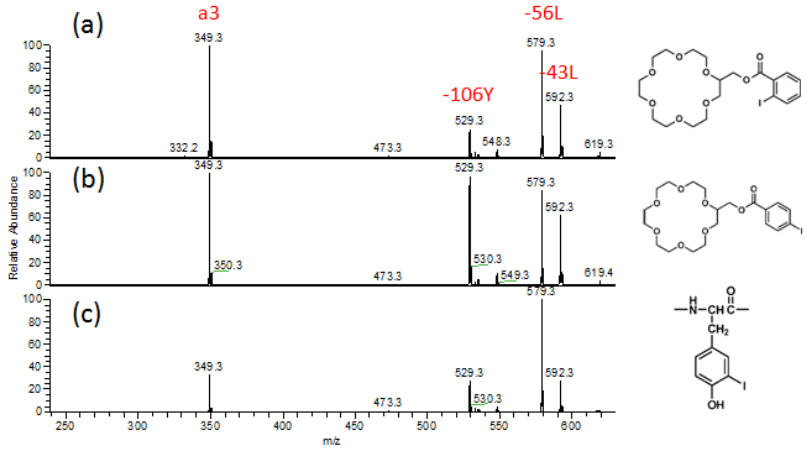

Figure 4.7. CID spectrum of RGYALG radical cation in the +1 charge state with radical introduced by (a) *ortho*-iodobenzoyl modified 18-crown-6 based non-covalent radical delivery; (b) *para*-iodobenzoyl modified 18-crown-6; (c) tyrosine iodination

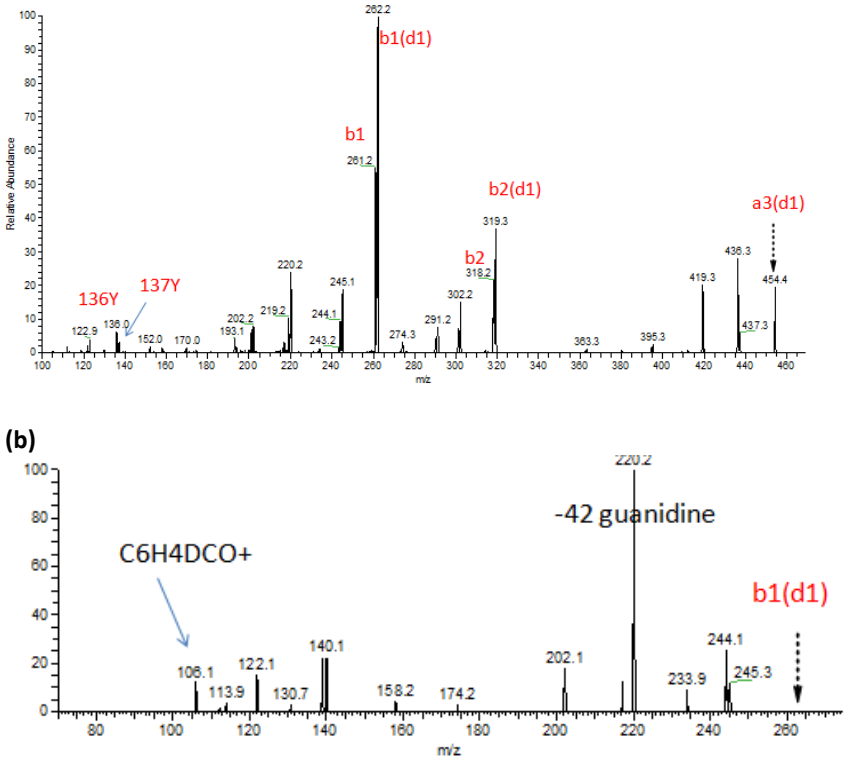

Figure 4.8. (a) CID spectrum of a_3(d1) ion in Figure 4e for *ortho*- radical peptide *N*-benzoyl-RGYA(α d1)LG. (b) CID spectrum of b_1(d1) in (a)

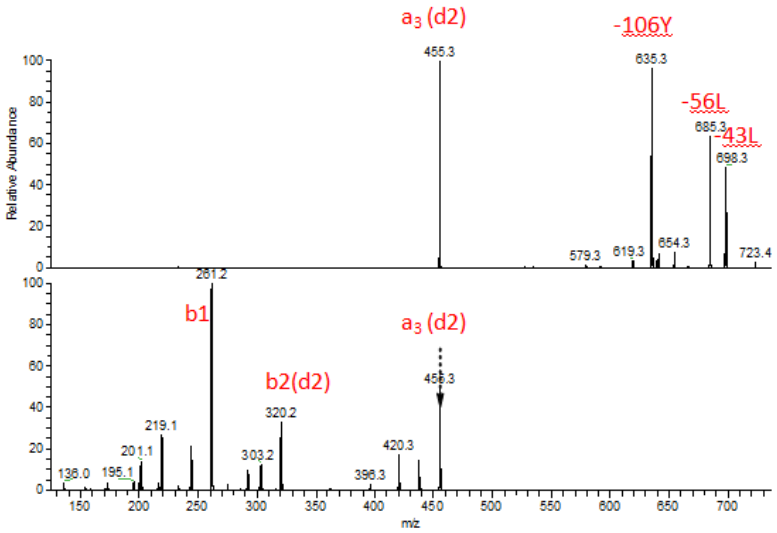

Figure 4.9. (a) CID spectrum of *ortho*- radical peptide *N*-benzoyl-RG(α d2)YALG (+1) with deuterium labeling at Gly2 α d2. (b) CID spectrum of a_3(d2) in (a)

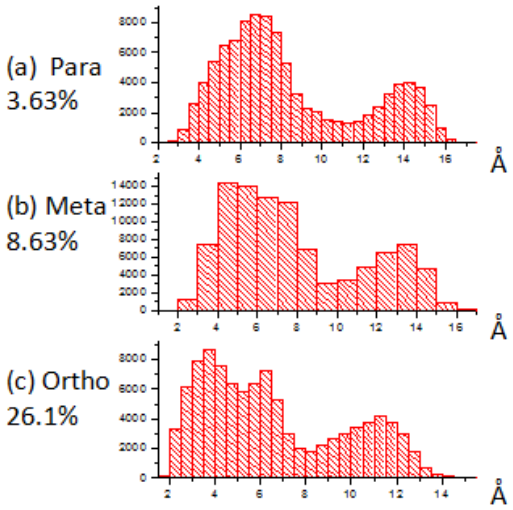

Figure 4.10. Statistical distance distributions from the Ala α hydrogen to the *para*-hydrogen (a), *meta*-hydrogen (b) and *ortho*-hydrogen (c) at benzoyl group of *N*-benzoyl-RGYALG during 10 ns MD with 100,000 saved conformations. The percentage represents the fraction with a distance below 4 Å

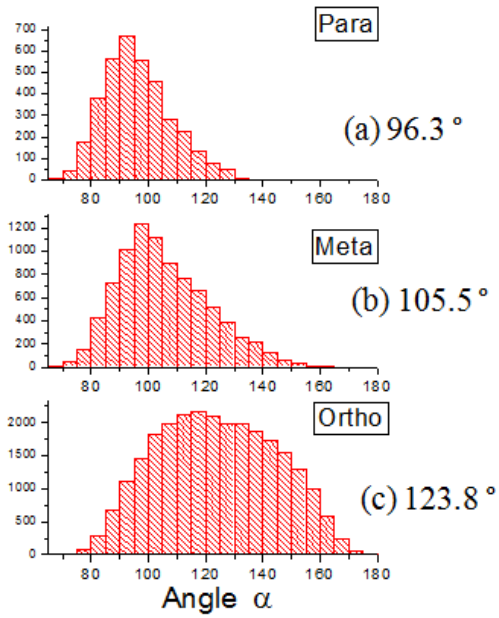

Angle α : for a radical migration reaction as below C_A• + H_B-C_B -> C_A-H_A + •C_B, the average angle of angle $C_AH_BC_B$ and angle $C_AH_AC_B$ is calculated and named α, which is used to characterize the linearity of the bond orientations during radical migration.

Figure 4.11. Statistical angle α distributions between bond Ala α C-H and the *para*-C-H bond (a), *meta*-C-H (b) and *ortho*-C-H (c) at benzoyl group of *N*-benzoyl-RGYALG during 10 ns MD at 500K with 100,000 saved conformations. Inserted value is the average angle. Angle α is only calculated when the H_A H_B distance is smaller than 4 Å

References

[1] Dean, R.T., Fu, S.L., Stocker, R., Davies, M.J.: Biochemistry and pathology of radical-mediated protein oxidation. *Biochem. J.* **324**, 1-18 (1997)

[2] Hawkins, C.L., Davies, M.J.: Generation and propagation of radical reactions on proteins. *Bba-Bioenergetics* **1504**, 196-219 (2001)

[3] Chu, I.K., Rodriquez, C.F., Lau, T.C., Hopkinson, A.C., Siu, K.W.M.: Molecular radical cations of oligopeptides. *J. Phys. Chem. B* **104**, 3393-3397 (2000)

[4] Headlam, H.A., Mortimer, A., Easton, C.J., Davies, M.J.: beta-scission of C-3 (beta-carbon) alkoxyl radicals on peptides and proteins: A novel pathway which results in the formation of alpha-carbon radicals and the loss of amino acid side chains. *Chem. Res. Toxicol.* **13**, 1087-1095 (2000)

[5] Masterson, D.S., Yin, H.Y., Chacon, A., Hachey, D.L., Norris, J.L., Porter, N.A.: Lysine peroxycarbamates: Free radical-promoted peptide cleavage. *J. Am. Chem. Soc.* **126**, 720-721 (2004)

[6] Hodyss, R., Cox, H.A., Beauchamp, J.L.: Bioconjugates for tunable peptide fragmentation: Free radical initiated peptide sequencing (FRIPS). *J. Am. Chem. Soc.* **127**, 12436-12437 (2005)

[7] Hao, G., Gross, S.S.: Electrospray tandem mass spectrometry analysis of S- and N-nitrosopeptides: Facile loss of NO and radical-induced fragmentation. *J. Am. Soc. Mass Spectrom.* **17**, 1725-1730 (2006)

[8] Lee, M.; Kang, M.; Moon, B.; Oh, H. B.: Gas-phase peptide sequencing by TEMPO-mediated radical generation. *Analyst* **2009,** *134* (8), 1706-1712.

[9] Ly, T., Julian, R.R.: Residue-specific radical-directed dissociation of whole proteins in the gas phase. *J. Am. Chem. Soc.* **130**, 351-358 (2008)

[10] Diedrich, J.K., Julian, R.R.: Site-specific radical directed dissociation of peptides at phosphorylated residues. *J. Am. Chem. Soc.* **130**, 12212-12213 (2008)

[11] Agarwal, A.; Diedrich, J. K.; Julian, R. R., Direct elucidation of disulfide bond partners using

ultraviolet photodissociation mass spectrometry. *Anal. Chem.* **2011,** *83* (17), 6455-6458.

[12] Tao, Y., Quebbemann N.R., Julian, R.R.: Discriminating D-Amino Acid-Containing Peptide Epimers by Radical-Directed Dissociation Mass Spectrometry. *Anal. Chem. Accepted.*

[13] Ly, T., Julian, R.R.: Elucidating the Tertiary Structure of Protein Ions in Vacuo with Site Specific Photoinitiated Radical Reactions. *J. Am. Chem. Soc.* **132**, 8602-8609 (2010)

[14] Zhang, X., Julian, R.R.: Investigating the gas phase structure of KIX with radical directed dissociation and molecular dynamics: Retention of the native structure. *Int. J. Mass Spectrom.* **308**, 225-231 (2011)

[15] Breuker, K., Bruschweiler, S., Tollinger, M.: Electrostatic Stabilization of a Native Protein Structure in the Gas Phase. *Angew. Chem. Int. Ed.* **50**, 873-877 (2011)

[16] Sun, Q.Y., Nelson, H., Ly, T., Stoltz, B.M., Julian, R.R.: Side Chain Chemistry Mediates Backbone Fragmentation in Hydrogen Deficient Peptide Radicals. *J. Proteome Res.* **8**, 958-966 (2009)

[17] Chu, I.K., Zhao, J., Xu, M., Siu, S.O., Hopkinson, A.C., Siu, K.W.M.: Are the radical centers in peptide radical cations mobile? The generation, tautomerism, and dissociation of isomeric alpha-carbon-centered triglycine radical cations in the gas phase. *J. Am. Chem. Soc.* **130**, 7862-7872 (2008)

[18] Ng, D.C.M., Song, T., Siu, S.O., Siu, C.K., Laskin, J., Chut, I.K.: Formation, Isomerization, and Dissociation of alpha-Carbon-Centered and pi-Centered Glycylglycyltryptophan Radical Cations. *J. Phys. Chem. B* **114**, 2270-2280 (2010)

[19] Wee, S., Mortimer, A., Moran, D., Wright, A., Barlow, C.K., O'Hair, R.A.J., Radom, L., Easton, C.J.: Gas-phase regiocontrolled generation of charged amino acid and peptide radicals. *Chem. Commun.* 4233-4235 (2006)

[20] Song, T., Ng, D.C.M., Quan, Q.A., Siu, C.K., Chu, I.K.: Arginine-Facilitated alpha- and pi-Radical Migrations in Glycylarginyltryptophan Radical Cations. *Chem-Asian J* **6**, 888-898 (2011)

[21] Ly, T., Zhang, X., Sun, Q.Y., Moore, B., Tao, Y.Q., Julian, R.R.: Rapid, quantitative, and site specific synthesis of biomolecular radicals from a simple photocaged precursor. *Chem. Commun.* **47**, 2835-2837 (2011)

[22] Dong, N.P., Liang, Y.Z., Yi, L.Z.: Investigation of Scrambled Ions in Tandem Mass Spectra. Part 1. Statistical Characterization. *J. Am. Soc. Mass Spectrom.* **23**, 1209-1220 (2012)

[23] Moore, B.N., Julian, R.R.: Dissociation energies of X-H bonds in amino acids. *Phys. Chem. Chem. Phys.* **14**, 3148-3154 (2012)

[24] Blanksby, S.J., Ellison, G.B.: Bond dissociation energies of organic molecules. *Acc. Chem. Res.* **36**, 255-263 (2003)

[25] Jorgensen, W.L., Maxwell, D.S., TiradoRives, J.: Development and testing of the OPLS all-atom force field on conformational energetics and properties of organic liquids. *J. Am. Chem. Soc.* **118**, 11225-11236 (1996)

[26] Tsaprailis, G., Somogyi, A., Nikolaev, E.N., Wysocki, V.H.: Refining the model for selective cleavage at acidic residues in arginine-containing protonated peptides. *Int. J. Mass Spectrom.* **195**, 467-479 (2000)

[27] Wee, S., O'Hair, R.A.J., McFadyen, W.D.: Comparing the gas-phase fragmentation reactions of protonated and radical cations of the tripeptides GXR. *Int. J. Mass Spectrom.* **234**, 101-122 (2004)

[28] Ly, T., Julian, R.R.: Tracking Radical Migration in Large Hydrogen Deficient Peptides with Covalent Labels: Facile Movement does not Equal Indiscriminate Fragmentation. *J. Am. Soc. Mass Spectrom.* **20**, 1148-1158 (2009)

[29] Moran, D., Jacob, R., Wood, G.P.F., Coote, M.L., Davies, M.J., O'Hair, R.A.J., Easton, C.J., Radom, L.: Rearrangements in model peptide-type radicals via intramolecular hydrogen-atom transfer. *Helv. Chim. Acta* **89**, 2254-2272 (2006)

Chapter 5

Radical additions to aromatic residues in peptides facilitate unexpected side chain and backbone losses

5.1 Introduction

Radical chemistry is emerging as an important tool in the arsenal of tandem mass spectrometry for peptide and protein characterization. A variety of radical directed dissociation (RDD) based methods have been recently developed to provide information about peptides and proteins including: sequence, post-translational modifications, and even higher-order structure [1-5]. Hydrogen deficient radical peptides can be generated in the gas phase by collision induced dissociation (CID) of modified peptides, including oxidative dissociation of peptide-metal complexes [6-8] and homolytic cleavage of labile bonds such as nitrate ester [9-10], peroxycarbamate [11], azo [12], nitroso [13], and tempo [14]. Low temperature plasma can also be used to generate peptide radicals in the source region of a mass spectrometer via ion/radical reactions [15-16]. Additionally, peptide radicals can be generated by photodissociation with site specificity and high yields, following homolytic bond cleavage of specific bonds. For example, 266 nm UV

photons can selectively cleave carbon–iodine (C–I), carbon–sulfur, or sulfur–sulfur bonds that are present in suitable chromophores. Subsequent to radical generation, RDD can be leveraged to facilitate both backbone and amino acid side chain fragmentation [17].

Numerous studies have investigated the mechanisms by which RDD occurs in peptides, and significant understanding has been achieved. Generally fragmentation in RDD is dictated by migration of the initially created radical to sites that are suitable for facile bond cleavage. The factors that influence radical migration and the most common dissociation pathways have been recently reviewed [18]. It is also well known within the odd-electron literature that radicals can undergo addition reactions, though these pathways have not been investigated in relation to hydrogen deficient peptide radicals. Nevertheless, experiments examining small neutral analogs, such as amino acids or dipeptides, have revealed that addition reactions are feasible, particularly where addition occurs at aromatic rings [19-25]. These studies revealed that branching ratios for addition versus migration or abstraction depend on both the reactivity of the aromatic σ-radical and the substrate target, and suggest the possibility that under appropriate conditions, radical addition reactions may be observed in larger, charged peptides.

In the present work, the gas phase reactions between large peptides and non-covalently attached radical benzoic acids are studied. A peptide complex with iodo-benzoic acid is isolated in the gas phase. Photodissociation mass spectrometry is used to cleave the C–I bond in the iodo-benzoic acid and generate a radical peptide complex. Further collisional

activation of the radical peptide complex results in radical migrations and also radical addition reactions at aromatic residues. The addition product can further dissociate via hydrogen loss or side chain fracture. For example, C_β–C_γ or C_α–C_β bond cleavage at tryptophan can be initiated by radical addition to the tryptophan indole ring. Intramoleuclar radical addition reactions in peptides are also studied by covalent modification with a radical precursor. A cross-linked peptide is generated after the intramolecular addition reaction, which subsequently dissociates into a variety of unexpected fragments including aromatic side chain migration products and internal fragment losses.

5.2 Experimental methods

Materials. Peptides (RGYALG, RYLPT, Ac-SYSMEHFRWGKPV-NH_2, VEPIPY) were purchased from American Peptide Company (Sunneyvale, CA, USA). Peptide RGY(O-methyl)ALG was purchased from QCB (Hopkinton, MA, USA). Fmoc-protected amino acids and Fmoc-Gly-Wang resin were purchased from Anaspec (San Jose, CA, USA) or LC Sciences (Houston, TX, USA). Fmoc-1-methyl-L-tryptophan was purchased from AstaTech (Bristol, PA, USA). Tetramethylammonium hexafluorophosphate (HCTU) (Chem-Pep Inc., Miami, FL, USA), 2-iodo benzoic acid, 3-iodo benzoic acid, 4-iodo benzoic acid, isopropylsilane (TIPS) and other solvents (Sigma-Aldrich, St. Louis, MO, USA) were also purchased. N-hydroxylsuccinimide activated 3-iodo-benzoyl ester was synthesized previously.

Peptide Synthesis and Derivatization. Peptides RGWALG and RGW(1-methyl)ALG were synthesized by solid phase methodology using Wang-resin and Fmoc chemistry. HCTU and piperidine were used for carboxyl group activation and amine group deprotection, respectively. Peptides were cleaved from the resin with 95:2.5:2.5 TFA:H_2O:TIPS. Peptide VEPIPY was labeled at *N*-terminus with *N*-hydroxylsuccinimide activated 3-iodo-benzoyl ester (2× molar ratio) in 1:3 borate buffer (0.2 M, pH 8.5):dioxane solution for 30 min at 40 ℃. Side products at tyrosine side chains were removed by incubation in 1 M hydroxylamine (adjusted pH to 8–9 by NaOH) for 4 h.

Photodissociation Mass Spectrometry. Peptides (10 μM) and 2-iodo benzoic acid (50 μM) were mixed in 20:80 H_2O:ACN with 10 mM NH_4Ac buffer and electrosprayed in negative mode into an LTQ linear quadrupole ion trap mass spectrometer (Thermo Fisher Scientific, San Jose, CA, USA). 10 μM *N*-benzoyl-VEPIPY peptide in 50:50 H_2O:ACN was electrosprayed in positive mode. 266 nm photons were generated from the fourth harmonic generation of a Nd:YAG laser (Continuum, Santa Clara, CA, USA). The back plate of the instrument was modified with a quartz window to transmit UV photons into the linear ion trap. Laser pulses were synchronized to the isolation step via a digital delay generator. The isolation window for precursor ions in collision induced dissociation and photodissociation was set between 1 to 10 *m/z* with an activation value q = 0.25 and default activation time 30 ms. Activation parameters were held constant for experiments where comparison of different fragmentation patterns are desired.

Computational Methods. GaussView 5.0 was used to build tryptophan amino acid, which was used to model aromatic radical addition reaction at position C2 of tryptophan

side chain in RGWALG. Energy calculations were performed at the B3LYP/6-31G(d) level of theory using Gaussian 09 Version 8.0. Transition state structures were found using the quasi-Newton synchronous transit (QST3) method. Harmonic vibrational frequency analysis revealed no imaginary frequency for structures at local minima and single imaginary frequency for transition state structures. The local minima associated with the transition state structures were verified using the intrinsic reaction coordinate (IRC) method. Activation energies were calculated from electronic energies and zero-point vibrational energies.

5.3 Results and Discussion

5.3.1Tryptophan Side Chain Fragmentation

A deprotonated non-covalent complex between RGWALG and 2-iodobenzoic acid is easily generated by electrospray ionization under gentle source conditions. The complex is formed due to hydrogen bonds between the guanidinium group in the arginine side chain and the carboxylic acid in benzoic acid. Collisional activation of this complex results simply in loss of neutral 2-iodobenzoic acid. In contrast, photoactivation (see Figure 5.1a) leads to homolytic cleavage of the carbon-iodine bond, generation of radical and non-radical RGWALG, and spontaneous fragmentation of radical RGWALG. Figure 5.1b shows the CID spectrum of the radical complex generated by loss of iodine (i.e., the peak labeled as –I in Figure 5.1a). The major product in Figure 5.1b is RGA(β•)ALG, which is generated by homolytic C_β–C_γ bond cleavage of tryptophan side chain leaving a primary radical at the C_β position. The tryptophan residue is therefore converted into an

alanine residue. Direct homolytic cleavage of the C_β–C_γ bond in tryptophan is not an energetically favorable pathway because it would generate two very unstable products, an aryl radical and a primary carbon radical. Recently, the Chu group reported C_β–C_γ bond cleavages of *N*-terminal tryptophan residues in peptide radical cations and proposed a hydrogen atom transfer mechanism that weakens the C_β–C_γ bond. However, tryptophan is not at the *N*-terminus in RGWALG and there is no proton present in our system. Instead, we consider homolytic aromatic substitution (or radical addition followed by dissociation) as a reasonable explanation for the C_β–C_γ bond cleavage as shown in Scheme 5.1. The benzoic acid radical adds to the tryptophan side chain at the C_γ position and breaks one double bond, leaving a radical at position C2 of the indole ring. The activation energy for this addition reaction is calculated to be 37.3 kJ/mol based on density functional theory when we used tryptophan amino acid to mimic the RGWALG peptide. Subsequently, the radical undergoes β cleavage to cleave the C_β–C_γ bond and rearomatize the indole ring.

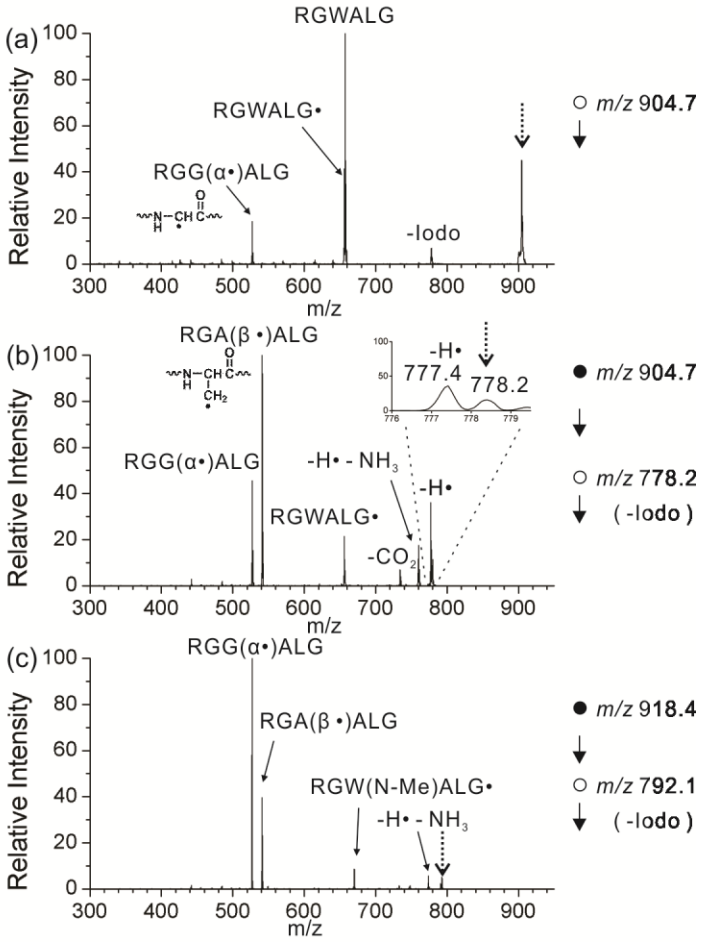

Figure 5.1. (a) Photodissociation spectrum of a non-covalent complex between singly charged RGWALG peptide anion and neutral 2-iodobenzoic acid. **(b)** CID spectrum of a radical complex between RGWALG and *ortho*-benzoic acid radical (i.e., the peak labeled as –I in Figure 5.1a). **(c)** CID spectrum of a radical complex between deprotonated RGW(*N*-Me)ALG and *ortho*-radical benzoic acid. W(*N*-Me) – N1-methylated tryptophan

Scheme 5.1 C_β–C_γ bond cleavage of tryptophan side chain by homolytic aromatic substitution reaction

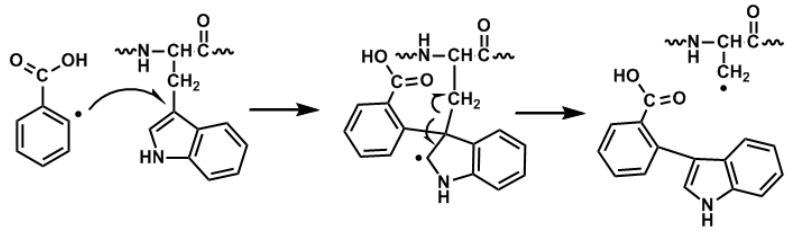

Scheme 5.5 shows a typical C_β–C_γ bond cleavage pathway for an amino acid side chain initiated by β cleavage from a C_α radical. Although this pathway is frequently observed for some amino acids such as leucine, it is not energetically favorable for aromatic side chains. Moreover, the dehydroalanine structure which is the product in Scheme 5.5 (theoretical *m/z* of 540.3) is not consistent with the experimental mass of RGA(β•)ALG that is observed in Figure 5.1b (*m/z* 541.3), indicating that this pathway does not occur. The radical nature of RGA(β•)ALG is further supported by reisolation and activation, which leads to radical directed dissociation (RDD) as discussed further below (see Figure 5.4c).

In Figure 5.1b, RGG(α•)ALG is generated by homolytic C_α–C_β bond cleavage and loss of the tryptophan side chain, which converts the tryptophan residue into a glycine residue. Further isolation and activation of RGG(α•)ALG leads to radical migration and side chain dissociation at leucine or arginine, confirming that the side chain loss produces a radical species (data not shown). Two reasonable mechanisms can explain tryptophan C_α–C_β bond cleavage as shown in Scheme 5.2. One route requires radical addition, where radical benzoic acid adds to the indole ring as shown in Scheme 5.2a with a calculated activation energy of 26.0 kJ/mol. The radical addition product then undergoes C_α–C_β bond cleavage to generate RGG(α•)ALG. This mechanism is analogous to one previously identified in radical ion/molecule reactions. Hydrogen atom abstraction at the N1 position of the indole ring can also account for the loss as shown in Scheme 5.2b. In the PD spectrum (see Figure 5.1a), RGG(α•)ALG has significant intensity whereas RGA(β•)ALG is barely seen. However, the situation reverses in RDD spectrum (see

Figure 5.1b). These observations are consistent with the mechanisms proposed in Schemes 5.1 and 5.2 because production of a primary radical for RGA(β•)ALG requires additional activation energy.

In order to further explore which mechanism (Scheme 5.2a vs. 5.2b) is the major pathway that gives rise to tryptophan C_α–C_β bond cleavage, the mechanism in Scheme 5.2b was blocked using *N*-methylated tryptophan and the same experiment was performed on RGW(*N*-Me)ALG. Methylation of tryptophan N1 atom prevents the radical from migrating to the indole nitrogen. The CID spectrum of radical RGW(*N*-Me)ALG peptide complex is shown in Figure 5.1c. Generation of the C_α–C_β bond cleavage product, RGG(α•)ALG (the base peak in Figure 5.1c), is not affected by tryptophan N1 methylation, indicating that the radical addition mechanism in Scheme 5.2a is the dominant pathway to cleave tryptophan C_α–C_β bond in this experiment. Previously, only the mechanism in Scheme 5.2b was used to explain tryptophan C_α–C_β bond cleavage. Our results reveal that radical addition reactions are also a plausible pathway in RDD of tryptophan-containing peptides and should be considered when assigning spectra.

Scheme 5.2

(a) C_α–C_β bond cleavage of tryptophan side chain initiated by aromatic addition reaction

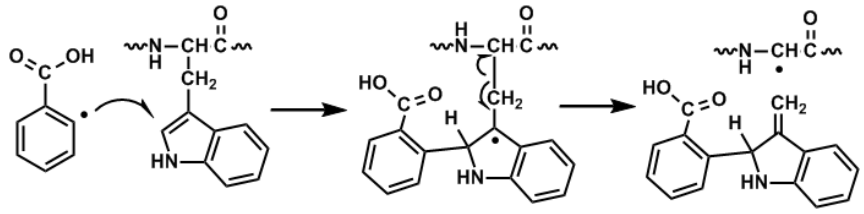

(b) C_α–C_β bond cleavage of tryptophan side chain by radical rearrangement initiated from a radical at position N1 of the indole ring

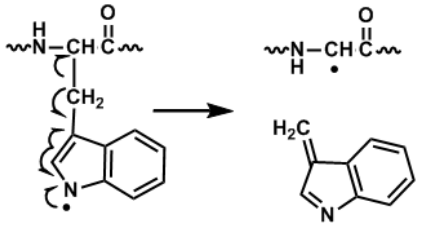

(c) Hydrogen loss and rearomatization after homolytic aromatic addition reaction

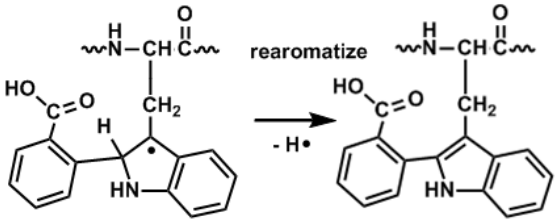

Another unusual product that is observed in Figure 5.1b is hydrogen atom loss. Although hydrogen atom loss is frequently observed in ECD (where hydrogen abundant radicals are generated), this dissociation pathway is atypical for the hydrogen deficient radicals generated here. The driving force behind this unusual loss is shown in Scheme 5.2c; the intermediate radical addition product can re-aromatize through loss of a hydrogen atom. The product ion should no longer be a radical, as indicated in Scheme 5.2c. Figure 5.2a shows the CID spectrum for the hydrogen atom loss product. The spectrum is dominated by ammonia loss and b/y fragments, which are consistent with an even electron ion. Furthermore, the fragments are consistent with benzoic acid modification at the tryptophan residue.

Figure 5.2b illustrates the RDD spectrum for the reaction between radical benzoic acid and a 13-residue peptide, Ac-SYSMEHFRWGKPV-NH_2. Both types of side chain cleavages at the tryptophan residue are observed and highlighted in Figure 5.2b. This data is shown to illustrate that these radical addition reactions are not specific to RGWALG, but can also occur in longer, more sequence complex peptides as well.

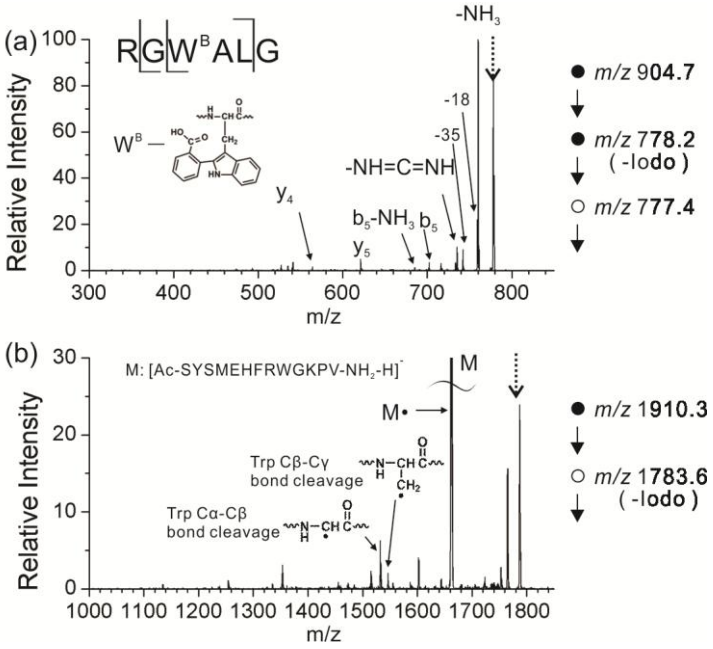

Figure 5.2 (a) CID spectrum of deprotonated RGW^{B}ALG peptide (i.e., the peak labeled as –H• in Fig5.1b). B – benzoic acid. W^{B} – benzoic acid modified tryptophan residue. **(b)** CID spectrum of a non-covalent complex between singly charged Ac-SYSMEHFRWGKPV-NH_2 anion and *ortho*-benzoic acid radical (generated from 2-iodobenzoic acid).

5.3.2 Tyrosine Side Chain Fragmentation

Figure 5.3a shows the CID spectrum of a radical complex between deprotonated RGYALG and radical benzoic acid. The [RGYALG]• product is generated by hydrogen atom abstraction from the peptide before separation of the complex. The tyrosine C_α–C_β bond cleavage product, RGG(α•)ALG, can potentially be generated by several pathways. Note that the base peak in Figure 5.3a corresponds to loss of CO_2 from the radical/peptide complex (i.e. loss of CO_2 prior to loss of benzoic acid). Further isolation and dissociation of this peak is shown in Figure 5.3b, producing RGG(α•)ALG in a very high yield. The peptide retains all carbonyl groups, suggesting that the initial CO_2 loss originated from the benzoic acid adduct. In the initially isolated complex, iodobenzoic acid forms a noncovalent bond with RGYALG via its carboxyl group; however, after radical activation and subsequent CO_2 loss, retention of the remaining benzene ring indicates that a new covalent bond has formed with the peptide. An aromatic addition reaction mechanism consistent with all of these observations is proposed in Scheme 5.3a. First, the benzoic acid radical adds to the C3 position of the tyrosine leaving a radical on the side chain. Second, the radical migrates back to the carboxyl group in benzoic acid and initiates decarboxylation, which generates the CO_2 loss in Figure 5.3a. Finally, further collisional activation leads to radical migration back to the tyrosine side chain at the phenolic oxygen which initiates C_α–C_β bond cleavage to generate RGG(α•)ALG.

If radical addition were to occur at position C2 or C4 of the tyrosine side chain, other pathways that do not involve CO_2 loss could also lead to C_α–C_β bond cleavage (see Scheme 5.3b). These pathways are analogous to several observed previously in radical

ion/ molecule reactions. Although possible, these pathways are not significant contributors as is demonstrated below. Additionally, Scheme 5.3c shows another potential tyrosine side chain loss pathway not involving CO_2 that is initiated by hydrogen abstraction from the phenol oxygen. This pathway can also account for observation of RGG(α•)ALG. However, since loss of CO_2 in Figure 5.3a is much larger than any other fragmentation channels, radical addition at position C3 (see Scheme 5.3a) appears to be the primary pathway that yields RGG(α•)ALG.

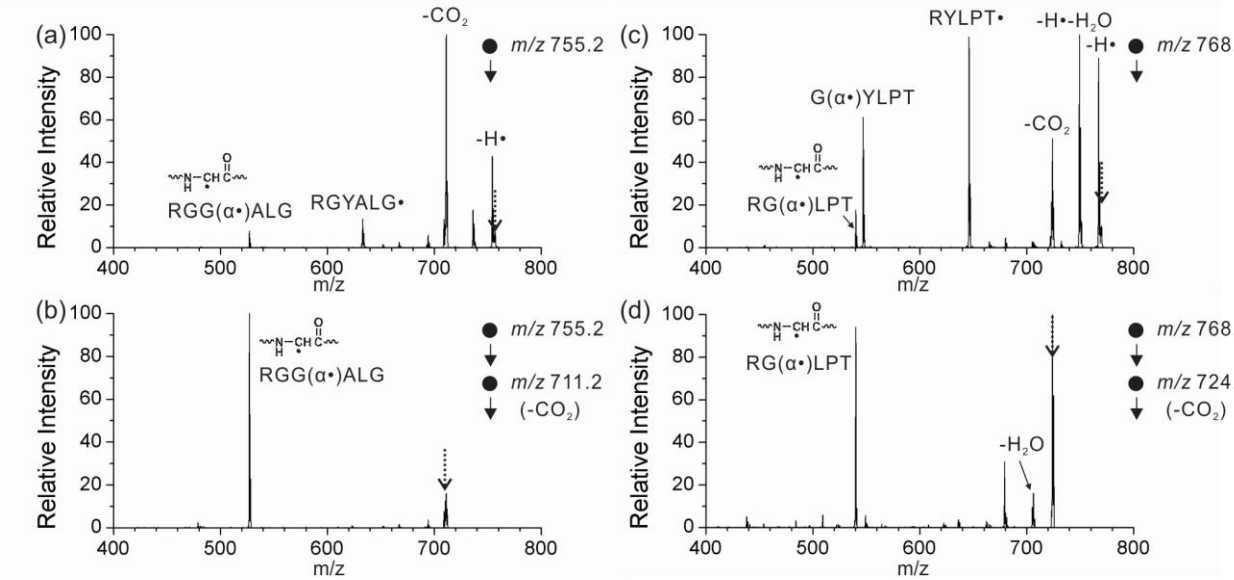

Figure 5.3. CID spectrum of a non-covalent complex between singly charged tyrosine peptide anion and *ortho*-benzoic acid radical (generated from 2-iodobenzoic acid). **(a)** RGYALG, **(c)** RYLPT. CID spectrum of the CO_2 loss fragment in (a) or (c) is shown in **(b)** or **(d)**, respectively

Scheme 5.3 Mechanisms for C_α–C_β bond cleavage of tyrosine side chain

(a) Homolytic aromatic addition reaction at position C3 – dissociation via CO_2 loss pathway

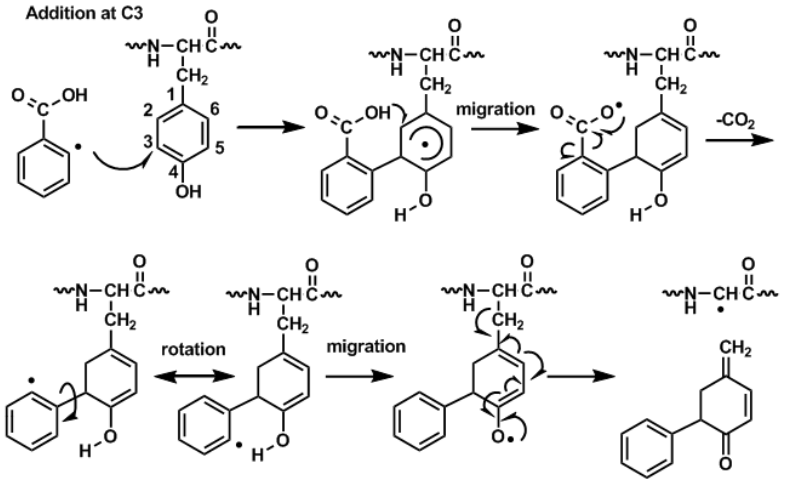

(b) Homolytic aromatic addition reaction at position C2 or C4

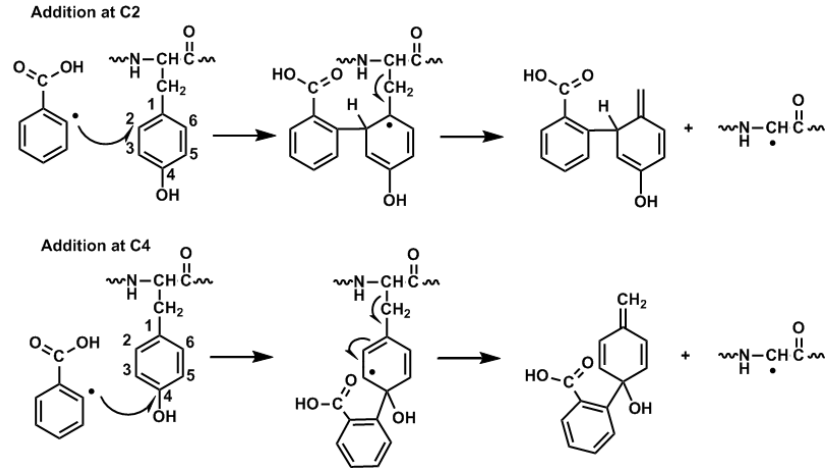

(c) Radical rearrangement initiated from phenol oxygen radical

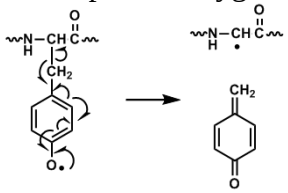

Figure 5.3c shows the analogous results for another tyrosine containing peptide, RYLPT. Both the CO_2 loss and the tyrosine C_α–C_β bond cleavage product (i.e., RG(α•)LPT) are observed, although other dissociation channels are more competitive for RYLPT. For example, side chain loss at arginine (producing G(α•)YLPT) is significantly more favorable. This suggests that for any given peptide, kinetics will dictate the dominant fragmentation pathways for both addition and migration initiated mechanisms. Figure 5.3d shows the CID spectrum of the CO_2 loss peak from Figure 5.3c, which preferentially generates the RG(α•)LPT, analogous to the situation for RGYALG in Figure 5.3b. The mechanism shown in Scheme 5.3a is again consistent with the data from RYLPT.

In order to verify the proposed mechanism of tyrosine C_α–C_β bond cleavage in Scheme 5.3a and evaluate the probabilities of the pathways in Scheme 5.3b, the tyrosine residue in RGYALG was replaced with O-methylated tyrosine (i.e., RGY(oMe)ALG). Absence of the phenolic OH should block the mechanisms in Scheme 5.3a and also 5.3c. Figure 5.4a shows the CID spectrum of the radical complex for RGY(oMe)ALG. Unlike the results for RGYALG in Figure 5.3a, RGG(α•)ALG is not observed at *m/z* 527 in Figure 5.4a, suggesting that the phenolic hydrogen is required and the mechanisms in Scheme 5.3b do not occur.

In Figure 5.4a, the C_β–C_γ bond cleavage product (i.e., RGA(β•)ALG at *m/z* 541.3) is favored. This product can be created by addition at the C1 position of tyrosine, followed by side chain loss as shown in Scheme 5.4. Further RDD of the RGA(β•)ALG product from Figure 5.4a is shown in Figure 5.4b. Extensive side chain losses (e.g., -43L, -56L, -

86R, -99R) are consistent with the radical nature of RGA(β•)ALG. For comparison, Figure 5.4c shows the CID spectrum of RGA(β•)ALG that is derived from RGWALG after tryptophan C_β–C_γ bond cleavage in Figure 5.1a. The nearly identical CID spectra in Figure 5.4b and 5.4c confirms the structure of RGA(β•)ALG and supports the aromatic substitution reaction mechanism in Scheme 5.4. However, in Figure 5.3a, RDD of RGYALG radical complex does not generate RGA(β•)ALG but results mainly in RGG(α•)ALG instead. This is different from tryptophan side chain dissociations in Figure 5.1b and 5.1c, where both the C_α–C_β and the C_β–C_γ bond cleavages are observed at the same time. The preferential tyrosine C_β–C_γ bond cleavage for RGY(oMe)ALG and C_α–C_β bond cleavage for RGYALG may be caused by two reasons. First, C_α–C_β and C_β–C_γ bond cleavages are two competitive fragmentation pathways. When C_α–C_β bond cleavage pathway is blocked after O-methylation, other dissociation pathways such as C_β–C_γ bond cleavage become kinetically more favored. Second, the peptide complex conformation may change significantly after tyrosine O-methylation. Although methyl group is small, phenol hydroxyl group is a polar group and may plays an important role towards the peptide conformational space. As a result, the interactions between the benzoic acid radical and the tyrosine side chain make radical attacking more favorable at the C1 position of tyrosine. This structure effect is elaborated further below.

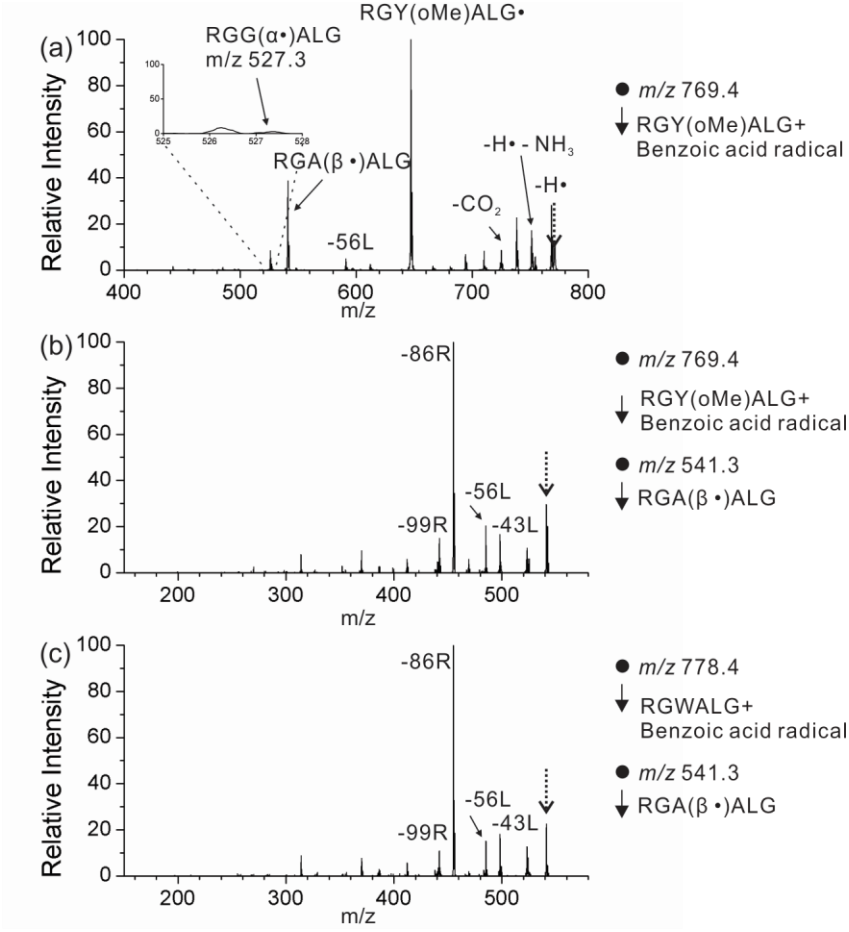

Figure 5.4 (a) CID spectrum of a non-covalent complex between singly charged RGY(oMe)ALG anion and *ortho*-benzoic acid radical (generated from 2-iodobenzoic acid). Y(oMe) – O-methylated tyrosine. **(b)** CID spectrum of RGA(β•)ALG in (a). **(c)** CID spectrum of RGA(β•)ALG peptide derived from RGWALG in Figure 5.1b.

Scheme 5.4 C_β–C_γ bond cleavage of tyrosine side chain in Figure 5.4a by homolytic aromatic substitution at position C1

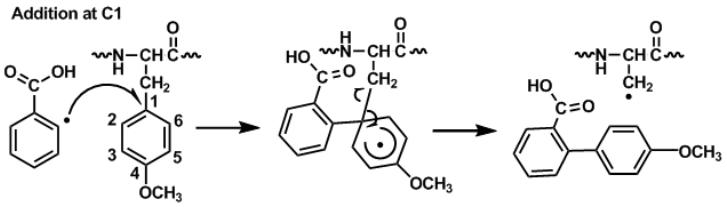

When *ortho*-benzoic acid radicals were replaced with *meta*- or *para*-benzoic acid radicals to react with RGYALG, the addition reaction rate is significantly decreased and intermolecular radical migration becomes the dominant pathway (generating hydrogen deficient radical peptides, see Figure 5.6 vs. Figure 5.1b). The relative position of the carboxyl group (*ortho*, *meta* or *para*) on the benzoic acid should not greatly influence the rates of attack because the singly occupied molecular orbital in each of the benzoic acid radicals lies in the plane of the ring. As a result, the ring position should not greatly influence the reactivity of benzoic acid radicals, which are already very reactive compared with alkyl radicals. However, intermolecular aromatic addition reactions within a non-covalent complex are different from bimolecular reactions where the relative orientations between reacting species are unlimited. Steric hindrance is more likely to be kinetically significant for a complex. Our previous molecular dynamics calculations on the kinetics of radical migration in peptides have shown that the *ortho*-position favors interacting with the peptide most among the *ortho*, *meta*, *para*- positional isomers. Analogously, since the benzoic acid must use the carboxyl group to interact with the peptide, a radical at the *ortho*-position is easily directed towards the partner molecule and thus appears to have the largest chance to undergo addition.

5.3.3 Intramolecular Radical Addition Reaction – Cyclization and Side Chain Migration

The results above clearly demonstrate that intermolecular radical addition reactions can occur between large peptides and reactive radical adducts. Similar functional groups can also exist within a single peptide, which could lead to intramolecular radical addition reactions. If such reactions occurred, they would be expected to significantly perturb the predicted fragmentation pattern for the peptide. Subsequent to our findings above, we re-examined previously obtained RDD spectra of peptides with abundant unassigned peaks. Figure 5.5 shows the results for one such peptide, VEPIPY. Following covalent modification with a radical precursor on the n-terminus, the CID spectrum of the radical peptide was acquired and is shown in Figure 5.5a. Only fragments that can be explained by radical migration or proton initiated fragmentation are assigned in Figure 5.5a. Both side chain loss fragments (e.g., –29I, C_β–C_γ bond cleavage at the isoleucine) and backbone dissociation products are observed. Without consideration of intramolecular radical addition reactions, only 42% of the peaks can be identified. The base peak (i.e., *m/z* 649.2) and several other intense fragments are not assigned. If radical addition reactions are taken into consideration, 81% peaks can be identified including the base peak and all abundant fragments (see Figure 5.5b). In this case, radical insertion followed by side chain dissociation leads effectively to migration of the tyrosine side chain to the *N*-terminus, which accounts for some of the products (e.g., b_4+107Y, a_4+107Y, b_3+107Y, b_2+107Y). Alternatively, radical addition followed by H• loss leads to a cyclized product from which internal fragment losses are observed (e.g., –H•–CO, –

H•–EPI, –H•–PI). The newly assigned peaks are highlighted in green in Figure 5.5b, and scheme 5.5 shows the corresponding reaction mechanisms. Tyrosine side chain losses from y ions are also observed in Figure 5.5 (e.g., $[y_4–107Y]•$, $[y_5–107Y]•$), which can be explained by two pathways. One pathway starts with radical migration to the phenol oxygen followed by the mechanism in Scheme 5.3c to cleave $C_\alpha–C_\beta$ bond. The other pathway is radical addition reaction at tyrosine residue followed by tyrosine side chain migration to the *N*-terminus. Observation of the complementary fragment for $[y_4–107Y]•$, (i.e., b_2+107Y) supports this pathway.

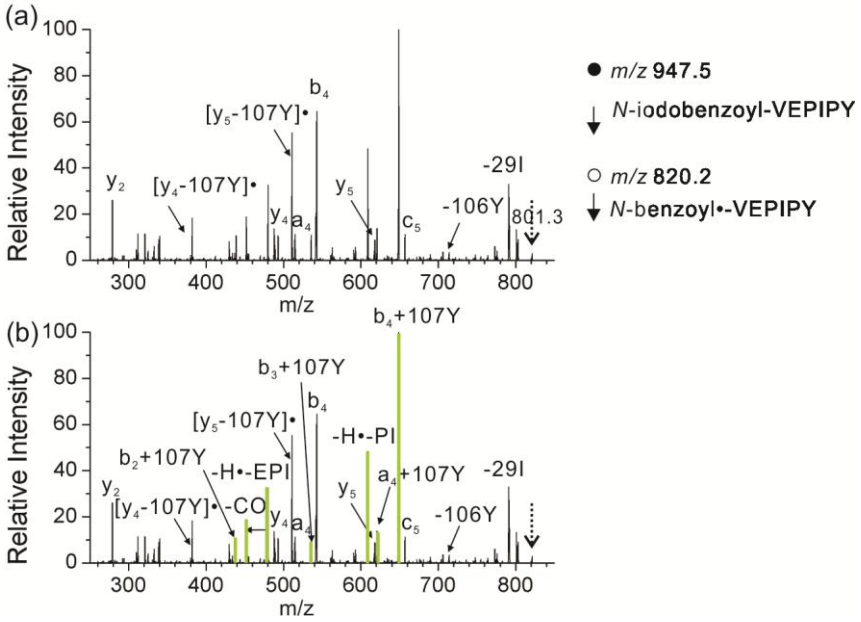

Figure 5.5. CID spectrum of radical peptide *N*-benzoyl-VEPIPY in the +1 charge state with the initial radical at the *meta*-position of *N*-terminal benzoyl group. Peaks are labeled without (a) and with (b) the knowledge of aromatic radical addition reactions. New identified peaks in (b) are highlighted in green. Side chain losses and migrations are abbreviated (i.e., 107Y represents 107 Da side chain from tyrosine). –CO, –EPI and –PI represent internal fragment losses from cyclized peptide

Scheme 5.5. Intramolecular radical addition reaction initiated peptide cyclization followed by tyrosine side chain and backbone dissociations in covalently labeled peptide radical cation *N*-benzoyl-VEPIPY

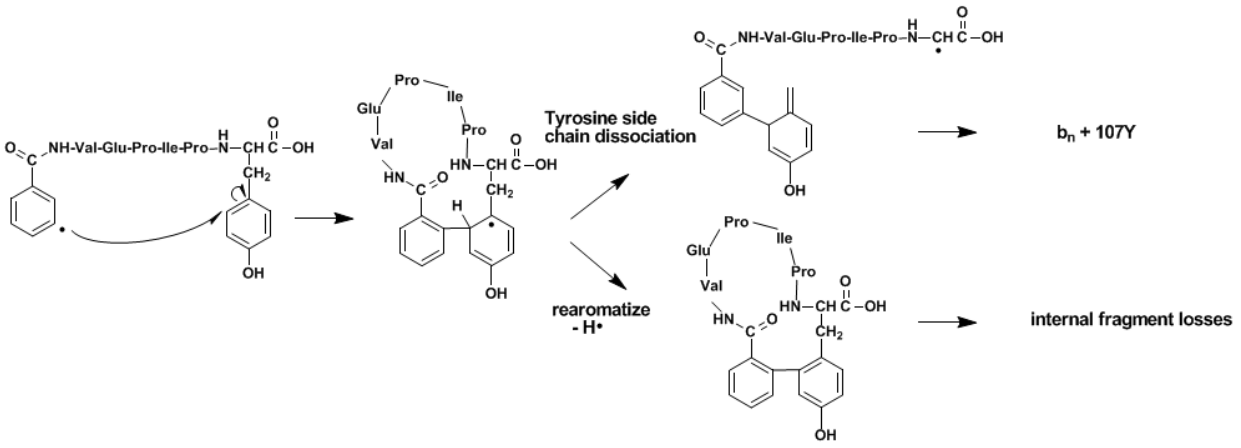

5.4 Conclusions

The present results illustrate that intermolecular radical addition at aromatic residues in peptides can lead to unusual side chain C_β–C_γ bond or C_α–C_β bond cleavage in the gas phase. To the best of our knowledge, this is the first study of side chain dissociations at tryptophan and tyrosine residues in large peptides initiated by radical addition reactions. In RGWALG and other tryptophan containing peptides, tryptophan C_β–C_γ bond cleavage and C_α–C_β bond cleavage are initiated by *ortho*-benzoic acid radical additions at the C_γ and C2 positions of the indole ring, respectively. In RGYALG and other tyrosine peptides, tyrosine C_β–C_γ bond cleavage is initiated by radical addition at the C_γ position whereas tyrosine C_α–C_β bond cleavage involves multiple steps and phenol hydrogen is indispensable. Results from covalently labeled radical *N*-benzoyl-VEPIPY suggest that intramolecular radical addition reactions in peptides can also occur to a significant degree, and that such mechanisms should be considered when assigning fragmentation spectra for hydrogen deficient peptides.

5.5 Supplemental information

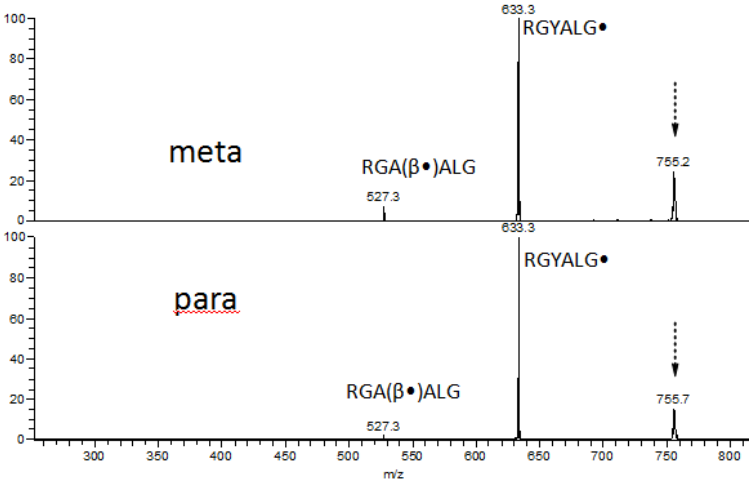

Figure 5.6. CID spectrum of the radical complex between RGYALG anion and (a) *meta*-benzoic acid radical (b) *para*-benzoic acid radical

References

[1] Zhang, X., Julian, R.R.: Photoinitiated intramolecular diradical cross-linking of polyproline peptides in the gas phase. *Phys. Chem. Chem. Phys.* 14, 16243-16249 (2012)

[2] Tao, Y.Q., Quebbemann, N.R., Julian, R.R.: Discriminating D-Amino Acid-Containing Peptide Epimers by Radical-Directed Dissociation Mass Spectrometry. *Anal. Chem.* 84, 6814-6820 (2012)

[3] Ly, T., Julian, R.R.: Elucidating the Tertiary Structure of Protein Ions in Vacuo with Site Specific Photoinitiated Radical Reactions. *J. Am. Chem. Soc.* 132, 8602-8609 (2010)

[4] Zhang, X., Julian, R.R.: Investigating the gas phase structure of KIX with radical directed dissociation and molecular dynamics: Retention of the native structure. *Int. J. Mass Spectrom.* 308, 225-231 (2011)

[5] Breuker, K., Bruschweiler, S., Tollinger, M.: Electrostatic Stabilization of a Native Protein Structure in the Gas Phase. *Angew. Chem. Int. Ed.* 50, 873-877 (2011)

[6] Chu, I.K., Rodriquez, C.F., Lau, T.C., Hopkinson, A.C., Siu, K.W.M.: Molecular radical cations of oligopeptides. *J. Phys. Chem. B* 104, 3393-3397 (2000)

[7] Barlow, C.K., McFadyen, W.D., O'Hair, R.A.J.: Formation of cationic peptide radicals by gas-phase redox reactions with trivalent chromium, manganese, iron, and cobalt complexes. *J. Am. Chem. Soc.* 127, 6109-6115 (2005)

[8] Laskin, J., Yang, Z.B., Ng, C.M.D., Chu, I.K.: Fragmentation of alpha-Radical Cations of Arginine-Containing Peptides. *J. Am. Soc. Mass Spectrom.* 21, 511-521 (2010)

[9] Headlam, H.A., Mortimer, A., Easton, C.J., Davies, M.J.: beta-scission of C-3 (beta-carbon) alkoxyl radicals on peptides and proteins: A novel pathway which results in the formation of alpha-carbon radicals and the loss of amino acid side chains. *Chem. Res. Toxicol.* 13, 1087-1095 (2000)

[10] Osburn, S., O'Hair, R.A.J.: Unleashing radical sites in non-covalent complexes: The case of the protonated S-nitrosocysteine/18-crown-6 complex. *Rapid Commun. Mass Spectrom.* 27, 2783-2788 (2013)

[11] Masterson, D.S., Yin, H.Y., Chacon, A., Hachey, D.L., Norris, J.L., Porter, N.A.: Lysine peroxycarbamates: Free radical-promoted peptide cleavage. *J. Am. Chem. Soc.* 126, 720-721 (2004)

[12] Hodyss, R., Cox, H.A., Beauchamp, J.L.: Bioconjugates for tunable peptide fragmentation: Free radical initiated peptide sequencing (FRIPS). *J. Am. Chem. Soc.* 127, 12436-12437 (2005)

[13] Hao, G., Gross, S.S.: Electrospray tandem mass spectrometry analysis of S- and N-nitrosopeptides: Facile loss of NO and radical-induced fragmentation. *J. Am. Soc. Mass Spectrom.* 17, 1725-1730 (2006)

[14] Lee, M.; Kang, M.; Moon, B.; Oh, H. B.: Gas-phase peptide sequencing by TEMPO-mediated radical generation. *Analyst* 2009, *134* (8), 1706-1712.

[15] Tan, L., Xia, Y.: Gas-Phase Peptide Sulfinyl Radical Ions: Formation and Unimolecular Dissociation. *J. Am. Soc. Mass Spectrom.* 23, 2011-2019 (2012)

[16] Tan, L., Xia, Y.: Gas-Phase Reactivity of Peptide Thiyl (RS center dot),Perthiyl (RSS center dot), and Sulfinyl (RSO center dot) Radical Ions Formed from Atmospheric Pressure Ion/Radical Reactions. *J. Am. Soc. Mass Spectrom.* 24, 534-542 (2013)

[17] Zhang, X., Julian, R.R.: Exploring Radical Migration Pathways in Peptides with Positional Isomers, Deuterium Labeling, and Molecular Dynamics Simulations. *J. Am. Soc. Mass Spectrom.* 24, 524-533 (2013)

[18] Turecek, F., Julian, R.R.: Peptide Radicals and Cation Radicals in the Gas Phase. *Mass Spectrom. Rev.* dx.doi.org/10.1021/cr400043s (2013)

[19] Xu, G.H., Chance, M.R.: Hydroxyl radical-mediated modification of proteins as probes for structural proteomics. *Chem. Rev.* 107, 3514-3543 (2007)

[20] Petzold, C.J., Ramirez-Arizmendi, L.E., Heidbrink, J.L., Perez, J., Kenttamaa, H.I.: Gas-phase reactions of charged phenyl radicals with neutral biomolecules evaporated by laser-induced acoustic desorption. *J. Am. Soc. Mass Spectrom.* 13, 192-194 (2002)

[21] Huang, Y.Q., Kenttamaa, H.: Theoretical and experimental investigations on the reactions of positively charged phenyl radicals with aromatic amino acids. *J. Am. Chem. Soc.* 127, 7952-7960 (2005)

[22] Huang, Y.Q., Guler, L., Heidbrink, J., Kenttamaa, H.: Reactions of charged phenyl radicals with aliphatic amino acids in the gas phase. *J. Am. Chem. Soc.* 127, 3973-3978 (2005)

[23] Pates, G.O., Guler, L., Nash, J.J., Kentamaa, H.I.: Reactivity and Selectivity of Charged Phenyl Radicals toward Amino Acids in a Fourier Transform Ion Cyclotron Resonance Mass Spectrometer. *J. Am. Chem. Soc.* 133, 9331-9342 (2011)

[24] Fu, M.K., Li, S., Archibold, E., Yurkovich, M.J., Nash, J.J., Kenttamaa, H.T.: Reactions of an Aromatic sigma,sigma-Biradical with Amino Acids and Dipeptides in the Gas Phase. *J. Am. Soc. Mass Spectrom.* 21, 1737-1752 (2010)

[25] Li, S., Fu, M.K., Habicht, S.C., Pates, G.O., Nash, J.J., Kenttamaa, H.I.: Phenyl Radical-Induced Damage to Dipeptides. *J. Org. Chem.* 74, 7724-7732 (2009)

Chapter 6

Radical mediated dissection of oligosaccharides

6.1. Introduction

Tandem mass spectrometry is a fast, accurate, and sensitive approach for structural characterization of oligosaccharides. Various ionization and dissociation methods have been used to obtain structural information from oligosaccharides including the compositions of substructures, the linkage positions, and even the epimeric nature. Collision induced dissociation (CID) is the most commonly used way to produce tandem mass spectra for oligosaccharides [1-6]. Low energy CID of even electron oligosaccharide ions generally results in abundant glycosidic bond cleavage but limited cross-ring cleavage. The advantage of cleavage at glycosidic bonds is that the generic monomeric substructure is revealed; however, linkage site information is often lost. In contrast, cross-ring cleavage is frequently observed in many activated ion dissociation methods including electron capture dissociation (ECD) [7-8], electronic excitation dissociation (EED) [9], electron transfer dissociation (ETD) [10-11], electron detachment dissociation (EDD) [12] and high energy photodissociation [13-15]. Odd-electron radical species and fragments are generated in most of these methods, which facilitate homolytic bond cleavage and ring-opening. For example, ECD of multiply charged oligosaccharides

generates charge reduced radical species. Compared with even-electron methods, radical directed dissociation is more likely to initiate cross-ring cleavage because cleavage of one bond frequently yields an equally reactive radical fragment as one of the products that can easily initiate a second bond fracture.

Direct capture of an electron in multiply charged molecules (e.g., peptides, proteins, saccharides) generates a hydrogen abundant species, which can convert to hydrogen deficient radicals [16]. Hydrogen deficient radical species can also be generated directly by homolytic bond cleavage. Various methods have been used to create hydrogen deficient radical peptides in the gas phase [17-21]. Subsequent radical migration and dissociation of peptides can provide structural information such as identification of isomeric residues [22] or investigation of peptide conformation [23]. In comparison, generation and dissociation of radical oligosaccharides by direct bond cleavage has been less studied. There are several advantages for studying oligosaccharide fragmentation with hydrogen deficient radical chemistry. First, the initial radical site can be controlled if the radical is generated by homolytic bond cleavage from a known position, providing an avenue for fragmentation mechanisms to be examined more easily. Second, most carbon atoms in oligosaccharides can donate a hydrogen atom and become free radical sites, which facilitates radical migration and increases the potential for backbone cleavage and generation of cross-ring fragments. Third, unlike ECD and ETD, singly charged ions can also be analyzed because generation of radicals does not involve charge reduction. Recently, Beauchamp and coworkers utilized collisional activation of TEMPO based radical precursors to generate radicals in covalently modified oligosaccharides [24].

Glycoside bond cleavage as well as two types of cross-ring fragments, $^{1,5}X$ and $^{0,2}X$, were observed in this study, suggesting that radical chemistry may be advantageous for the study of oligosaccharides.

Herein, we have developed two radical directed dissociation methods for characterizing oligosaccharides based on photodissociation mass spectrometry. Radicals are introduced to saccharides by covalent derivatization or noncovalent attachment with highly reactive phenyl radical precursors. The radical precursors used in this study are iodoaniline or iodophthalic acid based, but both have a carbon-iodine bond on the benzene ring. The benzene ring serves as a UV chromophore to absorb a photon, leading to homolytic dissociation of the carbon-iodine bond and generation of a highly reactive radical. The phenyl radical can subsequently migrate to other positions and initiate radical directed dissociation (RDD) of the molecule. More types of fragmentation are generated by RDD compared with CID of protonated species, which provides more information about structure. For example, positional isomers of fucopentaose can be easily distinguished based on RDD mass spectra. In addition, $^{1,5}X$ ions are the dominant cross-ring fragments generated in RDD. $^{0,2}X$ ions are also observed with a lower abundance.

6.2. Experimental methods

6.2.1. Materials

Oligosaccharides (Lacto-N-fucopentaose I (LNFP I), Lacto-N-fucopentaose II (LNFP II), Lacto-N-difucohexaose I (LNDFH I), Lacto-N-difucohexaose II (LNDFH II)) were

purchased from Dextra Laboratories Limited (Reading, UK). Maltoheptaose, $NaBH_3CN$ and other solvents were purchased from Sigma-Aldrich (St. Louis, MO, USA).

6.2.2. Saccharide Derivatization

Saccharides were reductively aminated in the reducing end. 200 nmol lyophilized maltoheptaose was mixed with 20 μL 0.5 M 2-iodoaniline in 70:30 DMSO : glacial acetic acid solution. 1 mg solid $NaBH_3CN$ was then added. The solution was incubated in 70 ℃ for 2 hrs before desalting with Oasis hydrophilic-lipophilic-balanced columns (Waters Corporation, Milford, MA, USA). The yield for this derivatization is close to 100%.

6.2.3. Photodissociation Mass Spectrometry

Covalently derivatized oligosaccharides (10 μM) in 50:50 H_2O:MeOH were electrosprayed in positive mode into an LTQ linear quadrupole ion trap mass spectrometer (Thermo Fisher Scientific, San Jose, CA, USA). Disaccharide (10 μM) and 4-iodophthalic acid (50 μM) were mixed with NH_4Ac buffer (10 mM) in 50:50 H_2O:ACN and electrosprayed in negative mode. 266 nm photons were generated from the fourth harmonic generation of a Nd:YAG laser (Continuum, Santa Clara, CA, USA). The back plate of the instrument was modified with a quartz window to transmit UV photons into the linear ion trap. Laser pulses were synchronized to the isolation step via a digital delay generator. The isolation window for precursor ions in collision induced dissociation and photodissociation was set between 1 to 10 *m/z* with an activation value q = 0.25 and default activation time 30 ms. Activation parameters were held constant for experiments where comparison of different fragmentation patterns are desired.

6.2.4 Nomenclature

Names of fragment ions are adopted from previous literature.

6.3. Results and Discussion

6.3.1 Maltoheptaose

The CID mass spectrum for singly protonated maltoheptaose is dominated by fragments resulting from glycosidic bond cleavages as shown in Figure 6.1a. Due to the structural symmetry of maltoheptaose, peaks can originate from either the non-reducing end (e.g., B, C ions) or reducing end (e.g., Y, Z ions). In order to facilitate radical directed dissociation (RDD), a radical precursor, iodoaniline, was attached to maltoheptaose by reductive amination. The CID mass spectrum for iodoaniline modified maltoheptaose is shown in Figure 6.1b. Significant differences are apparent in Figure 6.1b even in the absence of photoactivation of the radical. First, the symmetry of the molecule is broken, allowing for confident assignment of product ions. Second, the charge is retained at the modification site due to increased proton affinity, yielding a full series of Y ions that reveal the nature of each monosaccharide building block. Furthermore, the loss of iodine during collisional activation (see the peak labeled as –Iodo in Figure 6.1b) generates a hydrogen deficient radical ion. This observation contrasts with previous experiments on peptides and proteins, where collisional activation was not observed to cleave comparable carbon-iodine bonds. Interestingly, if the charge carrier is changed from a proton to a sodium ion, homolytic cleavage of carbon-iodine bond by CID is not observed. Calculation of the relevant bond dissociation energies (BDE) using density functional

theory reveals that the BDE of carbon-iodine in protonated iodoaniline is 8 kJ/mol lowered than neutral iodoaniline, which may account for the difference. Finally, close inspection of Figure 6.1b reveals that there are additional low abundance peaks (shown in greater detail in Figure 6.1c). These peaks are not noise, but represent secondary fragments derived from the radical ion (the CID spectrum of the reisolated radical maltoheptaose generated Figure 6.1b is shown in Figure 6.7) and will be described in greater detail in relation to the results in Figure 6.1d.

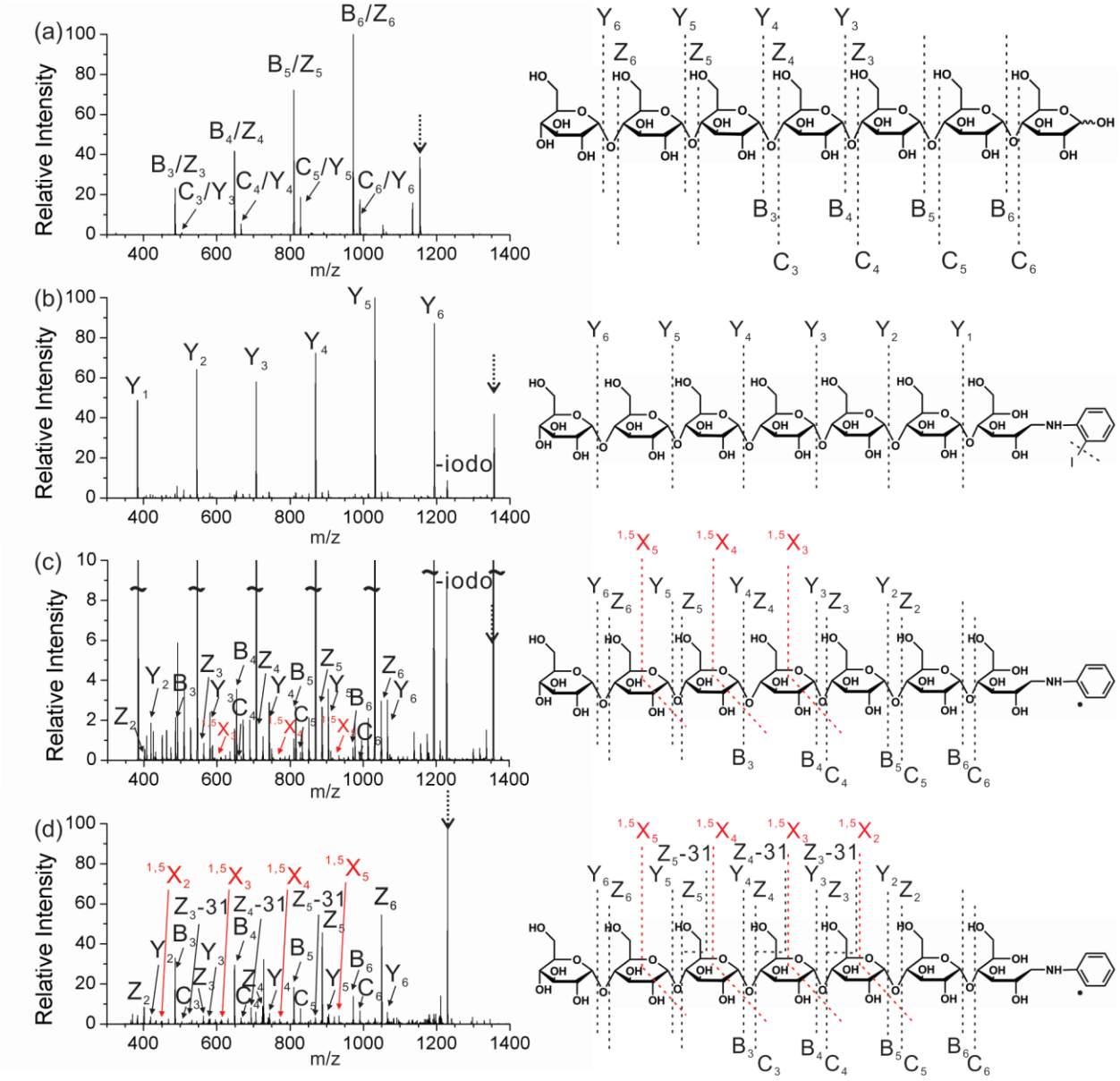

Figure 6.1. (a) CID of protonated maltoheptaose. Assignment of peaks is ambiguous due to symmetry. (b) CID of protonated maltoheptaose modified with 2-iodoaniline. (c) Zoom in of Fig.6.1(b), X, Y, Z fragments are assigned based on radical precursor with the structure shown on the right. (d) CID of protonated radical maltoheptaose, which was generated by photodissociation of 2-iodoaniline modified maltoheptaose

UV photodissociation (PD) can also be used for more selective radical generation as described in the introduction. Photoactivation of iodoaniline labeled maltoheptaose with 266nm photons yields loss of iodine almost exclusively, generating radical saccharide (see supporting information Figure 6.6). Subsequent collisional activation of the radical maltoheptaose results in radical migration and RDD as shown in Figure 6.1d. Importantly the radical precursor generated by loss of iodine is a highly reactive phenyl radical, which is thermodynamically favored to migrate to any position in a saccharide, and is therefore more likely to produce cross-ring fragmentation. Indeed, more cleavage sites and fragmentation types are observed in Figure 6.1d compared with the spectra in Figures 6.1a and 6.1b. Glycosidic bond cleavage fragments (i.e., B, C, Y, Z ions) can be generated by either proton or radical driven chemistry. However, cross-ring cleavage fragments, such as ^{1,5}X ions, must be generated by RDD because there are no cross-ring fragments in Figure 6.1a. The major types of glycoside bond cleavage fragments (e.g., Z ions) and cross-ring fragments observed herein (^{1,5}X ions) are consistent with Beauchamp and coworkers' data from CID of covalently modified radical maltoheptaose. However, there are more fragments from non-reducing end (i.e., B and C ions) in Figure 6.1d than were observed previously.

One possible radical pathway that generates ^{1,5}X fragments is shown in Scheme 6.1a. First, the radical migrates from benzene ring to C3 carbon after abstracting a hydrogen atom. Second, radical directed β cleavage reaction occurs and generates ^{1,5}X fragment. In Figure 6.1d, Z ions are often accompanied with secondary fragments which are 31 Da less than the corresponding Z ions. A reaction mechanism that leads to 31 Da loss from Z

ions is proposed in Scheme 6.1b. When Z ions are reisolated and collisionally activated, Z-31 is the major product, which supports the proposed fragmentation mechanism. Examination of a sodiated radical ion (see Figure 6.8) yielded mostly similar products to those for the protonated molecule in Figure 6.1d; however, generation of some $^{0,2}X$ fragments (e.g., $^{0,2}X_2$, $^{0,2}X_3$, $^{0,2}X_4$) was noted and is useful for obtaining branching information on position C2 of the pyranose. The effect of the benzene radical site on fragmentation was also investigated. Shifting the initial radical position on aniline from the ortho- to the para- position changes the fragmentation pattern (e.g., Z ions and Z-31 pathways are more favored for 4-iodoaniline in Figure 6.9). Nevertheless, the major fragmentation types (Z, Y, $^{1,5}X$) are not affected.

Scheme 6.1 (a) Radical directed dissociation mechanism for $^{1,5}X_i$ (i = 2, 3, 4 5) fragments in Figure 6.1d.

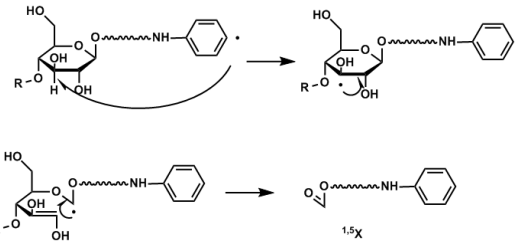

(b) Radical directed dissociation mechanism for Z-31 fragments in Figure 6.1d.

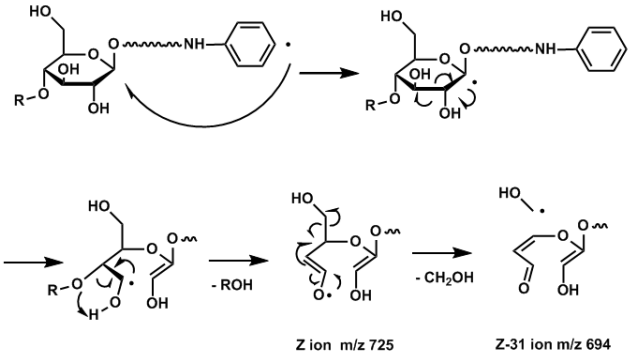

6.3.2 Lacto-N- fucopentaose isomers

LNFP I and LNFP II are two pentasaccharide isomers with the same monosaccharide composition but differ in linkage positions (see structures in Figure 6.2). Tandem mass spectrometry is usually a powerful method for distinguishing positional isomers; however, the CID spectra for protonated LNFP isomers (see Figure 6.10) are very similar. Some of the fragments generated by CID of the two isomers have different structures, but they are isomeric and are observed at the same m/z.

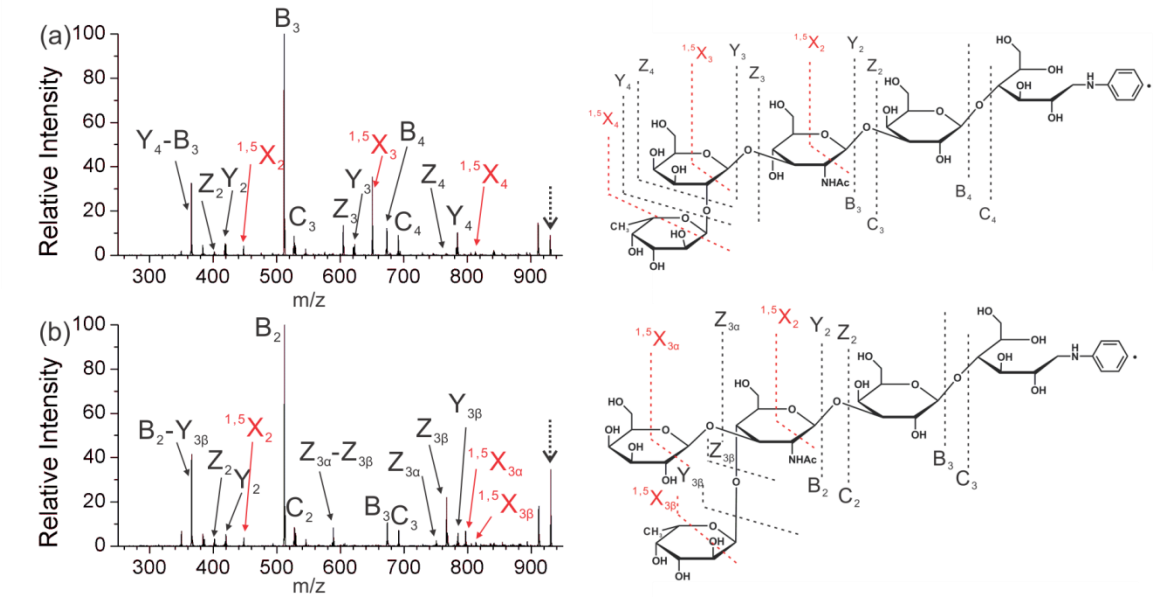

Figure 6.2. (a) RDD of protonated Lacto-N-fucopentaose I (LNFP I) modified with 4-iodoaniline. (b) RDD of protonated LNFP II isomer modified with 4-iodoaniline

Spectra illustrating collisional activation of the two LNFP radical isomers generated by PD are shown in Figure 6.2. Extensive glycosidic bond cleavage as well as some cross-ring cleavage fragments are observed. It is clear that the two spectra are different, and each has several diagnostic peaks that are unique to one isomer. For example, the cross-ring cleavage fragment, $^{1,5}X_3$, is unique for LNFP I in Figure 6.2a; whereas in Figure 6.2b, $^{1,5}X_{3\alpha}$ is unique for LNFP II. The major cross-ring cleavage fragments in these RDD spectra are $^{1,5}X$ ions, indicating that it is a particularly low energy dissociation pathway compared with other possible cross-ring cleavages. There are also some internal fragments which are generated by multiple bond cleavages in different rings, such as Y_4-B_3 (or Y_3-B_4) in Figure 6.2a and its isomeric fragment in Figure 6. 2b, B_2-$Y_{3\beta}$.

6.3.3 Lacto-N-difucohexaose isomers

LNDFH I and LNDFH II are two hexasaccharide isomers which differ only in the linkage position of one fucose group (see structures in Figure 6.3). Collisional activation of the radical isomers is shown in Figure 6.3. Extensive cleavage between all monosaccharide units is observed and many of the fragments result from glycosidic bond cleavage. However, there are still several unique fragments in Figure 6.3 that explicitly distinguish the two isomers, such as B_3, $^{1,5}X_{3\alpha}$ in Figure 6.3a and $Y_{1\alpha}$, $^{1,5}X_{2\alpha}$ in Figure 6.3b. In fact, $^{1,5}X$ cross-ring cleavages are observed for every ring except the second monosaccharide from the reducing end. This is consistent with the results from the two LNFP isomers in Figure 6.2. Absence of $^{1,5}X_1$ in the second ring could be explained by the rigid structure of benzene ring at the reducing end, which may make migration to the

adjacent ring kinetically disfavored. Observation of cross-ring cleavage at all other $^{1,5}X_n$ fragments suggests that radical is able to freely migrate to these rings.

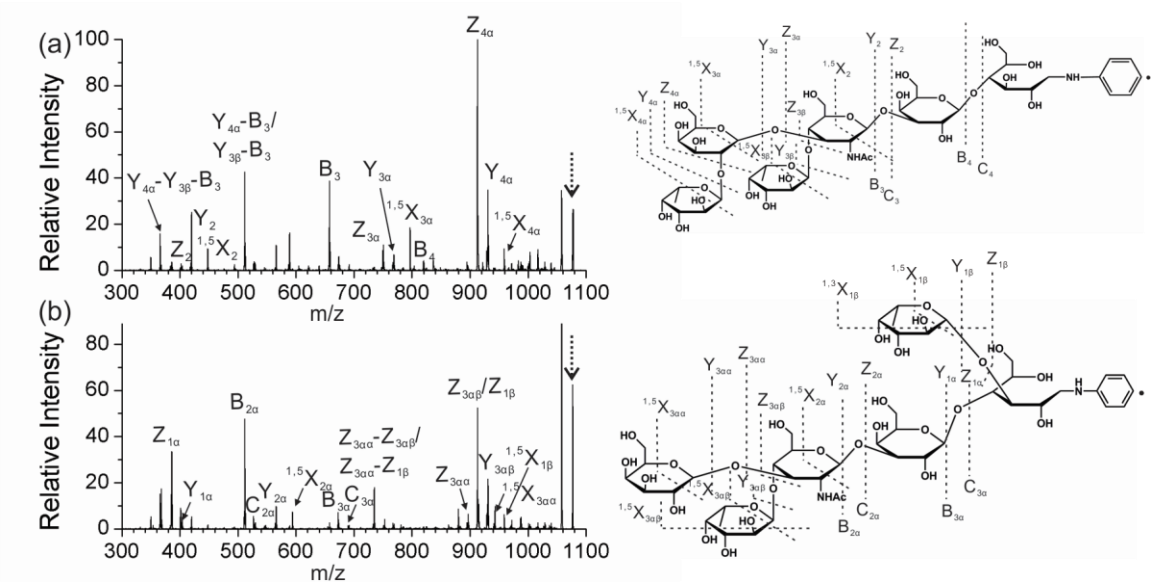

Figure 6.3. (a) RDD of protonated Lacto-N-difucohexaose I (LNDFH I) modified with 4-iodoaniline. (b) RDD of protonated LNDFH II isomer modified with 4-iodoaniline

6.3.4 Disaccharides

Although disaccharides are small molecules, they can still have numerous isomers with different combinations of monosaccharide types, linkage positions, and anomeric carbons. Tandem mass spectrometry is well-suited for distinguishing isomeric disaccharides, but de novo structural characterization without a standard for comparison is more challenging. This limitation can be mitigated by building a reference library of spectra for comparison against an unknown analyte. Various methods have been used to collect characteristic tandem MS spectra for disaccharides, and it has been found that generally the more fragments that are generated the higher the probability of identifying the unknown species. Due to these constraints, CID of protonated disaccharides is not effective because most fragments come from glycoside bond cleavage. Electron based activation methods are not a good choice either because disaccharide ions exist primarily in the singly charged state. Within these parameters, RDD may be advantageous since both glycosidic bond cleavage and cross-ring cleavage are observed, and fragmentation can be carried out regardless of charge state. However, modification of disaccharides by reductive amination to install a radical precursor leads to very little RDD (data not shown). One potential explanation is that in small molecules, the number of kinetically available radical migration sites is likely limited. Moreover, reductive amination is undesirable because it alters the molecule and makes it impossible to produce cross-ring cleavage fragments for one of the saccharides. Therefore a different strategy for introducing radicals was implemented, namely noncovalent attachment of 4-iodophthalic acid. When a solution containing cellobiose and 4-iodophthalic acid is electrosprayed in

anion mode, a noncovalent complex based on hydrogen bonds between the carboxyl group in 4-iodophthalic acid and the hydroxyl groups in the disaccharide is formed. The 1:1 ratio complex can be isolated and photodissociated as shown in Figure 6.4. The carbon-iodine bond on iodophthalic acid of this noncovalent complex is selectively cleaved by photoactivation and a radical complex is generated. The reaction pathway is shown in Scheme 6.2. The benzene radical is highly reactive and migrates to cellobiose immediately. Spontaneous separation of the radical cellobiose and phthalic acid is facilitated by the excessive energy from photoexcitation, which leads to hydrogen deficient, negatively charged radical cellobiose ($[M-2H]^{-\bullet}$ at m/z 340.2 in Figure 6.4). In this way, radical disaccharides can be easily generated in sufficient yield for further characterization without the need for covalent derivatization.

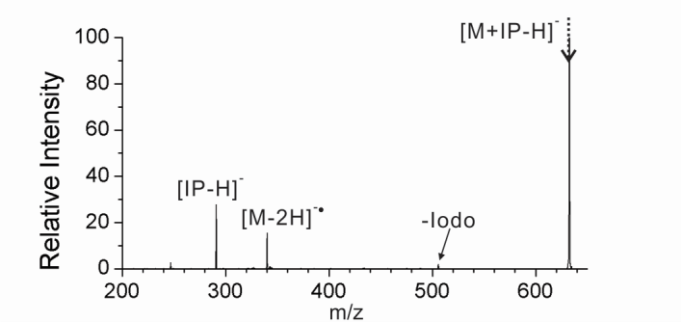

Figure 6.4. Photodissociation of anionic complex between cellobiose and 4-iodophthalic acid.

Scheme 6.2. Generation of radical cellobiose by photodissociation followed by spontaneous radical migration and complex separation.

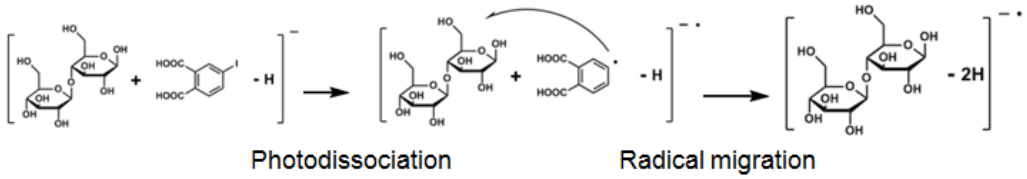

Four isomeric radical disaccharides (cellobiose, leucrose, melibiose and palatinose) were generated by this noncovalent radical delivery strategy and further activated by CID. Figure 6.5 shows PD-CID spectra of these disaccharides and their corresponding structures. Compared with CID spectra of even electron species for these isomers, RDD generates significantly more cross-ring cleavage fragments. All the four isomers can be distinguished from each other based on the unique signature fragments characteristic to each of them; cellobiose m/z 158, 262 and 293, leucrose m/z 99, 248, 267, 292; melibiose m/z 294; palatinose m/z 117.

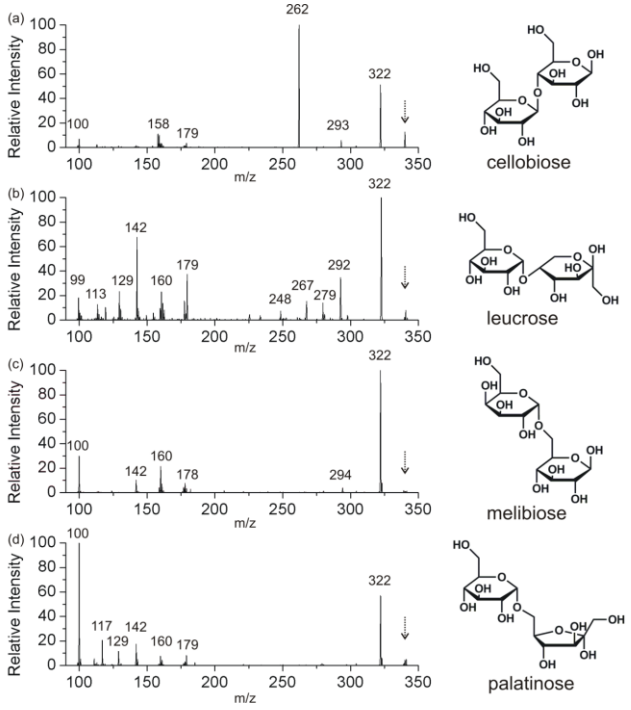

Figure 6.5. Radical directed dissociation of anion radical disaccharide isomers for (a) cellobiose, 4-O-β-D-Glucopyranosyl-D-glucose ; (b) leucrose, 5-O-(α -D-Glucopyranosyl)-D-fructose ; (c) melibiose**,** 6-O-α-D-Galactopyranosyl-D-glucose **;** (d) palationose, 6-O-α-D-Glucopyranosyl-D-fructose

Noncovalent attachment of larger oligosaccharides with iodophthalic acid was also investigated; however, separation of the oligosaccharide/phthalic acid complex proved to be difficult, presumably due to a stronger hydrogen bonding network. Instead of spontaneous separation of the oligosaccharide from the phthalic acid, covalent bond cleavage at glycosidic bonds was found to be preferred, limiting the utility of the phthalic acid noncovalent approach for larger oligosaccharides.

6.4. Conclusions

In the present work, a highly reactive phenyl radical is used to generate hydrogen deficient radical oligosaccharides and for subsequent fragmentation by RDD. The radical precursor can be attached to saccharides by either covalent derivatization with iodoaniline in the reducing end or by noncovalent attachment of iodophthalic acid for small disaccharides. Following covalent modification, CID of the protonated oligosaccharide results typical glycosidic bond cleavage as well as homolytic carbon-iodine bond cleavage and secondary fragmentation due to RDD. Alternatively, UV photodissociation of the carbon-iodine bond can be used to specifically generate radical ion in a high yield. Compared with CID of even electron saccharides, RDD generates extensive fragmentation types including both glycoside bond cleavage and cross-ring cleavage, which is helpful for characterization of positional oligosaccharide isomers, such as lacto-N-fucopentaose and lacto-N-difucohexaose. For all the oligosaccharides studied in this work, radical initiated cross-ring fragment is dominated by $^{1,5}X$ type. This suggests that this cross ring fragmentation occurs via a low energy pathway that is favored by the

slow activation process in CID. Overall, it appears that the energetic landscape for radical chemistry is significantly flatter than that for proton initiated chemistry, allowing for many more dissociation channels to be accessed and yield significantly more information.

6.5. Supporting information

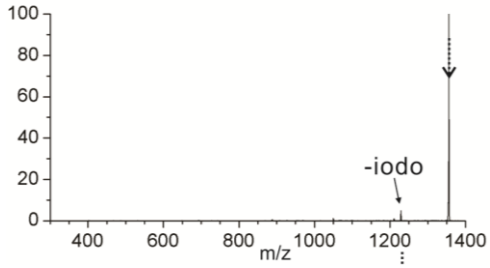

Figure 6.6. Photodissociation (single laser shot) of 2-iodoaniline labeled maltoheptaose

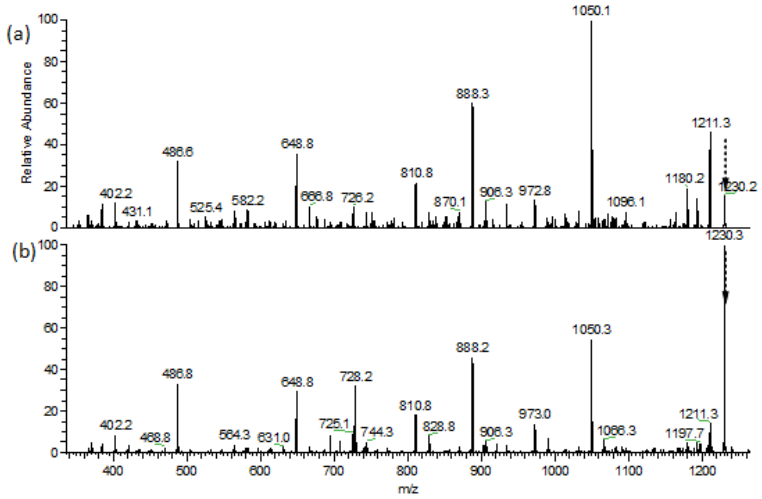

Figure 6.7. (a) CID of protonated radical maltoheptaose in Figure 6.1(b) (i.e, the peak labeled as –iodo, which was generated by CID of 2-iodoaniline modified maltoheptaose). (b) The same as Figure 6.1d, which is shown here for comparison with (a)

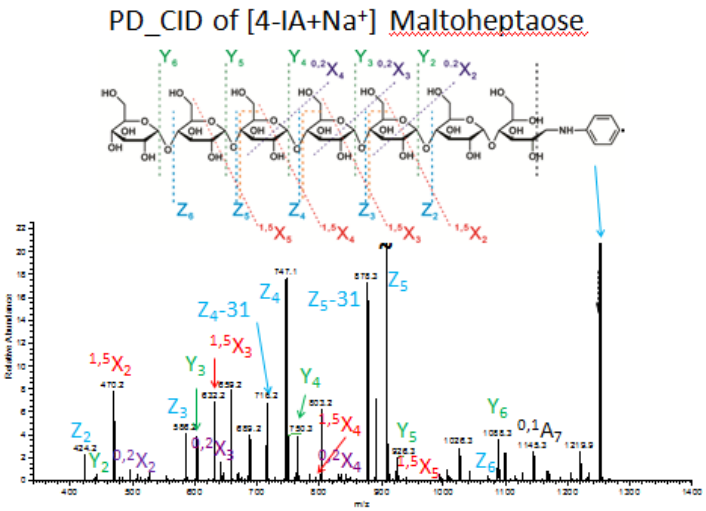

Figure 6.8. Radical directed dissociation of 4-iodoaniline labeled sodiated maltoheptaose

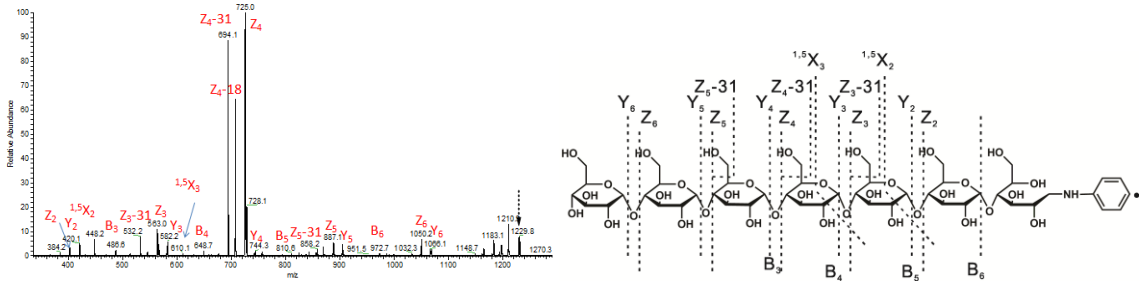

Figure 6.9. Radical directed dissociation of 4-iodoaniline labeled protonated maltoheptaose

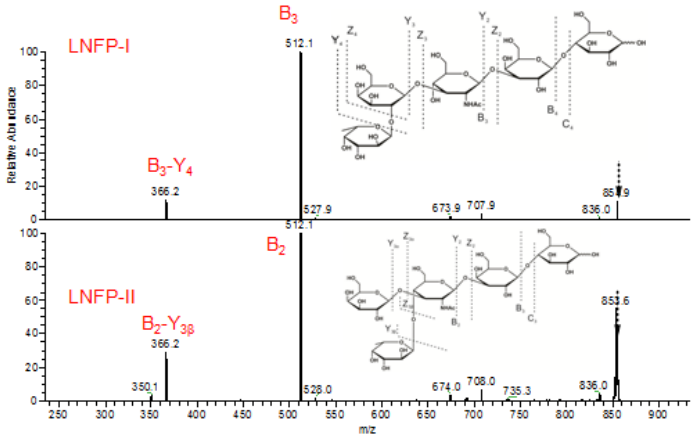

Figure 6.10 (a) CID of protonated Lacto-N-fucopentaose I (LNFP I) modified with 4-iodoaniline. (b) CID of protonated LNFP II isomer modified with 4-iodoaniline

References

[1] Domon, B., Costello, C.E.: A Systematic Nomenclature for Carbohydrate Fragmentations in Fab-Ms Ms Spectra of Glycoconjugates. *Glycoconjugate J.* **5**, 397-409 (1988)

[2] Medzihradszky, K.F., GilleceCastro, B.L., Townsend, R.R., Burlingame, A.L., Hardy, M.R.: Structural elucidation of O-linked glycopeptides by high energy collision-induced dissociation. *J. Am. Soc. Mass Spectrom.* **7**, 319-328 (1996)

[3] Domon, B., Muller, D.R., Richter, W.J.: Identification of Interglycosidic Linkages and Sugar Constituents in Disaccharide Subunits of Larger Glycosides by Tandem Mass-Spectrometry. *Org. Mass Spectrom.* **24**, 357-359 (1989)

[4] Garozzo, D., Giuffrida, M., Impallomeni, G., Ballistreri, A., Montaudo, G.: Determination of Linkage Position and Identification of the Reducing End in Linear Oligosaccharides by Negative-Ion Fast Atom Bombardment Mass-Spectrometry. *Anal. Chem.* **62**, 279-286 (1990)

[5] Hofmeister, G.E., Zhou, Z., Leary, J.A.: Linkage Position Determination in Lithium-Cationized Disaccharides - Tandem Mass-Spectrometry and Semiempirical Calculations. *J. Am. Chem. Soc.* **113**, 5964-5970 (1991)

[6] Konig, S., Leary, J.A.: Evidence for linkage position determination in cobalt coordinated pentasaccharides using ion trap mass spectrometry. *J. Am. Soc. Mass Spectrom.* **9**, 1125-1134 (1998)

[7] Adamson, J.T., Hakansson, K.: Electron capture dissociation of oligosaccharides ionized with alkali, alkaline earth, and transition metals. *Anal. Chem.* **79**, 2901-2910 (2007)

[8] Yu, X.A., Lin, C., Costello, C.E.: Electron Energy Dependent Electron Capture Dissociation, an Informative Tool for Structural Characterization of Oligosaccharides. *Glycobiology* **20**, 1513-1513 (2010)

[9] Yu, X., Huang, Y.Q., Lin, C., Costello, C.E.: Energy-Dependent Electron Activated Dissociation of Metal-Adducted Permethylated Oligosaccharides. *Anal. Chem.* **84**, 7487-7494 (2012)

[10] Han, L., Costello, C.: Electron Transfer Dissociation of Milk Oligosaccharides. *J. Am. Soc. Mass Spectrom.* **22**, 997-1013 (2011)

[11] Wolff, J.J., Leach, F.E., Laremore, T.N., Kaplan, D.A., Easterling, M.L., Linhardt, R.J., Amster, I.J.: Negative Electron Transfer Dissociation of Glycosaminoglycans. *Anal. Chem.* **82**, 3460-3466 (2010)

[12] Wolff, J.J., Chi, L.L., Linhardt, R.J., Amster, I.J.: Distinguishing glucuronic from iduronic acid in glycosaminoglycan tetrasaccharides by using electron detachment dissociation. *Anal. Chem.* **79**, 2015-2022 (2007)

[13] Devakumar, A., Mechref, Y., Kang, P., Novotny, M.V., Reilly, J.P.: Laser-induced photofragmentation of neutral and acidic glycans inside an ion-trap mass spectrometer. *Rapid Commun. Mass Spectrom.* **21**, 1452-1460 (2007)

[14] Han, L., Costello, C.: Electron Transfer Dissociation of Milk Oligosaccharides. *J. Am. Soc. Mass Spectrom.* **22**, 997-1013 (2011)

[15] Ko, B.J., Brodbelt, J.S.: 193 nm Ultraviolet Photodissociation of Deprotonated Sialylated Oligosaccharides. *Anal. Chem.* **83**, 8192-8200 (2011)

[16] Moore, B.N., Ly, T., Julian, R.R.: Radical Conversion and Migration in Electron Capture Dissociation. *J. Am. Chem. Soc.* **133**, 6997-7006 (2011)

[17] Chu, I.K., Rodriquez, C.F., Lau, T.C., Hopkinson, A.C., Siu, K.W.M.: Molecular radical cations of oligopeptides. *J. Phys. Chem. B* **104**, 3393-3397 (2000)

[18] Chu, I.K., Lam, C.N.W., Siu, S.O.: Facile generation of tripeptide radical cations in vacuo via intramolecular electron transfer in Cu-II tripeptide complexes containing sterically encumbered terpyridine Ligands. *J. Am. Soc. Mass Spectrom.* **16**, 763-771 (2005)

[19] Song, T., Hao, Q., Law, C.H., Siu, C.K., Chu, I.K.: Novel C-beta-C-gamma Bond Cleavages of Tryptophan-Containing Peptide Radical Cations. *J. Am. Soc. Mass Spectrom.* **23**, 264-273 (2012)

[20] Tan, L., Xia, Y.: Gas-Phase Peptide Sulfinyl Radical Ions: Formation and Unimolecular Dissociation. *J. Am. Soc. Mass Spectrom.* **23**, 2011-2019 (2012)

[21] Sun, Q.Y., Nelson, H., Ly, T., Stoltz, B.M., Julian, R.R.: Side Chain Chemistry Mediates Backbone Fragmentation in Hydrogen Deficient Peptide Radicals. *J. Proteome Res.* **8**, 958-966 (2009)

[22] Wee, S., O'Hair, R.A.J., McFadyen, W.D.: Side-chain radical losses from radical cations allows distinction of leucine and isoleucine residues in the isomeric peptides Gly-XXX-Arg. *Rapid Commun. Mass Spectrom.* **16**, 884-890 (2002)

[23] Zhang, X., Julian, R.R.: Photoinitiated intramolecular diradical cross-linking of polyproline peptides in the gas phase. *Phys. Chem. Chem. Phys.* **14**, 16243-16249 (2012)

[24] Gao, J.S., Thomas, D.A., Sohn, C.H., Beauchamp, J.L.: Biomimetic Reagents for the Selective Free Radical and Acid-Base Chemistry of Glycans: Application to Glycan Structure Determination by Mass Spectrometry. *J. Am. Chem. Soc.* **135**, 10684-10692 (2013)